Titel der Arbeit:

Studies on the formation of cortical circuits

The role of Ire1α in the developing neocortex

Identification of epilepsy-associated genes by ENU-induced mutagenesis in mice

D I S S E R T A T I O N

zur Erlangung des akademischen Grades

Doctor of Philosophy (Ph.D.)

eingereicht an der

Lebenswissenschaftlichen Fakultät der Humboldt-Universität zu Berlin

von

Ekaterina Borisova

Präsidentin/Präsident der Humboldt-Universität zu Berlin

Prof. Dr. Julia von Blumenthal

Dekanin/Dekan der Lebenswissenschaftlichen Fakultät

der Humboldt-Universität zu Berlin

Prof. Dr. Dr. Christian Ulrichs

Vorsitxende/Vorsitzender

1. Prof. Dr. Ana Pombo

Gutachter/innen

2. Prof. Dr. Victor Tarabykin
3. Prof. Dr. Matthew Larkum
4. Prof. Dr. Peter Robin Hiesinger

Weiteres Mitglied

5. Prof. Dr. Marina Mikhaylova

Tag der mündlichen Prüfung: 04.11.2022

Berlin 2022

Table of Contents

1. List of abbreviations

AAV – adeno-associated virus

AcX – Acryloyl-X

AGS – Audiogenic Stimulation

AIS – axon initial segment

AMPA – α-amino-3-hydroxy-5-methyl-4-isoxazolepropionic acid

ANL – azidonorleucine

AP – apical progenitor

APS – Ammonium Persulfate

ARX – Aristaless-related homeobox protein

bp – base pair

BrdU – Bromodeoxyuridine

BSA – Bovine Serum Albumin

CDKL5 – Cyclin-dependent kinase-like 5

cKO – conditional knockout

CP – cortical plate

CTIP2 – Chicken ovalbumin upstream promoter Transcription Factor-Interacting Protein 2

Cux1 – Cut like Homeobox 1

DIV – Day *in vitro*

dNTP – Deoxynucleosidtriphosphate

E – Embrionic day

E/I – Excitation/Inhibition

EDTA – Ethylenediaminetetraacetic acid

eEF2 – eukaryotic elongation factor 2

eIF4A1 – eukaryotic initiation factor 4A1

ENU – N-ethyl-N-Nitrosourea

FBS – Fetal bovine serum

FISH – Fluorescent *In situ* Hybridization

FYNCAT – Fluorescent Noncanonical Amino Acid Tagging

G – generation

G4 – guanine-quadruplex

GABA – γ-aminobutyric acid

GE – Ganglionic Eminence

GFP – Green Fluorescent Protein

HBSS – Hanks Balanced Salt Solution

HEPES – 4-(2-hydroxyethyl)-1-piperazineethanesulfonic acid

HPG – 4-Hydroxyphenylglycine

HPR – Horseradish Peroxidase

ICC – Immunocytochemistry

ICH – Immunohistochemistry

Ire1α – Inositol-Requiring Enzyme

IUE – *In Utero* Electroporation

IZ – intermediate zone

KO – knockout

LP – leading process

MAP2 – Microtubule-associated protein 2

MEFs – murine embryonic fibroblasts

MZ – marginal zone

NEM – N-Ethylmaleimide

OCT – Optimal Cutting Temperature Compound

OD – Optical Density

PBS – Phosphate-buffered saline

PCDH19 – Protocadherin 19

PCR – Polymerase Chain Reaction

PFA – Paraformaldehyde

PLA – Proximity Ligation Assay

PTEN – Phosphatase and tensin homolog

Satb2 – Special AT-rich sequence-Binding protein

SDS – Sodium dodecyl sulface

SDS-PAGE – Sodium Dodecyl Sulfate Polyacrylamide gel electrophoresis

SNP – Single Nucleotide Polymorphism

SP – subplate

SPR – signal recognition particle

STXBP1 – Syntaxin-binding protein 1

TBS-T – Tris-buffered saline with Tween20

THPTA – 3-hydroxypropyl-triazolyl methyl

TP – trailing process

UBE3A – Ubiquitin protein ligase E3A

UPR – Unfolded Protein Responce

VZ – ventricular zone

WB – Western blot

2. Abstract

English

Higher cognitive abilities of human neocortex comprise abstract thinking, complex comprehension, language and learning capacity. Formation of the cerebral cortex begins in the middle of embryogenesis and is a tightly organized and highly regulated process. Asymmetric divisions of neuronal stem cells give rise to immature neurons that migrate to consequently assume their specific position in the cortical plate. Correct acquisition of a single-axon morphology and specification of the dendritic tree complexity sets grounds for establishment of cortical connectivity. These morphological characteristics are encoded by intrinsic genetic programs of postmitotic differentiation and regulated by developmental cues in the extracellular milieu.

Endoplasmic Reticulum resident Inositol-Requiring Enzyme 1α (Ire1α) is one of the main regulators of the unfolded protein response. In this study, we demonstrate that Ire1α is pivotal for specification of upper layer cortical neurons and the acquisition of the neuronal morphology by regulating mRNA translation rates.

This work also shows that early and late cortical neuronal progenitors and early- and late-born postmitotic neurons exhibit different translation rates, indicative of the specific requirements for the proteome synthesis machinery for the development of cortical layers.

Disturbances of any cortical developmental milestones due to either environmental factors or gene mutations may result in aberrant physiology of cortical circuits. High number of such abnormalities can lead to serious neurological diseases such as epilepsy or complex disorders with epilepsy such as Rett syndrome, Angelman syndrome, Mowat-Wilson syndrome, Lafora disease and/or Kaufman oculocerebrofacial syndrome. One major hypothesis of the causes of epilepsy links its molecular pathology to alterations in excitation/inhibition (E/I) balance in the neuronal networks. According to this hypothesis, E/I imbalance can be then caused by, inter alia, altered synaptic strength in single neurons within the network, different number of excitatory or inhibitory neurons, abnormalities in neuronal morphology or the number of neurons of a given fate. In order to broaden the scope of molecular and cellular processes leading to epilepsy and its mechanisms, we used ENU mutagenesis in mice to investigate novel mutations linked to the disease. Using these models, we also characterize the molecular and cellular underpinnings of the disease.

Deutsch

Zu den höheren kognitiven Fähigkeiten des menschlichen Neokortex gehören abstraktes Denken, komplexes Verstehen, Sprache und Lernfähigkeit. Die Bildung der Großhirnrinde beginnt in der mittleren Phase der Embryogenese und ist ein hochgradig organisierter und streng regulierter Prozess. Durch asymmetrische Teilung neuronaler Stammzellen entstehen unreife Neuronen, die im Anschluss an ihre Migration ihre spezifische Position innerhalb des Cortex einnehmen. Der korrekte Erwerb der axonalen Morphologie und die Spezifizierung des Dendritenbaums bilden die Grundlage für die Etablierung der kortikalen Konnektivität. Diese morphologischen Merkmale werden durch intrinsische genetische Programme der postmitotischen Differenzierung kodiert sowie durch entwicklungsbedingte Einflüsse im extrazellulären Milieu reguliert.
Das im endoplasmatischen Retikulum lokalisierte Inositol-Requiring Enzyme 1α (Ire1α) ist einer der Hauptregulatoren der entfalteten Proteinantwort. In dieser Studie zeigen wir, dass Ire1α für die Spezifizierung der Neurone der oberen Cortexschichten sowie den Erwerb der neuronalen Morphologie von zentraler Bedeutung ist, indem es mRNA-Translationsraten reguliert.
Diese Arbeit zeigt auch, dass frühe und späte kortikale neuronale Vorläuferzellen sowie früh und spät geborene postmitotische Neurone unterschiedliche Translationsraten aufweisen, was auf differenzierte Anforderungen an die Proteom-Synthesemaschinerie bezüglich der Entwicklung der kortikalen Schichten hinweist.
Störungen in allen Phasen der kortikalen Entwicklung, welche entweder auf Umweltfaktoren oder Genmutationen zurückzuführen sind, können zu einer abweichenden Physiologie der kortikalen Schaltkreise führen. Eine große Anzahl solcher Anomalien kann zu schweren neurologischen Erkrankungen wie Epilepsie oder komplexen Störungen mit Epilepsie wie Rett-Syndrom, Angelman-Syndrom, Mowat-Wilson-Syndrom, Lafora-Krankheit und/oder Kaufman-Okulozerebrofazial-Syndrom führen. Eine der wichtigsten Hypothesen zur Ursache der Epilepsie verbindet die molekulare Pathologie mit Veränderungen des Gleichgewichts zwischen Erregung und Inhibition (E/I) in neuronalen Netzwerken. Nach dieser Hypothese kann ein E/I-Ungleichgewicht unter anderem durch eine veränderte synaptische Stärke einzelner Neurone innerhalb des Netzwerks, eine unterschiedliche Anzahl erregender oder hemmender Neurone, Anomalien in der neuronalen Morphologie oder die Anzahl bestimmter neuronaler Subtypen verursacht werden. Um das Spektrum der zugrundeliegenden molekularen und zellulären Prozesse der Epilepsie zu erweitern, haben wir die ENU-Mutagenese bei Mäusen eingesetzt, um neue Mutationen, die mit der Krankheit in Verbindung stehen, zu untersuchen. Diese Modelle erlauben es

uns die molekularen und zellulären Grundlagen der Krankheit näher zu charakterisieren.

3. Introduction

3.1. Cerebral cortex development

Uninterrupted establishment of the neocortex and evolutionary expansion of upper layers are the biological substrates of higher cognitive capabilities of humans (Rakic P., 2009). The mammalian cerebral cortex displays a highly organized structure composed of six layers of defined excitatory and inhibitory neuronal subpopulations (Lodato S. and Arlotta P., 2015). The cortical layers display their own cytoarchitecture and transcriptomic signatures of single neurons comprising each layer (Fishell G. and Hanashima C., 2008). Tightly orchestrated timing and localization of proliferation of progenitors determine the fate identity, laminar positioning, morphology and connectivity of a single neuron in the cerebral cortex (Guarnieri F.C. et al., 2018). Each cortical layer comprises radially organized units of pyramidal projection neurons with distinct physiological properties and extrinsic connectivity and local circuit interneurons (Schubert D. et al., 2007; Staiger J.F. et al., 2016). The cerebral cortex mainly consists of two types of neurons: pyramidal and interneurons. Pyramidal neurons or projection neurons originate from the dorsal cortical ventricular zone (VZ) progenitors and are glutamatergic excitatory neurons. Projection neurons account for about 80% of all neurons in the neocortex (Wonders C.P. and Anderson S.A.. 2006). Interneurons originate from progenitors in ventral ganglionic eminence (GE), and they are GABAergic inhibitory neurons (Gorski J.A. et al., 2002; Marín O. and Rubenstein J.L.R., 2003; Wonders C.P. and Anderson S.A., 2006; Dehay C. and Kennedy H., 2007; Gelman D.M. and Marin O., 2010).

3.2. Neurogenesis and migration

The neocortex formation starts in the middle of embryogenesis after the neural tube closure (Dwyer N.D. et al., 2016; Toma K. and Hanashima C., 2015). Most cell types in the cerebral cortex originate from neural stem and progenitor cells, except microglia, which originates from yolk sac erythromyeloid precursors (Ginhoux F. et al., 2010; Hoeffel G. and Ginhoux F., 2015; Ginhoux F. and Guilliams M., 2016). Neurons are generated from neural stem and progenitor cells through a process called neurogenesis (Götz M. and Huttner W.B., 2005; Noctor S.C. et al., 2007; Sun T. and Hevner R.F., 2014). Early during gestation at the beginning of neurogenesis neuroepithelial cells divide symmetrically and later asymmetrically to generate apical radial glia cells (Götz M. and Huttner W.B., 2005; Kriegstein

A. and Alvarez-Buylla A., 2009). In turn, radial glia cells in the ventricular region initially divide symmetrically to increase the pool of radial glial cells (Romero C.D.J. and Borrel V., 2015). Then they switch to asymmetrical mitoses for neuronal production and self-renew, or by indirect neurogenesis and producing various intermediate neuronal progenitors with proliferative activity, thereby enhancing neuronal production (Taverna E. et al., 2014; Cardenas A. and Borrell V., 2019). Intermediate progenitors located in the subventricular zone further divide to generate two postmitotic neurons (Haubensak W. et al., 2004; Miyata T., 2004; Noctor S.C. et al., 2002; Noctor S.C. et al., 2004). Newly born neurons migrate radially toward the pial surface along the radial glia fibers and populate the cortical plate. Neurons of each layer are born in the inside-first outside-last manner (Finlay B.L. and Darlington R.B., 1995; Molyneaux B.J. et al., 2007; He S. et al., 2015; Luzzati F. et al., 2015). In Mus musculus, at embryonic day 12 (E12) progenitors generate neurons that populate deeper cortical layers, whereas upper layer neurons are born later at E14-E15 and move through their younger siblings in deeper layers (Caviness V.S. and Takahashi T., 1995; Desai A.R. and McConnell S.K., 2000; Tarabykin V. et al., 2001; Molyneaux B.J., 2007; Greig L.C. et al., 2013). Pyramidal neurons of different layers exhibit specific transcriptional signatures. Transcription factors are signatures of pyramidal neurons of different layers. Neurons of the deeper layers (layer V-VI) are characterized by the expression of CTIP2 (Chicken ovalbumin upstream promoter Transcription Factor-Interacting Protein 2) and have subcortical projections. Neurons of the upper layers express Satb2 (Special AT-rich sequence-Binding protein) and have intracortical projections, also forming the corpus callosum (Molyneaux B.J. et al., 2007; Britanova O. et al., 2008; Fishell G. and Hanashima C., 2008; DeBoer E.M. et al., 2013). With the course of development, the multipotency of ventricular progenitors is being restricted in the direction of generating exclusively Satb2-positive upper layer neurons. Current models of development suggest that temporal progression of upper and deeper layer neurons differentiation is conserved, but initial ground states are already embedded in their progenitors (Telley L. et al., 2019). During migration, neurons specify their axons and dendrites. Upon migration termination, neurons send axons to their target neurons, establish their dendritic trees, and induce synapses to form complex neuronal network architecture. Axons of earlier born deeper layer neurons form subcortical tracts, later born upper layer neurons establish interhemispheric connections, including the most extensive axonal tract in placental mammals, the corpus callosum (Koester S.E. and O'Leary D.D., 1993; Migliore M. and Shepherd G.M., 2005; Molnár Z. and Cheung A.F.P., 2006; Dehay C. and Kennedy H., 2007; Han W. and Šestan N., 2013). The formation and connectivity of upper layers can be disrupted by genetic deletion of Satb2 and results in the corpus callosum agenesis (Britanova O. et al., 2008).

Prior to migration initiation from their birthplace to their defined position in the cerebral cortical plate, newly born neurons undergo a dramatic change of shape called a multipolar-to-bipolar transition (Cooper J.A., 2014; Boitard M. et al., 2015). The first step of neuronal radial migration is the detachment of the newly born neurons from the progenitor cell in the ventricular zone (VZ). Immature neurons exit the VZ with bipolar or "pin-like" morphology and move to the intermediate zone (IZ) (Tabata H. and Nakajima K., 2003; Hatanaka Y. et al., 2004; Noctor S.C. et al., 2004; Ochiari W. et al., 2007; Cooper J.A., 2014; Namba T. et al., 2014; Bonnefont J. and Vanderhaeghen P., 2021). When these cells enter the IZ of the neocortex, they become multipolar with multiple immature neurite extensions that dynamically extend and retract while their cell bodies move moves at a lower velocity (Kreigstein A.R. and Noctor S.C., 2004; Barnes A.P. and Polleux F., 2009). Then a ventricle-directed process adjacent to the centrosome starts to extend and become the trailing process (TP). In the next step, the neuron reorients the Golgi apparatus and centrosome toward the pia and consecutively establishes a single pia-directed leading process (LP) (Hatanaka Y. et al., 2004; de Anda F.C. et al., 2010; Cooper J.A., 2014). The bipolar cells migrate toward the cortical plate in two modes of radial migration: somal translocation and glia-guided locomotion (Nadarajah B. et al., 2001; Ayala R. et al., 2007; Cooper J.A., 2014; Hirota Y. and Nakajima K., 2017). During further development of pyramidal neurons, the leading process becomes the main shaft of the dendritic tree, and the trailing process extends into a single axon (Cooper J.A., 2013; Lambert de Rouvroil C. and Goffinet A.M., 2001). Previously, we reported that defects in polarity specification observed as multiple trailing processes are associated with loss of bipolar axon-dendrite polarity in developing neurons and the emergence of multiple axons (Ambrozkiewicz M.C. et al., 2018). Many pathways are involved in cell fate acquisition and the establishment of neuronal morphology, but we focused on the translation aspect of these processes in this study.

3.3. The mechanism of eukaryotic translation

It still remains unclear how intra- and extracellular signals that determine neuronal polarity interplay with the determinants of neuronal fate to form the correct architecture of neural networks. Many recent works addressing the cortical cell fate focus mainly on measuring transcription levels, leaving post-transcription as a poorly understood process (Jabadoun D., 2017, Nowakowski T.J. et al., 2017, Telley L. et al., 2019). Previously, it was shown that high-fidelity protein translation is necessary for synaptic transmission in the adult brain (Biever A. et al., 2020; Hafner A.-S. et al., 2019). It is, however, still unknown how spatiotemporal mechanisms of translation rates regulation

overlay transcriptionally primed progenitor states to specify cellular diversity in the neocortex.

Gene expression is a multilevel highly orchestrated process consisting of two main steps: transcription and translation. During transcription, an RNA copy of the DNA sequence of a gene is generated, called the messenger RNA (mRNA). The DNA molecule serves as a matrix for the construction of a complementary strand by RNA polymerases II, which catalyze the formation of pre-mRNA, which is subsequently converted to mature mRNA. The mature mRNA is transported from the nucleus to the cell cytoplasm, where it is used for protein synthesis (Liu S.J. et al., 2016).

The translation is a cyclic process consisting of initiation, elongation, and termination stages. The overwhelming majority of proteins are synthesized in the cytoplasm and only a small number of specialized proteins are synthesized in the mitochondria. Translation initiation is a multistep process in which the 80S ribosome subunit is assembled onto mRNA. This step can be subdivided into two sub-stages: assembly of the 48S complex and coupling this complex to the 60S subunit. At least nine eukaryotic initiation factors (eIF) are involved in the regulation of translation initiation. The small 40S subunit of the ribosome binds to the initiator methionyl-tRNA and to the GTP-eIF2 complex; this binding occurs with the participation of other eIFs (eIF1, eIF1A, eIF3 and eIF5). As a result, a 43S preinitiation complex is formed (Kapur M. et al., 2017). eIF4F translocates the 43S subunit to the 5' cap mRNA. eIF4A unwinds the 5'UTR of mRNA, making this site available for scanning and searching for the starting AUG codon. Once the start codon is recognized, a 48S complex is formed. The 60S subunit of the ribosome is then attached by eIF5B (Jackson R.J. et al., 2010; Hinnebusch A.G., 2014).

Elongation of translation is a highly conservative and less multi-component process than initiation. After initiation, the 80S ribosome has three binding sites: acceptor (A), peptidyl (P) and exit site (E). Initially, the ribosome is positioned on the mRNA so that the start codon is located at the P site, and the next codon is located at the A site and awaits the necessary tRNA. Polypeptide transfer from the tRNA in the P site is performed on the aminoacyl-tRNA in the A site. This addition involves a global rearrangement of the ribosome, rotating the large and small subunits relative to each other to release the A site for the new tRNA. Stable movement of the ribosome along the mRNA requires the participation of eEF2, which promotes the movement of the newly synthesized protein chain from the A site to the P site (Prabhakar J. et al., 2017). As ribosomes translocate on mRNA, they may pause, for example, due to tRNA availability, mRNA structure, protein properties, or changes in the cell's need for specific proteins. Depending on the conditions, the pause can be short-term or permanent (Neubauer C. et al., 2012; Brandman O. and Hegde R.S., 2016).

The cycle of attaching a new amino acid and moving the ribosome repeats until the A site of the ribosome reaches the stop codon (UAA, UAG or UGA), which initiates translation termination. At this point, two release factors (eRF) release the produced polypeptide and promote the dissociation of the ribosome into the 60S and 40S subunits. The 40S subunit remains bound to the mRNA and is released by several factors, including initiation factors (Dever T.E. and Green R., 2012; Jackson R.J. et al., 2012).

3.4. Principles of translation regulation

The translation is a tightly regulated process, mainly at the initiation stage. One of the main pathways of regulation at the initiation stage is phosphorylation of eIF2 by one of the stress kinases, resulting in total inhibition of translation (Barbosa C. et al., 2013). Another regulation pathway is the phosphorylation of eIF4G and eIF4B regulated by mTOR, which enhances protein synthesis and explicitly enhances the translation of proteins involved in cap-dependent translation (León K. et al., 2013). Moreover, mTOR signaling enhances the assembly of the eIF4F complex, which includes eIF4A1. As a result of the enhancement of helicase eIF4A1 activity, some proteins possessing a particular structure of 5'UTR of mRNA can gain an advantage in synthesis (Andreou A. Z. et al., 2019). The low availability of eIF4 in cells, combined with the tight regulation of its activity, leads to the advantage of so-called "eIF4E-sensitive" mRNAs during translation initiation (Mamane Y. et al., 2007).

Moreover, control can be exerted at the elongation stage; for example, a lack of nutrients leads to phosphorylation of eEF2 and a decrease in binding affinity to the ribosome (Carlberg U. et al., 1990). Interestingly, phosphorylation of eEF2 mainly blocks translation, but it has been shown that in neurons an increased level of phosphorylated eEF2 leads to enhanced synthesis of proteins involved in postsynaptic endocytosis (Park S. et al., 2008).

The secondary structures in RNA such as stem-loops and more complex structures that occur on RNA folding, play an essential role in translation regulation. According to the literature, RNA sequences without secondary structures form stable initiation complexes at a higher rate, ensuring more efficient translation (Zhang W. et al., 2006). G-quadruplexes (G4) is an element of RNA secondary structure, formed in RNA regions containing spaced guanine repeats, which fold into square planar structures – G-quartets (Bochman M.L. et al., 2012). G4 structures are mainly represented in the 5’UTR and greatly influence the efficiency of translation (Hinnebusch A.G. et al., 2016). The eIF4A1 factor is required to unwind the secondary structures in 5’UTR (Jackson R.J. et al., 2010). G4s in 5’UTR are involved in the cap-dependent regulation of translation, so the presence of an excessive

number of G4s in this region prevents the initiation of translation (Koromilas A.E. et al., 1992). It was also shown that eIF4A unwinds such secondary structures as R-loops (Rogers G.W. et al., 2001).
The data on mRNA of a specific gene obtained, for example, by single-cell RNA sequencing do not provide the information about the protein that will be translated from this mRNA. Therefore, the study of translation can provide information about the participation of a specific gene in determining the cell fate, morphology establishment, migration, and other aspects. Moreover, the role of translation and its regulation during development is not sufficiently understood, which makes this direction very promising for research.

3.5. Endoplasmic reticulum

The majority of ribosomes during translation are located on the membrane of rough ER, making this organelle a translation hub in the cell. The endoplasmic reticulum is a continuous membrane system that forms a system of flattened sacs in the cytoplasm of eukaryotic cells. All eukaryotic cells have ER, and in animal cells it occupies more than half of the cell membrane content (Rapoport T.A., 2007; Fagone P. and Jackowski S., 2009; Braakman I. and Hebert D.N., 2013; Reid D.W. and Nicchitta C.V., 2015). The ER has many functions, including protein synthesis, folding, modification and transport, lipid and steroid synthesis and calcium storage. Depending on the physical and functional characteristics of the ER, it is divided into two subtypes rough ER and smooth ER (Hebert D.N. et al., 2005; Clapham D.E., 2007; Westrate L.M. et al., 2015; Schwarz D.S. and Blower M.D., 2016).
The rough ER is located next to the cell nucleus, and its membrane forms an integral unit with the outer nuclear membrane. There are ribosomes on the cytosolic surface of the rough ER, which is essential for protein synthesis (Jan C.H. et al., 2014). These ribosomes specialize in synthesizing secreted and integral membrane proteins and a subpopulation of cytosolic proteins (Jan C.H. et al., 2014; Reid D.W. and Nicchitta C.V., 2015). Several proteins including mitochondrial and nuclear proteins are synthesized on free ribosomes not attached to the ER. Translation of integral or secreted proteins begins in the cytosol, followed by docking the mRNA-ribosome complex on the ER membrane. A signal sequence of amino acids achieves recognition at the beginning of the newly synthesized protein, which binds to the signal recognition particle (SPR) (Walter P. and Blobel G., 1981; Walter P. et al., 1981; Metcalf M.G. et al., 2020). The produced mRNA-ribosome-nascent protein-SPR complex binds to ER via the SPR receptor (Gilmore R. et al., 1982; Meyer D.I. et al., 1982; Shan S. et al., 2009). The emerging protein can be co-translationally transferred into the ER through a dynamic complex of membrane proteins called translocon. The translocon is an aqueous pore that cyclically transitions from ribosome-free to ribosome-bound state and also

transitions from protein translocation mode inside the ER to integration mode into the ER membrane (Deshaies R.J. et al., 1991; Johnson A.E. and van Waes M.A., 1999; Rapoport T.A. et al., 2007).
In contrast, the smooth ER is not bound to ribosomes and has other functions, like lipid synthesis (Jacquemyn J. et al., 2017).

3.6. Endoplasmic Reticulum Stress

ER stress is caused by an imbalance between the ER's ability to fold proteins and the cell's requirement for adequately folded proteins, resulting in the accumulation of unfolded proteins in the ER lumen. This imbalance can occur under physiological stress (hypoxia, increased secretory load, glucose deficiency, calcium depletion) or under pathological stress (genome instability, mutated proteins, introduction of cytotoxic compounds) [Walter P. and Ron D., 2011]. Some of these factors occur in oncogenesis during the uncontrolled proliferation of transformed cells, so ER stress is observed during tumor growth and progression (Corazzari M.. et al., 2017). ER stress is also an essential factor in the development of diseases such as diabetes, inflammatory diseases and neurodegeneration (Oakes S.A. and Papa F.R., 2015; Wang M. and Kaufman R.J., 2016). ER stress results in the activation of a conserved signal transduction pathway called unfolded protein response (UPR) [Lin H. et al., 2008; Walter P. and Ron D., 2011].

3.7. Unfolded protein response

The main goal of UPR is to restore homeostasis in the cell, but under long-term and sustained stress induction of cell death takes place. This explains the numerous studies that focus on the relationship between UPR signaling and human diseases in which ER stress is observed (Oakes S.A. and Papa F.R., 2015). UPR is controlled by three stress sensors located on the ER membrane: inositol-requiring enzyme 1α (IRE1α), activating transcription factor 6 (ATF6) and pancreatic endoplasmic reticulum kinase (PERK) [Wang X.Z. et al., 1998; Shen J. et al., 2002; Huang G. et al., 2006]. These transmembrane proteins have a luminal domain that senses ER stress and transmits the signal to the cytosolic effector domain. Under normal physiological conditions, sensor activation is inhibited by the chaperone protein BiP (Binding immunoglobulin protein), which binds to the luminal domain. When a large number of misfolded proteins accumulate in the lumen, BiP dissociation occurs, which makes the luminal domains of the sensors accessible and leads to their activation. Generally, the UPR to eliminate the stress state ether activates the translational response and thereby increases ER capacity, or through translational control mRNA decay reduces the

loading of proteins in the ER (Walter P. and Ron D., 2011). The primary regulator of UPR is IRE1, which was first appeared in the evolution, later followed by PERK and ATF6.

3.8. Inositol-requiring enzyme 1α (IRE1α)

IRE1 is a type I transmembrane protein with a luminal domain and cytosolic serine/threonine kinase and RNase domains. It is present on the ER membrane as a monomer in an inactive state. Its lumenal site is bound by BiP, which exhibits high affinity towards the unfolded proteins, as a chaperone protein. In the presence of misfolded proteins, BiP detaches from Ire1a allowing its oligomerization and auto-phosphorylation through the cytoplasmic kinase domain. The cytoplasmic domain has a dual function and exhibits both kinase and endoribonuclease activity. The primary manifestation of RNase activity of IRE1 is unconventional splicing of XBP1 resulting in the formation of the transcriptionally active form XBP1s (spliced) [Aragón T. et al., 2009; Korennykh A.V. et al., 2009]. The active transcription factor translocates into the nucleus and regulates the expression of genes such as ER chaperones, genes responsible for protein transport and genes involved in the ER-associated protein degradation program (ERAD). During ERAD, misfolded proteins are removed from the ER into the cytoplasm, where they undergo proteasomal degradation. This is the canonical pathway for the regulation of UPR by IRE1 (Corazzari M. et al., 2017). On the other hand, IRE1 conducts UPR through regulated IRE1-dependent decay (RIDD). IRE1 reduces the number of proteins entering the ER lumen through the degradation of mRNAs localized near the ER membrane (Coelho D.S. and Domingos P.M., 2014). Furthermore, the proapoptotic pathway of IRE1 signaling has been shown to occur via c-Jun N-terminal kinase (JNK) activation. IRE1 binds to TNF receptor-associated factor 2 (TRAF2) that activates apoptosis signal-regulating kinase 1 (ASK1), which in turn activates JUN N-terminal kinase (JNK). Therefore, activation of JNK by the IRE1/TRAF2/ASK1 complex can lead to cell death in response to ER stress (Urano F. et al., 2000; Nishitoh H. et al., 2002). Recent advances in the study of UPR processes have shown their role in synaptic signaling and neuronal physiology (Martínez G. et al., 2016).

3.9. Excitation/Inhibition (E/I) imbalance and Epilepsy

The brain consists of neuronal circuits, the correct functioning of which enables a wide range of adaptive and dynamic behavior (Kramer M.A. and Cash S.S., 2012). Time-limited and undisrupted development of the cerebral cortex involving such aspects as cell fate acquisition, formation of proper

neuronal morphology, and neuronal migration is the basis of brain connectivity and function. Genetic mutations that lead to changes in neuronal morphology, cell fate acquisition and synaptogenesis can affect elements of this network and engender pathological changes such as epilepsy.

Aberrances in cortical development leading to defects in network formation or E/I imbalance can result from abnormal neuronal proliferation, migration defects of inhibitory and excitatory neurons, altered synaptogenesis and neuronal network formation, and thereby lead to epilepsy in at least 75% of patients (Leventer R.J. et al., 1999; Bozzi Y. et al., 2012; Guerrini R. and Parrini E., 2010; Manzin M.C. and Walsh C.A., 2011). About 40% of intractable or medication-resistant childhood epilepsy cases are caused by developmental cortical malformations (Barkovich A.J. et al., 2012; Guerrini R. and Dobyns W.B., 2014).

One out of every 26 people is diagnosed with epilepsy, making it the world's most severe prominent brain disorder (Sirven J.I., 2015). Despite the development of new antiepileptic drugs, a third of these patients remain refractory to treatment and are diagnosed with drug-resistant epilepsy (Duncan J.S. et al., 2006; Kwan P. et al., 2010; Dalic L. and Cook M.J., 2016; Fattorusso A. et al., 2021). In addition, controlling epilepsy with surgery or medication leads to significant, sometimes debilitating, side effects including dizziness, drowsiness, movement disorders, behavioral disorders, visual side effects, mental slowing, hepatotoxicity, nephrotoxicity, nephrolithiasis, dermatological reactions, metabolic acidosis, hypohydrosis (Kramer M.A. and Cash S.S., 2012, Perucca P. and Gilliam F.G., 2012). The development of epilepsy can be caused by congenital malformations of the central nervous system, head injuries, central nervous system infections, hereditary metabolic conditions, and genetic predisposition (Covan L., 2002). Recently, cortical malformations have been referred to as an etiology of epilepsy, especially in the drug-resistant form of epilepsy (Wyllie E. et al., 1996; Lortie A. et al., 2002; Sisodiya S.M., 2004; Palmini A., 2011; Liu W. et al., 2015).

About 30% of people with epilepsy are resistant to standard therapies and drugs (Dalic L. and Cook M.J., 2016), as there is a multitude of signaling pathways leading to an imbalance in the E/I, whereby decreased or increased inhibition or decreased or increased excitation or combination of these factors induce a hyperexcitable state (Bozzi Y. et al., 2012; Löscher W. et al., 2020). The dysfunction of synaptic receptors and/or their signaling pathways play a crucial role in the E/I disruptions (Badawy R.A.B. et al., 2012; Needs H.I. et al., 2019). It was shown that changes in the level of neurotransmitter receptor proteins (AMPA, kainite, metabolic glutamate, presynaptic cannabinoid and GABA receptors) are involved in the mechanism of E/I imbalance (Paoletti P. et al., 2013; Busquets Garcia A. et al., 2016; Henley J.M. and Wilkinson K.A., 2016; Evans A.J. et al., 2017; Sieghart W. and Savic M.M., 2018; Suh Y.H. et al., 2018).

Recent studies demonstrate an imperative of expansion and reconsideration of the E/I theory with strong developmental contributions. For several epileptic syndromes, mutations in genes that do not affect the regulation of the E/I balance have been found (McTague A. et al., 2016; Shao L.-R. et al., 2019). For example, the mutation in syntaxin-binding protein 1 (STXBP1) leads to severe neurodevelopmental disease with epilepsy, but this mutation does not affect the E/I balance (Suri M. et al., 2017; Kovacevic J. et al., 2018). Other genetic mutations causing epilepsy lack the developmental mechanism to explain the E/I imbalance, for example, Aristaless-related homeobox protein (ARX; Colasante G. et al., 2008), Cyclin-dependent kinase-like 5 (CDKL5; Chen Q. et al., 2010), Protocadherin19 (PCDH19; Pederick D.T. et al., 2016), Phosphatase and tensin homolog (PTEN; Endersby R. and Baker S.J., 2008).

In this work, we used ENU mutagenesis to broaden the scope of genetics of epilepsy and thoroughly analyze the cortical network physiology addressing the E/I balance. We also provided the developmental insights that precede synapse formation but could contribute to disease formation.

4. Materials and methods

4.1. Animals

Colonies of mice for this study have been maintained in the animal facilities of Charité University Hospital and Institute of Neuroscience of Lobachevsky University of Nizhny Novgorod. All animals were housed at 25 ± 3°C with a 12-h light/dark cycle and free access to food and water.

All animal experiments conducted on mice have been performed in compliance with the guidelines for welfare of experimental animals approved by the State Office for Health and Social Affairs, in accordance with the animal welfare guidelines of the Charite University Hospital approved by the Landesamt für Gesundheit und Soziales der Stadt Berlin Council in Berlin, and by the Ethical Committee of The Lobachevsky State University of Nizhny Novgorod for experiments at the Institute of Neuroscience.

4.1.1. Mutagen preparation and injection

The ENU (Sigma) was dissolved by injection 10 ml of 95% ethanol into the commercial bottle. ENU mutagen is sensitive to light, humidity and acidity. The solution of the mutagen was always protected from light with foil paper. One gram of ENU was diluted by adding 90 ml of phosphate/citrate buffer (100 nM sodium phosphate, 50 nM sodium citrate, pH 5.0). The concentration of ENU was determined by spectrophotometry (wavelength 398 nm). The following formula calculated the required volume of ENU for a single injection per animal: 0,001*W+Y/X=Z, where W – animal weight in grams; Y – the required ENU dose in microgram per gram of body weight; X – stock solution concentration in milligrams per milliliter; Z – injection volume in milliliters (Stottman R. and Beier D.R., 2014).

4.1.2. Breeding scheme

In this study, we used a three-generation screen with a backcross stage to obtain recessive mutations (Fig.1). C3H/HeJ males were injected three times intraperitoneally with 60-100 μg/kg body/weight ENU at one-week intervals. After a period of recovery and sterility, when spermatogonial cells repopulate the testes, males were mated with C3H/HeJ females to generate G1 animals (Salinger A.P. and Justice M.J., 2008). G1 males ("founders") were subsequently crossed with C57BL/6 females for obtaining generation 2 (G2). G2 females were crossed with their G1 father to generate G3 animals. These animals were expected to be homozygous for 6.25% of the mutations initially induced in the C3H/HeJ mice.

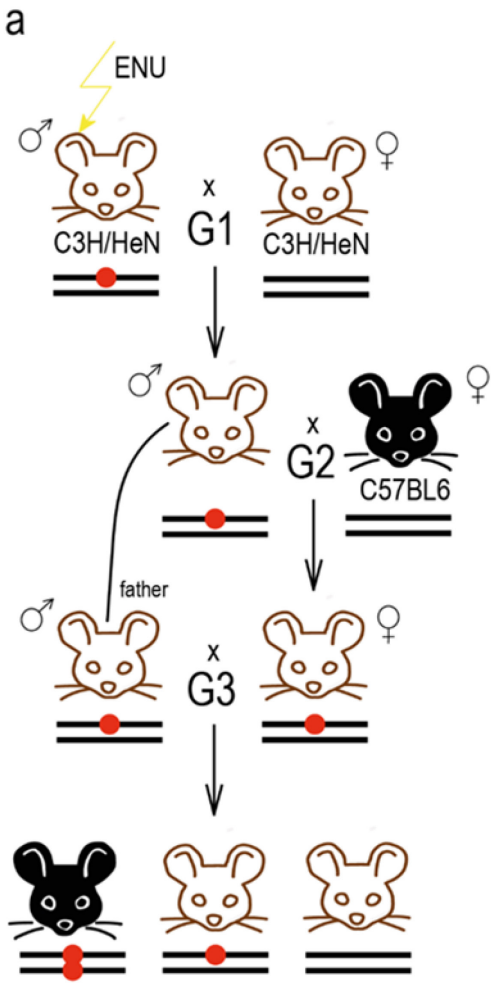

Fig.1. Breeding strategy to identify the recessive genetic mutations after ENU mutagenesis. Red circle depicts the mutation. The mouse strains used are indicated. For details, see text. (adopted from Borisova E. et al., 2021)

4.1.3. DNA isolation from tail biopsies

DNA was extracted from 0,5-1 cm tail cuts using proteinase K digestion and double precipitation (Green M.R. and Sambrook J., 2018). Tissue was lysed at 55°C overnight in 300 µl buffer containing 200 mM NaCl (Carl Roth), 100 mM Tris pH 7,5 (Carl Roth), 200 mM EDTA (Carl Roth), 0.5% SDS (Carl Roth) and 100 µg/ml proteinase K (Carl Roth). Following centrifugation at 13000×g for 10 min the supernatant was mixed with 300 µl 100% isopropanol (Carl Roth). The DNA was pelleted by second centrifugation and washed twice with 300 µl 80% ethanol (Carl Roth). Then steps with isopropanol precipitation of DNA and washing by ethanol were repeated once. After drying at room temperature for 15 min the sample was resuspended in 50 µl dH_20.

4.2. Polymerase Chain Reaction (PCR)

4.2.1. Determination of DNA concentration

DNA concentrations of samples were estimated using a nanophotometer (Implen) by absorption measurement at 260 and 280 nm wavelength. The ratio between these two readings was calculated as a mean of assessing the purity of the sample. Solutions with OD 260nm/OD 280nm ratio within the range 1.8 to 2.0 were treated as pure preparations, relatively free from RNA and protein contaminants.

4.2.2. PCR

The polymerase chain reaction (PCR) is a technique that allows the amplification of a specific DNA sequence (Borisova E. et al., 2021). PCR consists of the following steps: denaturation, annealing and elongation. The first stage of PCR is a denaturation step at about 95°C in order to melt apart the two strands of the DNA template by breaking the hydrogen bonds between complementary bases. After this stage DNA template is accessible for the primers to adhere. The second is an annealing step, and the reaction temperature is lowered to 50-65°, which allows the primers complementary bind to the fragment of template DNA. The third, is an elongation stage at 72°, which enables the polymerase enzyme to synthesize new strands of DNA complementary to the template strands by adding free dNTPs from the reaction mix. This is followed by further cycles of the three temperature phases, resulting in an exponential increase in the number of copies of the amplified DNA fragment.

PCR was performed in tubes or strips cut from a 96-well microtiter plate (ABgene) in a T3 Thermocycler (Biometra) under the following condition:

Step 1: 95°C for 3 minutes

Step 2: 95°C for 30 seconds

Step 3: annealing temperature for 30 seconds

Step 4: 72°C for extension time (1 kb of DNA per 1 minute) (35 cycles Step 2 to 4)

Step 5: 72°C for 5 minutes

Prime STAR GXL DNA polymerase (TaKaRa) was used for cloning applications, GoTaq G2 DNA polymerase (Promega) was used for genotyping, and Taq DNA polymerase (Evrogen) was applied for SNPs mapping PCR.

3.2.3. Agarose gel electrophoresis

PCR products, digested DNA and isolated RNA were subjected to electrophoresis in 1-2% (2% for most PCR amplified products and 1% for fragments over 1kb) agarose (Biozym) gel. Agarose gels were prepared by dissolving 1-2 g of agarose in 100 ml Tris-acetate-EDTA (TAE) buffer using brief heating in a microwave oven. Serva DNA stain G (SERVA) As an intercalating agent was used as an intercalating agent in concentration 1:10000. 20 µl of sample mixed with 1 µl DNA loading Dye (Bioline) and 3 µl of 1 Kb marker (Bioline) were loaded into wells.

Electrophoresis was performed in 1x Tae at 130 volts for the time required to obtain satisfactory separation, judged by eye, typically 35 minutes. DNA bands were visualized under UV light on a transilluminator (Intas) and digitally photographed using INTAS software (Intas science imaging).

TAE buffer: 40 mM Tris Base, 20 mM Acetic Acid, 1 mM EDTA Sodium Salt

4.2.4. 1kb DNA Ladder (Bioline)

It consists of 14 bands ranging from 200 bp to 10037 bp with higher intensity reference bands at 1000 bp and 10037 bp and a doublet band at 1500/1517 bp.

4.2.5. Mutant mouse genotyping

The genotype of mutant mice (control – *Ire1α*$^{f/f}$ and cKO – *Ire1α*$^{f/f}$;*Emx1*$^{Cre/+}$) was determined by PCR with the following conditions:

Ire1α-flox PCR (*Ire1α*-floxed allele) (Iwawaki T. et al., 2009)

Primers (Metabion):

Ire1_WT: CCG AGC CAT GAG AAA CAA GG

Ire1_neo: CCC TGC CAG GAT GGT CAT GG

Reaction mix:

5x buffer (Promega) 4µl

10 mM dNTPs (Invitrogen) 0,4µl

10 nmol/mL Ire1_WT and Ire1_neo primers 0,4µl each

Go-taq polymerase (Promega) 0,2 µl

Distilled deionized H_2O (ddH_2O) 13,6 µl

Template 100-500 ng per reaction

Program:

Step 1 97°C 3 min

Step 2 97°C 15 sec

Step 3 70°C 15 sec

Step 4 66°C 10 sec

Step 5 72°C 2 min 20 sec

Step 6 72°C 5 min

Step 7 12°C store

Steps 2 to 5 are repeated 40 cycles.

The presence of the allele with flox cassette amplified a fragment of 229 bp.

EmxCre PCR (*Emx* allele) (Gorski J.A. et al., 2002)

Primers (Metabion):

CRE159: TCG ATG CAA CGA GTG ATG AG

CRE160: TTC GGC TAT ACG TAA CAG GC

oIMR4170: AAG GTG TGG TTC CAG AAT CG

oIMR4171: CTC TCC ACC AGA AGG CTG AG

Reaction mix:

5x buffer (Promega) 4µl

10 mM dNTPs (Invitrogen) 0,4 µl

10 nmol/mL CRE159, CRE160; oIMR4170 and oIMR4171 primers 0,4µl each

Go-taq polymerase (Promega) 0,2 µl

Distilled deionized H_2O (ddH_2O) 12,8 µl

Template 100-500 ng per reaction

Program:

Step 1 95°C 2 min

Step 2 95°C 10 sec

Step 3 55°C 20 sec

Step 4 72°C 30 sec

Step 5 72°C 2 min

Step 6 12°C store

Steps 2 to 4 are repeated 34 cycles.

In wild-type animals the PCR amplified a fragment of 378 bp, where the presence of *Emx* allele generated a longer fragment of 450 bp.

4.3. *In Utero* electroporation

4.3.1. Glass capillary preparation

Micropipettes for IUE were prepared from 1,5-1,8*100 mm borosilicate glass capillaries (Kimble) using HEKA temperature-controlled pipette puller PIP6. The filament was heated to 1250°C to ensure the appropriate tip diameter. In order to achieve a slow expansion of heated glass the pulling of the glass capillary was controlled manually. Before the operation, the needle tip was cut at approximately a 30° angle using fine forceps to enable liquid flow.

4.3.2. Plasmid DNA for IUE

Plasmid DNA was purified using NucleoBond Xtra Maxi kit (Macherey-Nagel) according to the manufacture's protocol with a final concentration of 2-3 µg/µl. Prior to IUE, DNA was diluted in endotoxin-free water and mixed with 0.1% Fast Green dye (Sigma-Aldrich). The final concentration of DNA used for transfecting cortical progenitors was 500 ng/µl. The plasmids used in this study are listed in the table 1.

Table 1. Recombinant DNA

Plasmid name	Source
pCX::myr-Venus	gift from A. Hadjantonakis
pCAG	gift from J. Miyazaki
pCAGIG	gift from J. Miyazaki

pRaichu205X	gift from M. Matsuda
pCAG-EGFP	Lois et al., 2002
pCAG-flox-Stop-flox-TdTomato	gift from B. Eickholt
pCAG-flox-Stop-flox-EGFP	gift from B. Eickholt
pCAG-EGFPiCre	gift from R. Huganir
pCAG-Cre	gift from S. Parathasarathy
pcDNA3.EGFP-IRE1α	Lipson et al., 2006
pRai-HA-Ire1α	was generated in the laboratory by T. Schaub
pNeuroD-GFP	gift from G. Fishell
pNeuroD-Cre	gift from S. Parathasarathy
pX335-sgRNA-EF(Cas9n)-Eif4a1-R	Ochiai et al., 2020
pX335-sgRNA-EF(Cas9n)-Eif4a1-L	Ochiai et al., 2020
pCAGIG-6XHis-eEF2	was generated in the laboratory by T. Schaub
pCAG-5'UTR-Satb2-EGFP	was generated in the laboratory by T. Schaub
pCAG-5'UTR-CTIP2-EGFP	was generated in the laboratory by T. Schaub
pcDNA4TO-24xGCN4_v4-BFP-24xPP7	Yan et al., 2016
pHR-scFv-GCN4-sfGFP-GB1-NLS	Yan et al., 2016
pHR-tdPP7-3xmCherry	Yan et al., 2016
EGFP-Sec61β	gift from Tom Rapoport
pCAG-Intron-dsRed	gift from H. Fuchs

4.3.3. Preparation for surgery

A surgery was performed by using aseptic procedures. Surgical instruments (hardened fine scissors, Dumond forceps, Ring forceps, Autoclip applier with clips, and needle holder) were sterilized.

4.3.4. Procedure

A timed-pregnant mouse was deeply anesthetized with isoflurane CP (CP-pharma)/ oxygen diffusor, transferred to a warm heating pad, and the nose and mouth were placed within a mask for delivery of isoflurane during surgery. Proper anesthetization was confirmed by observing a loss of the pedal reflex (toe pinch). Eye ointment was applied to prevent the eyes from drying during the procedure (Bepanthen, Bayer). The surgical area was washed with 70% Ethanol and iodine. To ensure intra and post-operative, 3 mg buprenorphine (Temgesic) was administered subcutaneously. In the abdominal cavity, an incision (2 cm or less) was made using fine scissors to expose the entire uterus with embryos. The uterus was taken out carefully by pinching gaps between embryos with ring forceps. During the surgery, the uterus was subsequently moistened with warm (37°C) 0,9% sodium chloride solution (WDT, B|BRAUN) supplied with penicillin 2000 U/mL and 2 mg/mL streptomycin (Gibco). 1-2 µl of the DNA solution was injected into the lateral ventricle of embryonic brain and exhausted by expiratory pressure through a pneumatic PicoPump PV820 (WPI). The forceps-type electrode was applied around the embryo's head accordingly to the targeted brain region. Electric pulses were delivered to the embryo with CUY21EDIT electroporator (Bex Co) with the following settings for electroporation of cortical and hippocampal progenitors: 6 pulses, each of 37 V, each pulse of 50 ms duration with 950 ms interval. After pulsing, the embryo head was thoroughly washed with a warm 0.9% sodium chloride solution with antibiotics (1x Penicillin/Streptomycin). The uterus was placed back into the abdominal cavity. The surgical incision in the peritoneum was closed with surgical sutures with simple interrupted stitches. The skin was closed with 9 mm Autoclips (Clay Adams). The animal was kept on the warm pad until recovery from anesthesia and then placed in the cage with drinking water supplied with tramadol (Tramal) and Butylscopolaminiumbromid (Buscopan) to a final concentration of 1 mg/ml final Tramadol and 12 µg/ml Buscopan. The mouse was monitored after the operation every day until the stage of brain preparation (Saito T., 2006).

4.4. Ex Utero Electroporation

Time pregnant females were sacrificed by a lethal injection of 600 mg/kg bodyweight Pentobarbital i.p. followed by neck dislocation 10 min later. Embryos were isolated via opening of the intraabdominal cavity. Then, the lateral ventricles of embryonic brains were injected with a glass capillary with plasmid DNA with a final concentration of 500 ng/µl. Then the platinum electrodes were positioned on the head, and 6 square pulses of 37 V for 50 ms at 950 ms inter-pulse intervals were delivered. The heads of embryos were isolated and placed in ice-cold HBSS without $MgCl_2$ and $CaCl_2$ (HBSS-/-, Gibco) until proceeding with primary cultures (Eid L. et al., 2018).

4.5. Primary neuron cell culture

For this study, neurons were prepared from E12.5 and E14.5 mouse embryonic cortex, as we described previously (Ambrozkiewicz M.C. et al., 2018). Neurons were seeded in 6-well or 24-well plates on 13 mm glass coverslips prepared with the following steps: coverslips were placed in a falcon tube with 100% ultrapure ethanol overnight while shacking. Then, they were washed with ddH2O three times. Afterward, coverslips were placed in 24-well plates and left to dry under UV light in the hood. One day before cell culture coverslips were coated with 0.008% Laminin (Sigma) and 0,1 mg/ml poly-L-lysine (Sigma) solution at 37°C. Before seeding, coverslips were washed with PBS three times and left to dry under the cell culture hood.

Following solutions were prewarmed in a 37°C water bath: Neurobasal media (Gibco) complete (with 1x B27 (Gibco), 1x Penicillin-Streptomycin (Gibco), 1x Glutamax (Gibco)) and without supplements; 2.5% Trypsin (Gibco); DNase (Roche); FBS (Gibco).

Mouse brains of E12.5 and E14.5 embryos were isolated in ice-cold Hank's Balanced Salt Solution without $MgCl_2$ and $CaCl_2$ (HBSS -/-, Gibco) to collect cortices in ice-cold HBSS with $MgCl_2$ and $CaCl_2$ (HBSS +/+, Gibco). During preparation, the meninges, the basal ganglia and the striatum were removed. The collected tissue was washed three times with HBSS +/+. The tissue was digested by adding 1 ml of 2.5 % trypsin and 200 µl DNase to 5 ml of HBSS +/+ and following incubation for 30 min at 37°C. The reaction was stopped by adding 2 ml of FBS. The tissue was washed three times with 10 ml of Neurobasal media without supplements. Further, the cortices were carefully triturated in 1 ml of Neurobasal media. After this step, cells were counted in the Neubauer counting chamber and plated 60.000-100.000 cells per well (depending on the experiment's goals) in 24-well plates. Cells were cultivated at 37°C in the presence of 5% CO_2.

Neurobasal media (Gibco) complete: 500 mL Neurobasal A (Gibco), 10 mL B-27 (Gibco), 5 mL GlutaMAX (Gibco), 5 mL penicillin/streptomycin (Gibco).

4.6. Nucleofection of primary neurons

After counting in Neubauer counting chamber for some experiments in this study cells were nucleofected according to the manufacturer's protocol (Mouse Neuron Nucleofector Kit and Amaxa 2b Nucleofection system). 1mg of DNA construct was transfected to one million cells. Cells were nucleofected with the O-05 program on the Amaxa 2b Nucleofection system and then plated as described previously (3.4).

4.7. Immunocytochemistry

The details of this procedure are described in our previous publications (Ambrozkiewicz M.C. et al., 2018, 2020). Shortly, neurons cultured on glass coverslips were fixed in 4% PFA 4% sucrose in 1x PBS for 15 minutes at room temperature, washed three times in 1x PBS, and then can be stored at +4°C in 1x PBS with 0.001% Sodium Azide.

The cells on the coverslips were firstly incubated in blocking solution (0.05% TritonX-100 (Roche), 10% horse serum (Gibco) in 1x PBS) for 30 min at room temperature to prevent unspecific binding of the antibody. Further, the coverslips were incubated with primary antibodies dissolved in the blocking solution diluted 1:1 in 1x PBS (according to Table 2) overnight at +4°C in a humid chamber. After incubation, they were washed three times in 1x PBS for 10 min per single wash, followed by incubation with secondary antibody coupled to appropriate fluorophore 1:300 diluted in 1:1 blocking solution with 1x PBS for 2 hours at room temperature. Finally, the unbound secondary antibody was removed by washing three times in 1x PBS (10 minutes each), then briefly rinsed in ddH2O, air-dried and mounted on Superfrost Plus glass slides with Immu-Mount mounting medium (Thermo-Scientific).

4.8. Antibodies

Table 2. Primary antibodies for immunohistochemistry and immunocytochemistry

Recognized protein	Host species	Company	Usage and dilution		Catalog number
			WB	ICC/IHC	
Tau-1	Mouse	Millipore		1:1000	MAB3420
MAP2	Chicken	Novus		1:1000	NB 300-213
GFP	Goat	Rockland		1:1000	600-101-215
GFP	Chicken	Abcam		1:1000	Ab13970
Ki67	Rabbit	Gift from Prim Singh		1:300	
Pax6	Rabbit	Abcam		1:300	Ab22345
Tbr1	Rabbit	Abcam		1:300	Ab31940
Satb2	Rabbit	Generated in-house		1:300	
Satb2	Mouse	SCBT		1:500	sc-81376
Cux1	Rabbit	SCBT		1:300	Sc-13024
CTIP2	Rat	Abcam		1:300	Ab18465
Bcl11b	Rabbit	CST		1:300	12120S
Ire1α	Rabbit	Abcam		1.300	Ab48187
Ire1α	Rabbit	CST	1:500	1:300	3294S
BrdU	Rat	Abcam		1:300	Ab6326-250
Gapdh	Mouse	Hytest	1:10000		5G4-6C5
AnkyrinG	Mouse	Antibodies Incorporated		1:1000	75-146
Sodium Channel Pan	Mouse	Sigma-Aldrich		1:500	S8809
RFP	Rabbit	Abcam		1:500	Ab62341
FoxP2	Rabbit	Abcam		1:300	Ab16046
P-S6 Ribosomal protein	Rabbit	CST	1:1000		2215S
eIF2α	Rabbit	CST	1:1000		9722
eIF2αP^{Ser51}	Rabbit	CST	1:1000		3398T
Xbp1S	Rabbit	CST	1:1000		12782
β-actin	Mouse	Millipore	1:1000		MAB1501R
β-tubulin	Mouse	BioLegend	1:10000		801201
eEF2P^{Thr56}	Mouse	CST	1:1000		2331S
eEF2	Mouse	CST	1:1000		2332S

RFP	Rat	Chromotek		1:1000	5f8-100

Table 3. Secondary antibodies for immunohistochemistry and immunocytochemistry

Recognized IgG	Species	Conjugated substrate/Fluorophore	Company	Dilution	Catalog number
Mouse	Donkey	(H+L)-HRPO	Jackson Immunoresearch	1:10000	715-035-150
Rabbit	Donkey	(H+L)-HRPO	Jackson Immunoresearch	1:10000	211-032-171
Goat	Donkey	AlexaFluor-488	Jackson Immunoresearch	1:300	705-545-003
Rat	Donkey	AlexaFluor-488	Jackson Immunoresearch	1:300	712-545-150
Rabbit	Donkey	AlexaFluor-Cy3	Jackson Immunoresearch	1:300	711-165-152
Rat	Donkey	AlexaFluor-Cy3	Jackson Immunoresearch	1:300	712-165-150
Rat	Donkey	AlexaFluor-647	Jackson Immunoresearch	1:300	712-605-153
Mouse	Donkey	AlexaFluor-Cy3	Jackson Immunoresearch	1:300	715-165-150
Rabbit	Donkey	AlexaFluor-647	Jackson Immunoresearch	1:300	711-605-152
Chicken	Donkey	AlexaFlour-647	Jackson Immunoresearch	1:300	705-605-147

4.9. Fluorescent Noncanonical Amino Acid Tagging (FUNCAT)

The previously published method (Dieck S.T. et al., 2012) was modified in this study to label newly synthesized proteins with a fluorescent mark and characterize translation rates.

Shortly, at indicated developmental timepoints (day in vitro; DIV; DIV1 and DIV5) medium for primary neuronal cell cultures was exchanged with 1 mM HPG-supplemented Methionine-free Neurobasal Medium for the indicated amount of time. After incubation cells were carefully washed with 1x PBS fixed with 4% PFA, 4% sucrose in PBS for 15 minutes. For visualization cells were fluorescently labeled with 1 µM Sulfo-Cyanine5 azide (Lumiprobe). An azide-alkyne binding reaction was performed in "click buffer" (0.2 mM Tris (3-hydroxypropyl-triazolyl methyl) amine (THPTA), 20 mM sodium L ascorbate, 0.2 mM copper (II) sulfate pentahydrate (Sigma) for 20 min at room temperature. Next, following washing with 1x PBS, cells were subjected to immunocytochemistry.

HPG-supplemented Methionine-free Neurobasal Medium: 100 mL Methionine-free Neurobasal Medium (Gibco), 2 mL B-27 (Gibco), 1 mL Glutamax (Gibco), 1mM HPG (Jena Bioscience), 0.4 mM L-Arginine (Cambridge Isotope Laboratories), 0.8 mM L-Lysine (Cambridge Isotope Laboratories).

4.10. Biochemistry

Protein samples for Western Blot were collected by prepping embryonic cortices at different developmental stages (E12.5, E14.5, E16.5, E18.5). Cortices were prepped in ice-cold 1x PBS, snap-froze in liquid nitrogen, and stored at -80ºC.

4.10.1. Protein isolation

Isolation of protein from embryonic cortices was performed on ice. Firstly, 500µl of Chromatin lysis buffer (20mM Tris pH7.5, 350 nM NaCl, 1% TritonX-100 in ddH2O) or E1A (50 mM HEPES (Thermo Fisher), 150 mM NaCl, 0.10% NP40 (Sigma) in ddH2O) with inhibitors cocktail (1mM PMSF, 5mM NaF, 1x NEM (Sigma), 10µM MG132 (Sigma), 10mM β-Glycerophosphate, 1x Protease cocktail Sigma) was added to the samples, and tissue was disrupted by pipetting. The lysates were sonicated briefly with BANDELIN SONOPLUS GM70 Sonicator with three pulses in a 1.5 ml Eppendorf tube. The tubes were spined down for 10 min 13000 rpm at 4ºC.

The supernatant was transferred to a new pre-cold tube and proceeded to protein concentration measurement.

4.10.2. Protein concentration measurement

Protein concentration was measured with a DC Protein-Assay kit (BioRad). The BSA standards (Thermo Scientific) and protein samples were pipetted into a clean microtiter plate (5 µl per well, three replicates per sample). The BSA standards were pipetted with a concentration gradient from a blank sample, 0.25 mg/ml to 2.5 mg/ml. Then 25 µl of reagent A '(20 µl of reagent S to each ml of reagent A) were mixed with samples, followed by pipetting 200 µl of reagent B into each well. The absorbance was measured after 5-10 minutes incubation at room temperature with SpectraMax iD3 (Molecular Devices) at 620 nm wavelength. Protein concentration in the sample was determined based on the absorbance value for BSA standards.

4.10.3. Sodium dodecyl sulfate polyacrylamide gel electrophoresis (SDS-PAGE)

Protein samples were separated and analyzed with SDS Polyacrylamide gel electrophoresis (SDS-PAGE) as described in our previous works (Ambrozkiewicz M.C. et al., 2018, 2020). After protein concentration measurement samples were dissolved in 1x Laemmli buffer (50mM Tris pH 7.5, 10% glycerol, 20% Sodium dodecyl sulfate (SDS), 1M DTT, 2mM EDTA, 2% Bromophenol Blue) according to final concentration. Samples were cooked for 20 min at 70ºC, cooled on ice and stored at -20ºC before use.

The consistency of two-layered acrylamide gel was:

Stacking gel (5%, 9.2 ml):

6 ml ddH_2O

1.8 ml 30% Acrylamide/Bisacrylamide 37.5:1 (Carl Roth)

1.2 ml Tris 1M pH 6.7

138 µl 10% SDS

72 µl 10% Ammonium Persulfate (APS)

12 µl TEMED

Running gel (8%, 10 ml):

4.5 ml ddH_2O

2.7 ml 30% Acrylamide/Bisacrylamide 37.5:1 (Carl Roth)

2.6 ml Tris 1.5M pH 9.1

100 µl 10% SDS

100 µl 10% Ammonium Persulfate (APS)

8 µl TEMED

4.10.4. Western blotting

Samples were loaded in the wells of this gel and subjected to electrophoresis in Running buffer (25mM Tris-HCl, 0.01% SDS, 250mM glycine) at 90 V.

Separated proteins were transferred on a nitrocellulose membrane (GE healthcare) in Transfer buffer (25mM Tris-base, 190mM glycine, 20% methanol) in an ice-cold chamber for 120 minutes at 90 V. After transfer membrane was briefly washed in 1x TBS-T (10mM Tris-HCl, 150mM NaCl pH 7.5, 0.1% Tween-20) and subjected to blocking solution (3% BSA in 1x TBS-T) for 30 minutes at room temperature with shaking. Next, the membrane was incubated in primary antibody dissolved in blocking solution according to Table 2 overnight at +4ºC while shacking. After washing three times in TBS-T (10 minutes each) membrane was incubated in secondary antibody conjugated with horseradish peroxidase (HRP) in 3% BSA in TBS-T for two hours at room temperature on a shaker. After incubation membrane was washed three times with TBS-T for 10 minutes. The protein bands were visualized using ECL western blotting solution (BioRad), and the signal was detected with the chemiluminescence detection system Chemi Doc XRS+ (BioRad). The signal was detected in two exposure time series: short – for total 30 seconds and images were acquired every second and long – usually for 300 seconds and images were taken every 10 seconds (Mahmood T. and Yang P.-C., 2012).

4.11. Perfusion and brain processing

Brains from animals older than P7 were fixed using the intracardiac perfusion with 4% PFA in 1x PBS. Mice were anesthetized by intraperitoneal injection of a lethal dose of Pentobarbital (600 mg/kg body weight). After that, the chest was opened by a crosscut of the rib cage and the diaphragm. The perfusion needle was inserted in the left ventricle, and a small cut was placed in the right atrium. The butterfly needle was connected via tubes with two 20 ml syringes system: first with ice-cold 1x PBS

and second with ice-cold 4% PFA in PBS. First, the blood vessels were washed from the blood by carefully injecting 10-20 ml of 1x PBS into the entire circulatory system. Further, 1x PBS was replaced with 4% PFA (5-10 ml). Microtremors and contractions of the skeletal muscles are signs of correctly performed perfusion. After that brain was isolated from the skull and placed in 4% PFA in 1x PBS for overnight fixation at +4ºC. Next, brains were washed twice with 1x PBS and then passed through a sucrose gradient for cryoprotection (Wu J. et al., 2021).

4.12. Cryosectioning

After fixation in 4% PFA in PBS and washing in 1x PBS, brains were passed through a discontinuous sucrose gradient starting from 10% sucrose and ending in 30% sucrose in PBS to cryoprotect the tissue. The brains were kept in 10% and consecutively 30% sucrose overnight.

For coronal sections with 12-16 µl thickness isolated brains were embedded in OCT (Tissue Tek) block. First, the cerebellum was removed and the brains were washed with OCT compound twice. Next, they were placed on the bottom of a plastic mold filled with OCT and transferred to dry ice to freeze the samples. The block was stored at -80ºC. Brains in the block were cut coronally with a thickness of 12-16 µm using Cryotome (Leica), and sections were collected on Super Frost Plus slides, air-dried for 20 minutes, and stored at -80ºC.

For free-floating sections isolated brains were frozen in a -40ºC isopentane bath (Roth). Coronal sections with a thickness of 50 µm were cut using a Cryotome (Leica) and collected in a 24-well plate filled with 1x PBS with 0.01% Sodium Azide and stored at +4ºC.

4.13. Immunohistochemistry

Before the blocking step, cryo-sections on the slides (16 µm thickness) were washed in 1x PBS to remove the rest of the OCT compound. Dako Pen (Dako) was applied on the borders of the slide to make a hydrophobic barrier and keep the solution in place. Free-floating sections of postnatal animals after P7 before blocking were incubated for 5 min in 1x PBS with 1 mg/ml Sodium Borohydride (Sigma) at room temperature to reduce the background signal and/or autofluorescence. Subsequently, the sections were washed three times in 1x PBS (10 min each). Further steps are the same for all types of sections. Firstly, sections were incubated with blocking solution [10% horse serum (Gibco), 0.05% TritonX-100 (Roche) in 1x PBS] for 30 min at room temperature. Next, sections were incubated with primary antibody and DAPI (Sigma) dissolved in blocking solution accordingly to Table 2

overnight at +4ºC with shacking (for free-floating sections). Further, sections were washed three times in 1x PBS (10 minutes each) and transferred to a blocking solution with a secondary antibody coupled to a fluorophore according to Table 3 for four hours at room temperature. After incubation, sections were washed three times with 1x PBS, placed on the SuperFrost Plus slides (for free-floating sections), air-dried and mounted with ImmoMount medium (Epredia) and a cover glass. The slides were stored at +4ºC in dark boxes to preserve the fluorophores (Ambrozkiewicz M. et al., 2018).

4.14. BrdU injection

Bromodeoxyuridine (BrdU, Sigma) was diluted in PBS to make a sterile solution of 10 mg/mL. Time-pregnant mice were injected intraperitoneally with 100 µg/g body weight (Tarabykin V. et al., 2001).

At P2, the animals were sacrificed (both genotypes: control – *Ire1α*$^{f/f}$ and cKO *Ire1α*$^{f/f}$; *Emx1*$^{Cre/+}$), brains were isolated and fixed in 4% PFA overnight, and then passed through sucrose gradient and frozen in -40°C isopentane (Roth). The brains were cryosectioned with 50µm thickness free-floating, then sections were placed on the Super Frost Plus glass slides and dried overnight at +4°C. Antigen retrieval was achieved by boiling in citrate-based Antigen Unmasking Solution (Vector, pH 6.0) for 10 min in a 750-W microwave oven and following 20 min cooling on ice. Slides were washed briefly in PBS, and then proceeded with immunolabeling according to the protocol.

4.15. Audiogenic epilepsy test

For generation audiogenic stimulation (AGS) in this study was created the system based on the Startle and Fear Conditioning System (PanLab, Stalting) (Borisova E.V. et al., 2018). The system is a transparent plastic chamber (25 cm in each dimension) placed in a soundproof box. A bell and a video camera (Lifecam cinema HD) were installed in the chamber. The test was performed on G3 animals at postnatal days 20-30 (P20-30). First, the animal was placed in the chamber. After one-minute adaptation, a loud acoustic stimulus (4 series of 20 seconds with two-second break between series) or when the animal had seizures. For the assessment of audiogenic response following criteria were used: intensity of seizures (score from 0 to 4), seizure latency (in seconds) and the latent period of motor excitation.

4.16. Tetra-primer ARMS-PCR

In this study, we developed a single nucleotide polymorphism (SNP) panel to identify loci of homozygosity and map the mutation. The panel consists of 114 SNPs (6 SNPs for each of 19 autosomes). Only SNPs that are different between C3H/HeN and C57Bl6 mouse lines were selected. The identification of SNPs was performed using ARMS-PCR. Primers were designed with primer design online software "Primer1" (Ye S. et al., 2001). Genomic DNA was extracted from tail biopsies as described earlier, including the second step of DNA precipitation and purification.

Reaction mix:

5x buffer (Evrogen) 5 µl

10 mM dNTPs (Evrogen) 0,5 µl

10 nmol/mL Outer_FW, Outer_REV, Inner_FW, Inner_REV primers 0,25 µl each

Taq polymerase (Evrogen) 0,25 µl

Distilled deionized H_2O (ddH_2O) 17 µl

Template 100 ng per reaction

Program:

Step 1 95°C 3 min

Step 2 95°C 30 sec

Step 3 55°C 30 sec

Step 4 72°C 40 sec

Step 5 72°C 5 min

Step 6 12°C store

Steps 2 to 4 are repeated 35 cycles

4.17. Expansion microscopy

In order to perform expansion of embryonic brain slices and take a more detailed look at the morphology of GFP-expressing neurons, we performed expansion microscopy according to previously published protocol (Asano S.M. et al., 2018). First, we did immunohistochemistry, but used an increased concentration of goat

anti-GFP antibody (Rockland) at 1:200 and secondary antibody anti-goat Alexa 488 (Jackson Immunoresearch) at 1:100. After incubation with antibody, sections were washed in 1x PBS and subjected to AcX (Thermo Fisher) crosslinker solution (10mg/ml) in 150 mM $NaHCO_3$ (Sigma) overnight at room temperature. Next, sections were washed with PBS and incubated in monomer solution (19% sodium acrylate, 10% acrylamide (Sigma), 0.1% bis-N',' N-methylene-bisacrylamide (Sigma), 0.01% 4-hydro-TEMPO (Sigma) in PBS) for one hour. Further, sections were placed on Super Frost Plus slides with spacers, and monomer solution mixed with 0.2% APS (Applichem), 0.2% TEMED (Sigma) for polymerization was applied on sections and incubated for two hours at 37ºC. The brain sections embedded in the gel were digested in digestion buffer with proteinase K (50 nM Tris-Cl, 800 nM guanidine-Cl, 2 mM $CaCl_2$, 0.5% TritonX-100, pH 8.0) overnight at 37ºC. Subsequently, sections were transferred to a Petri dish filled with ddH_2O to expand, and water was changed at least five times for 48 hours. Sections were measured before and after expansion to identify the expansion factor. Next, sections were carefully placed in the glass-bottom chambers (Ibidi) and imaged with Leica Sp8 confocal microscope.

4.18. Microscopy

For imaging the overview of GFP signal after IUE Leica SL confocal microscope with 20x objective was used.
To acquire images of brain sections and cells from primary neuronal cell cultures to analyze the colocalization with cell fate markers, the morphology of neurons and for quantitative imaging, Leica SL microscope with 40x oil objective and Zeiss Spinning Disk microscope with 40x objective were used.
For imaging the brain sections after expansion, the Leica Sp8 microscope with a 40x objective was used.

4.19. Data analysis

Colocalization with cell type markers was analyzed using Fiji software. Satb2, CTIP2, Cux1-positive electroporated neurons were counted manually using the Cell Counter plugin.

Cell morphology in brain sections and primary neuron cultures were characterized by reconstructing in Fiji of the cell shape with simple neurite tracer, cell counter and Sholl analysis plugins. Axons were defined as neurites with prominent Tau-1 staining and no MAP2 signal. To quantify the number of axons projected from single neuron, the number of cells projecting 0, 1 or multiple axons were counted. The number of primary branches from the soma of the cell and primary branches of the

axon was counted using the Cell Counter plugin. For analysis of the complexity of the dendritic arbor we applied the Sholl analysis plugin with starting radius of 10 nm with a 1 nm interval between Sholl circles on thresholded images using ImageJ software. We quantified the number of crossings with Sholl circles by dendrites of an individual cell. For analysis of cell morphology after IUE in brain slices number of cells projecting a single trailing process (normal morphology) or cells with multiple trailing processes and atypical morphology were quantified. Tracing of representative neurons was performed manually after thresholding of binarized images.

Quantification of neuronal distribution in the cortex was performed with the cell counter plugin (Fiji) with selection of two references the pia and the ventricular zone (the cortical plate [CP] area). All electroporated GFP-positive cells were marked manually with the Cell Counter plugin. The position of a given cell in the CP was visualized using the y-coordinate and presented on a graph as % CP, where 0% is the bottom of the CP / the subplate (SP), and 100% is the pia / the marginal zone (MZ). Every single cell was plotted individually on the graph (Graph Pad Prism).

For HPG signal quantification, we used maximum intensity projection of Z-stack images from the primary cell cultures. The soma of the neuron was manually outlined, and the signal of intensity was measured. Raw integrated densities (the sum of all the pixel intensities in the selected area) of all cells were plotted individually on a graph.

Quantifications of the western blots were performed in Image Lab Software. The bands that represent respective proteins were selected manually and outlined, and the signal of adjusted volume intensity of a band after background subtraction was measured and represented on a graph.

4.20. Statistical analyses

We used Prism Graph Pad software for statistical analyses and tested the distribution of data points using D'Agostino and Pearson normality test. We used a two-tailed unpaired t-test, or one/two-way Anova for data that distributed normally, and Mann-Whitney test to compare two groups of data with not normal distribution, and a Kruskal-Wallis test with Dunn's Multiple comparisons to compare multiple groups. For binomial data sets such as number of axons projected from a single neuron or the percentage of cells with different types of morphology, we used the Chi-square test. For statistical analysis of categorical data (quantification of the cell identity markers, quantification of subcellular distribution of axonal markers) we used Fisher’s test.

5. Essential new results

In this project, we investigated the molecular mechanisms of cell fate decisions in the developing neocortex. One of the most important findings of the work is that Ire1α regulated mRNA translation rate is a process that supervises the fate acquisition and morphology of developing cortical neurons. Neocortical development has been recently thoroughly characterized by substantial works focused on the transcriptome level, where many conclusions about the sources of cellular diversity and the mechanisms of neuronal lineage progression and differentiation are based on mRNA transcription (Nowakowski T.J. et al., 2017; Telley L. et al., 2019; Bandler R.C. et al., 2021; Manno G.L. et al., 2021). It is important to emphasize that in this study, we demonstrate that neuronal diversity in the cerebral cortex is generated as well by translation rate regulation.

Figures of this chapter were adapted from Ambrozkiewicz M.*, Borisova E.* et al., * equal contribution, biorxiv, 2021, https://doi.org/10.1101/2021.06.23.449563.

5.1. Ire1α acts as a regulator of Satb2 expression and specification of axons during cortical development

To identify signaling pathways involved in the specification of neuronal subtypes the method previously developed in our institute for high-throughput screening of small molecule inhibitors involved in the determination of cell fate was used (Ambrozkiewicz M. et al., 2017). This method is based on the *Satb2*$^{Cre/+}$ mouse line in which Cre recombinase is expressed at the *Satb2* locus (Britanova O. et al., 2006). In primary cortical cell culture obtained from *Satb2*$^{Cre/+}$ mouse line was co-expressed Cre-inducible construct loxP-Stop-loxP-tdTomato together with the green fluorescent protein-expressing construct (pCAG-EGFP) for normalization of transfection efficiency (Fig. 2). As a result, all Satb2-negative cells express GFP, and Satb2-positive cells co-express GFP with tdTomato. Then cell sorting was used to quantify the proportion between Satb2-expressing cells (yellow or red) to EGFP-expressing cells (green). Primary cell culture was prepared from E13.5 *Satb2*$^{Cre/+}$ cortices, including apical progenitors (AP) potent to generate upper and deeper layer neurons. Transfected cells were maintained in culture in the presence of 0.2 μM or 1 μM of a control vehicle or an active compound for two days in vitro (DIV2). At DIV2 a library of 450 kinase inhibitors was tested for their ability to change the proportion of Satb2-expressing neurons (Grinshtein N. et al., 2016). The proportion of Satb2-positive neurons in cell cultures was quantified using flow cytometry. Compounds altering Satb2-positive cell numbers revealed candidate molecules at play in the regulation of upper layer neurogenesis. The experiment was conducted by Mateusz Ambrozkiewicz.

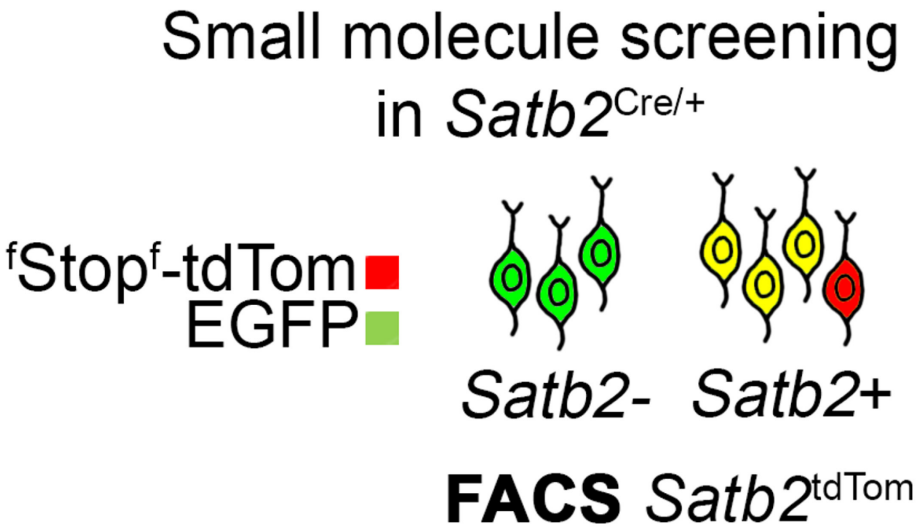

Fig. 2. Screening setup for identification of upstream targets of *Satb2* expression. Primary cell culture was prepared from E13.5 *Satb2*$^{Cre/+}$ cortices. Cells were transfected with Cre-inducible tdTomato together with EGFP expressing constructs. Using FACS, the proportion of Satb2-negative cells (green) and Satb2-positive cells (yellow and red) was determined.

Using this method, APY69 was identified as a strong inhibitor of Satb2 expression in dose-dependent manner (Fig. 3) [0,2μM: DMSO – 1 ± 0,01; Untreated – 0,99 ± 0,003; APY69 – 0,55 ± 0,04; 1μM: DMSO – 1,02 ± 0,04; Untreated – 1 ± 0,02; APY69 – 0,08 ± 0,01]. It was shown that APY69 specifically inhibits Ire1α (Lee K.P.K. et al., 2008). Ire1α is a transmembrane protein located on the endoplasmic reticulum membrane and acts as a key activator of unfolded protein response (Mori K. et al., 1993; Cox J.S. and Walter P., 1996; Adams C.J. et al., 2019). Recently, it has been demonstrated that Ire1α acts as a regulator of cell migration during development and this regulation is independent of the unfolded protein response (Urra H. et al., 2018). Given all these findings, we hypothesized that Ire1α plays a pivotal stress-independent role in the specification of Satb2 identity in the developing neocortex.

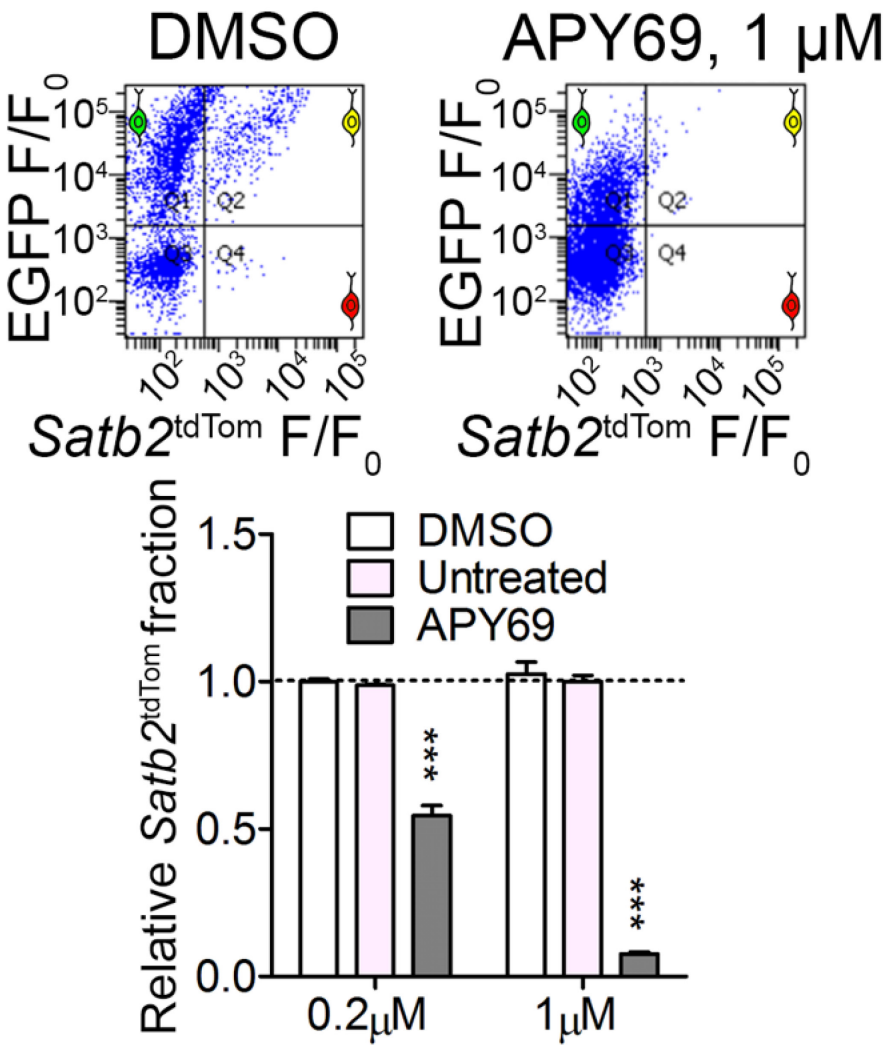

Fig. 3. Kinase inhibitor APY69 is a modulator of Satb2 expression. Top panel: representation of flow cytometry results from DIV2 cortical cell culture treated with kinase inhibitor APY69 and control treated with DMSO. Bottom panel: quantification of the proportion of Satb2tdTom cells using different inhibitor doses. Bar graphs show averages ± S.D. Statistics: one-way ANOVA with Bonferroni post-hoc test. *** p<0,001.

We then used mouse genetics to further validate ours *in vitro* findings. For this purpose, we used a mouse line to delete *Ire1α* conditionally. In this mouse line, a Cre-dependent deletion of exon 20-21 from the *Ire1α* floxed allele leads to the formation of the mutated version of Ire1α protein without the kinase-extension nuclease domain including the RNase active site. In the *Ire1α* cKO mouse line *Ire1α* is conditionally inactivated in the progenitors of dorsal telencephalon using *Emx1*-Cre deleter.

To study the pattern of Ire1α expression at the mRNA level, Fluorescence *in situ* hybridization (FISH) on coronal cortical sections from E12.5, E14.5 and E18.5 was performed by technical assistant Rike Danneberg. Using this method, we demonstrated that Ire1α expresses homogenously throughout the developing cortex (Fig. 4b). Most cells showed perinuclear punctate staining, but at stages E12.5 and E14.5 cells with a diffuse cytoplasmic signal were also detected. In VZ, enlarged fragments shown on insets were observed (Fig. 4b). Using western blotting, we characterized the expression pattern of Ire1α at the protein level. We used cortical lysates from different developmental stages: E12.5, E14, E15.5, E17 and P0 (Fig. 4a). As a loading control we used Gapdh. Using FISH and western blotting, we demonstrated that Ire1α expression is the highest at E12 during development and then downregulated on both protein and mRNA levels. Therefore, it appears most likely that Ire1α is involved in the regulation of Satb2-identity specification at E12 stage.

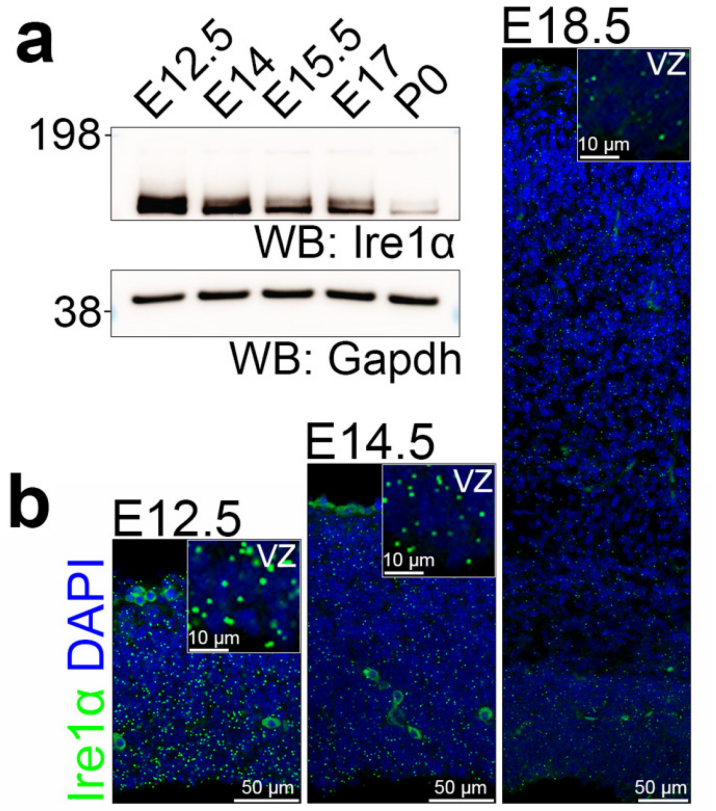

Fig. 4. The pattern of developmental expression of Ire1α. (a) Western blotting in cortical lysates with Ire1α antibodies and Gapdh as a loading control on indicated developmental stages. (b) FISH for Ire1α on E12.5, E14.5 and E18.5 stages. Insets showed enlarged fragments of VZ.

In order to study the effects of Ire1α on aspects of neuronal development, we used the powerful *in utero* electroporation technique (Saito T., 2006). This method allows the delivery of DNA to the neuronal precursors in the ventricular zone and to study developmental aspects such as cell fate determination and formation of bipolar neuronal morphology.

At E12.5, early neuronal progenitors are characterized by multipotency and can give rise to both CTIP2-positive and Satb2-positive neurons, whereas at E14.5 precursors have already limited potency and produce solely Satb2-expressing upper layer neurons.

To inactivate *Ire1α* in early cortical progenitors, we performed IUE in *Ire1α*$^{f/f}$ mice at E12.5 to transfect in control condition EGFP and EGFP together with Cre to induce *Ire1α* KO (Fig. 5). At E16.5 brains were sectioned, coronally and stained for GFP and cell fate markers CTIP2 (deeper layers) and Satb2 (upper layers). We quantified that *Ire1α* KO leads to a loss of upper layer identity in the cortex (Satb2-positive neurons) [EGFP – 81,5 ± 9,12%; EGFPiCre – 52,68 ± 13,63%] at the expense of the identity of the deeper layers (CTIP2-positive neurons) [EGFP – 24,77 ± 14,28%; EGFPiCre – 39,99 ± 10,08%].

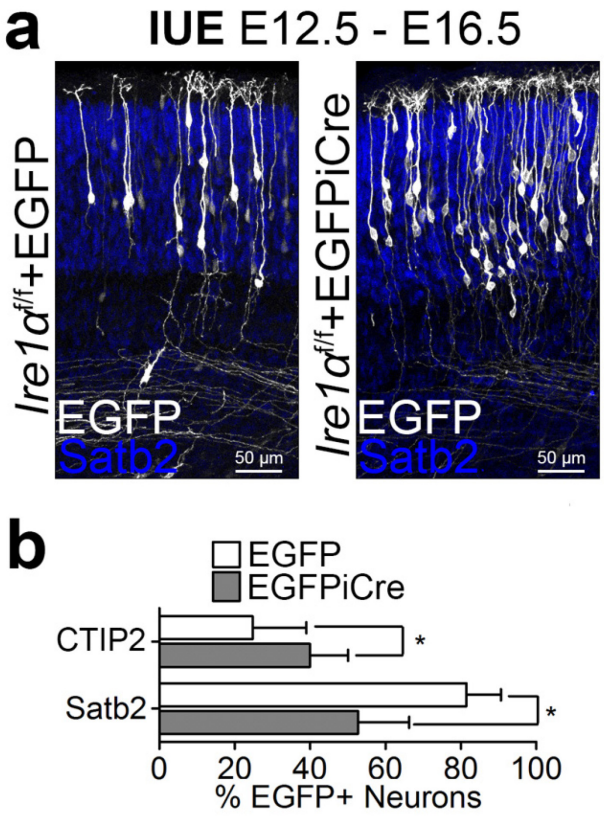

Fig. 5. *Ire1α* loss leads to alterations in the fate of cortical neurons. (a) Representative images of immunostaining of section from E16.5 *Ire1α*$^{f/f}$ brains transfected using IUE with EGFP plasmid and EGFP and Cre plasmids simultaneously. Sections were stained against EGFP and Satb2. (b) Quantification of neuronal fate markers Satb2 and CTIP2. Bar graphs show averages ± S.D. Statistics: D'Agostino-Pearson normality test and unpaired t-test. 0,01<*p<0,05.

On the other hand, using IUE, we overexpressed human ortholog IRE1α in a wild-type E12.5 cortex, immunostained the cortical cryosections for identity markers and analyzed at E18.5 (Fig. 6). Quantification demonstrated that overexpression of IRE1α leads to specification of ultimate neurons of upper layer fate (EGFP – 54,3 ± 12,2%; EGFP+IRE1α – 83,9 ± 13,6%) and almost total absence of CTIP2-positive neurons (EGFP – 43,9 ± 8,9%; EGFP+IRE1α – 1,04 ± 1%). Altogether, these findings indicate the importance of Ire1α for the correct proportion between upper and deeper layer neurons during cortical development.

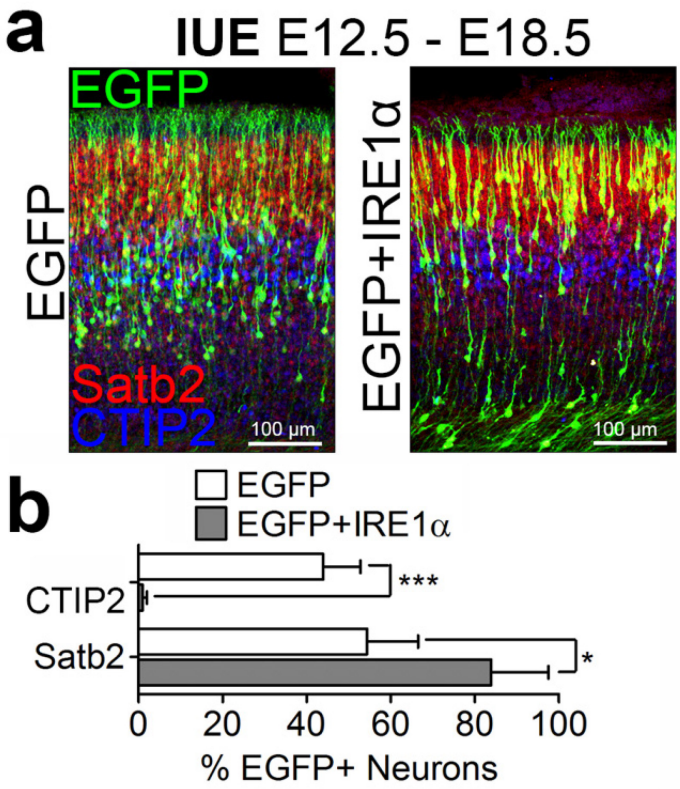

Fig. 6. Overexpression of IRE1α leads to complete KOdeeper layer identity. (a) Representative images of neuronal cell fate markers Satb2 and CTIP2 six days after IUE in wild-type E12.5 embryos with plasmids encoding EGFP and EGFP with human IRE1α simultaneously. (b) Quantification of neuronal identity after IUE. Bar graphs show averages ± S.D. Statistics: D'Agostino-Pearson normality test and unpaired t-test. 0,01<*p<0,05; *** p<0,001.

Additionally, inactivation of *Ire1α* in a defined cell population with the IUE approach showed that loss of *Ire1α* leads to disrupted, highly branched morphology of neurons (Fig. 7). In contrast, the control neurons have a bipolar morphology with a single LP perpendicular to the pia and a single TP, leaving the soma as an axon further in development. These data indicate that Ire1α has an additional role in the formation of polarity during neuronal development.

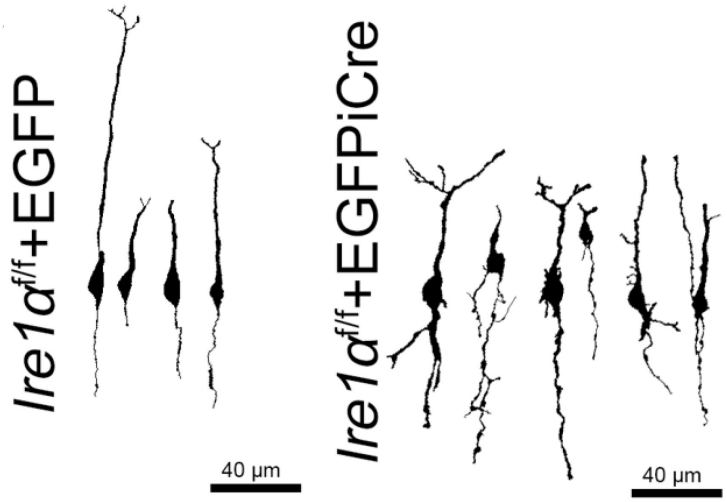

Fig. 7. Representative tracings of EGFP-positive neurons after IUE at E12.5 in *Ire1α*$^{f/f}$ brains with EGFP and EGFP with Cre simultaneously.

In order to test the hypothesis that Ire1α-mediated neuronal fate switch is due to its role in postmitotic cells, we induce *Ire1α* KO specifically in postmitotic neurons. We performed IUE in *Ire1α*$^{f/f}$ mice using EGFP and Cre targeting constructs under *NeuroD1* promoter (Fig. 8a,d). *NeuroD1* promoter is exclusively activated upon cell cycle exit of immature neurons. Expression of *Ire1α* only in postmitotic neurons at E12.5 or E14.5 and quantification of EGFP-positive neurons for Satb2 and CTIP2 markers four days after IUE showed no differences between the two conditions (Fig. 8b,e). These findings indicate that role of Ire1α in neuronal fate acquisition is embedded in progenitors and importance of Ire1α for correct proportion between upper and deeper layer neurons during cortical development (E12.5-E16.5: Satb2 NeuroD1-EGFP – 61,67 ± 2,39%; Satb2 NeuroD1-Cre 63,81 ± 14,82%; CTIP2 NeuroD1-EGFP – 36,01 ± 2,06%; CTIP2 NeuroD1-Cre – 30,79 ± 13,53%; E14.5-E18.5: Satb2 NeuroD1-EGFP – 81,65 ± 9,9%; Satb2 NeuroD1-Cre – 95,06 ± 3,59%; CTIP2 NeuroD1-EGFP – 0,73 ± 1,06%; CTIP2 NeuroD1-Cre – 0,14 ± 0,2%) . Additionally, using the *NeuroD1*-promoter we found analogous changes in neuronal morphology (disrupted, highly branched) with the changes that was observed using CAG-promoter (Fig. 8; E12.5-E16.5: NeuroD1-EGFP – 90,09 ± 1,92% of bipolar

neurons; NeuroD1-Cre – 60,43 ± 7,36%; E14.5-E18.5: NeuroD1-EGFP – 89,58 ± 7,18%; NeuroD1-Cre – 42,37 ± 4,38%) [Fig. 8c,f].

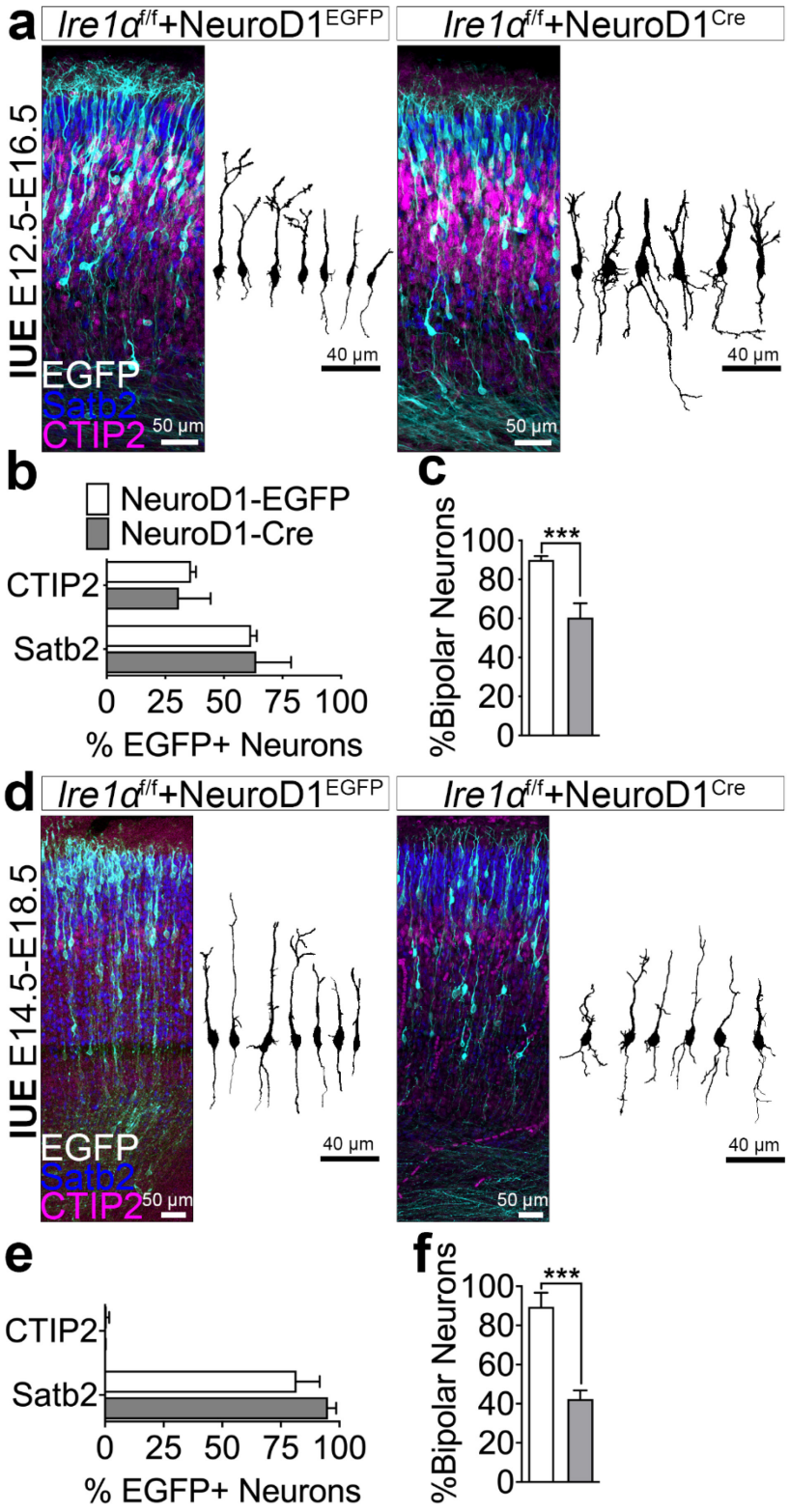

Fig. 8. Ire1α-dependent cell fate acquisition but not the establishment of bipolar neuronal morphology is embedded in progenitors. (a,d) Representative images of immunostained E16.5 (a) and E18.5 (d) brain sections after IUE at E12.5 (a) and

E14.5 (d) with EGFP and Cre under *NeuroD1* promoter. Representative tracings of EGFP-positive neurons. (b,e) Quantifications of neuronal fate identity. (c,f) The proportion of EGFP-positive bipolar neurons. Bar graphs show averages ± S.D. D'Agostino-Pearson normality test and unpaired t-test. *** p<0,001.

The BrdU approach allows us to perform the lineage tracing of progenitors at the given day of birth. We used the BrdU labeling approach to analyze laminar positioning and cell fate of neurons of a given date of birth. 5'-bromo-2'-deoxyuridine (BrdU) is an exogenous cell tracer that applies for monitoring cell proliferation and birth dating. BrdU is a thymidine analog that incorporates into the new DNA chain during the S phase of the cell cycle (Wojtowic J.M. and Kee N., 2006).

Using mouse line with conditional deletion of *Ire1α* (*Ire1α*$^{f/f}$*Emx1*$^{Cre/+}$), we injected intraperitoneally pregnant mice at E12.5 and E14.5 and performed immunostaining and analysis at the stage when neurogenesis is already complete – at P2 (Fig. 9). At P2 coronal brain sections were stained for BrdU, Satb2 and CTIP2 to quantify the proportion of BrdU-positive cells for upper and deeper layers markers.

At P2 stage there were fewer Satb2-positive and more CTIP2-positive neurons among the cells born at E12.5 compared to the control (Satb2 CTR – 78,21 ± 1,37%; Satb2 cKO – 57,84 ± 3,31%; CTIP2 CTR – 48,89 ± 4,91%; CTIP2 cKO – 61,56 ± 8,12%; both CTR – 37,91 ± 1,96%; both cKO – 34,91 ± 1,96%) [Fig. 9a-c], which is consistent with the data obtained before using IUE. Remarkably, at P2 stage we found BrdU-positive CTIP2-positive cells among the cells born at E14.5 in the area of CP closer to the pia (Satb2 CTR – 78,04 ± 5,41%; Satb2 cKO – 72,96 ± 9,27%; CTIP2 CTR – 4,72 ± 2%; CTIP2 cKO – 13,4 ± 4,89%; both CTR – 1,75 ± 0,52%; both cKO – 5,25 ± 3,55) [Fig. 9h]. These results could be explained by a temporary shift in cell fate determination in the case of *Ire1α* loss. Additionally, we noted an alteration in the cortical positioning of the BrdU-positive Satb2-positive neurons; they occupied a lower position in the CP compared to the control neurons. These findings suggest that Ire1α plays a critical role in cell fate determination and the proper ratio between upper and deeper layer neurons during cortical development and this process is distinctly time-limited.

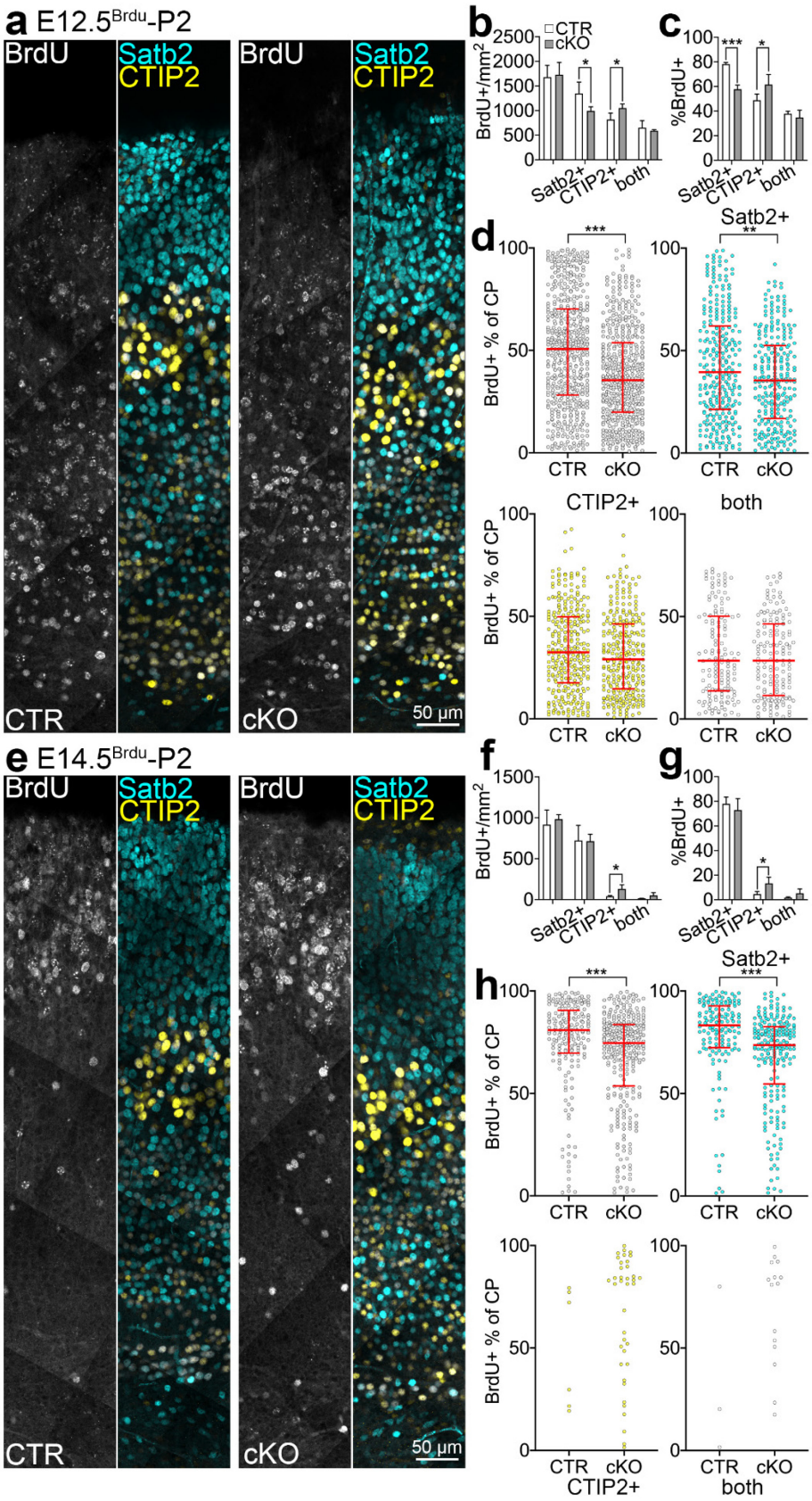
a E12.5Brdu-P2
BrdU
Satb2
CTIP2
CTR
cKO
50 µm
b
CTR
cKO
BrdU+/mm2
Satb2+
CTIP2+
both
c
%BrdU+
d
Satb2+
CTIP2+
both
BrdU+ % of CP
e E14.5Brdu-P2
f
g
h

Fig. 9. Cortical distribution of early and later born Satb2- and CTIP2 -positive neurons in *Ire1α* cKO cortex. (a,e) Representative images of control and *Ire1α* cKO sections after BrdU injection at E12.5 (a) and E14.5 (e) stained with Satb2 and CTIP2 markers. (b,f) Quantification of cell density with corresponding markers: Satb2, CTIP2 or both. (c,g) Quantification of the proportion of neurons expressing an indicated nuclear stain. (d,h) Representation of laminar distribution of neurons stained with indicated marker. 0% CP – bottom of the CP, 100% - pia. (b,c,f,g) Bar graphs show averages ± S.D. (d,h) Line and error bars show median and interquartile range. Statistics: D'Agostino and Pearson normality test, (b,c,f,g) unpaired t-test, (d,h) Mann-Whitney test. 0,01< * p <0,05; 0,001< ** p <0,01; *** p <0,001.

5.2. Ire1α controls axon specification in upper layer neurons during corticogenesis.

Previously, we showed that loss of *Ire1α* leads to alterations in neuronal morphology (Fig. 7 and 8). During cortical development, the correct ratio between upper and deeper layer neurons and the specification of axons is the basis for the formation of proper brain connectivity. Upper layer neurons have been shown to be a model for studying neuronal polarity formation (Barnes A.P. and Polleux F., 2009). In order to study the morphology of upper layer neurons, we performed IUE in the *Ire1α*$^{f/f}$ line at E14.5 using the EGFP-encoding construct or the EGFP- and Cre-encoding constructs simultaneously under the CAG promoter and performed the analysis four days later (Fig. 10). According to the literature, *Ire1α* KO alters the laminar position of upper layer neurons (Urra H. et al., 2008). In the case of *Ire1α* loss, we showed that the neurons have an abnormal cortical positioning and localize in the lower CP (EGFP – 82,1 ± 18,22%; Cre – 76,34 ± 32,48%) [Fig. 10b]. The control neurons are located in the upper part of CP, occupying the upper layers, which is characteristic of the neurons born on E14.5. As predicted, we detected no alterations in the determination of cell fate compared to the control (Satb2 EGFP – 96,91 ± 2,43%; Satb2 Cre – 94,68 ± 4,56%; CTIP2 EGFP – 1,89 ± 3,21%; CTIP2 Cre – 1,23 ± 0,92%) [Fig. 10d]. Additionally, 54% (± SD) of the neurons in *Ire1α* KO were characterized by disrupted highly branched morphology, while the control had only 6% (± SD) of such neurons (Fig. 10c).

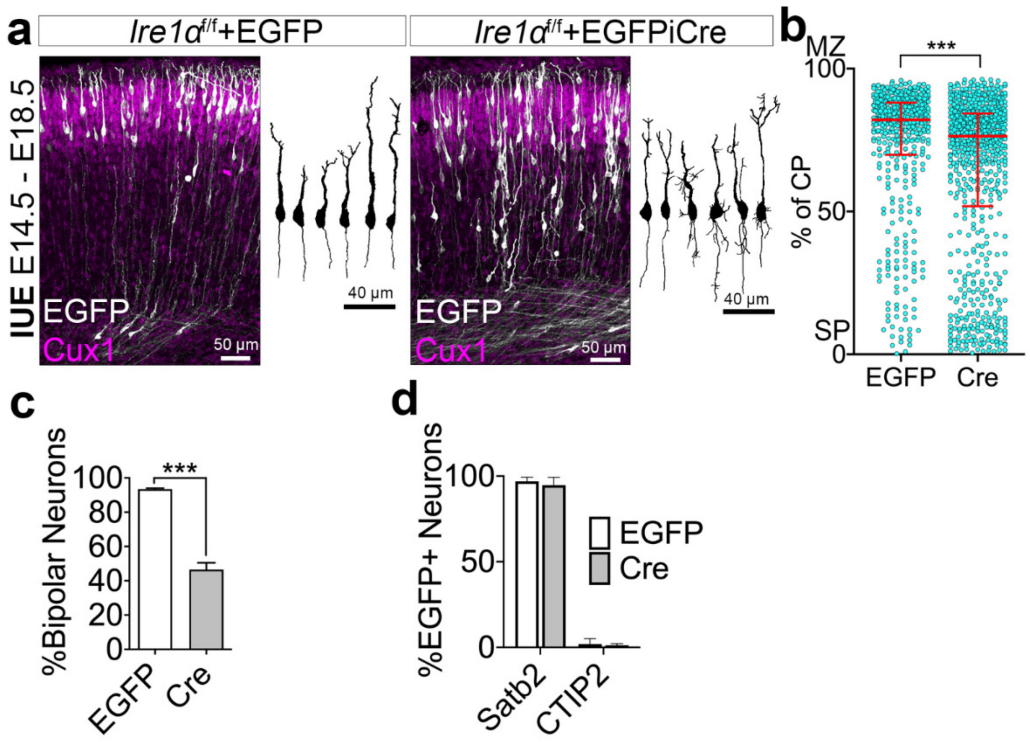

Fig. 10. Ire1α controls cell fate acquisition in upper layer neurons, morphology and laminar positioning. (a) Representative pictures of cortical coronal sections at E18.5 after IUE at E14.5 with EGFP and EGFP and Cre simultaneously. (b) Cortical distribution of EGFP-positive neurons. 0% CP – bottom of the CP, 100% - pia. (c) The proportion of bipolar neurons after IUE from (a). (d) The proportion of cells with corresponding markers. (b) Line and error bars show median and interquartile ranges. (c,d) Bar graphs show averages ± S.D. Statistics: D'Agostino and Pearson normality test, Mann-Whitney test. 0,001< *** p <0,01.

In order to characterize the changes in morphology in more detail, we have taken advantage of expansion microscopy, and we visualized in 3D the role of Ire1α in neuronal morphology establishment (Fig. 11). Expansion microscopy allows physically uniform enlargement of a biological sample by synthesizing a hydrogel over the entire surface of the biological sample and further isotropic expansion, which removes diffraction limitations and allows more detailed examination of features that were not previously discernible (Wassie A.T. et al., 2018). *Ire1α* KO upper layer neurons exhibit multiple trailing processes and many short lamellipodia-like processes originating from the soma. In contrast, wild type neurons exhibit bipolar morphology and lack additional neurites originating from cell soma.

Disruption of bipolar morphology was shown after IUE at both E12.5 and E14.5 stages in Satb2-positive and CTIP2-positive neurons, using constructs under CAG

and NeuroD1 promoters, suggesting that the role of Ire1α in the formation of neuronal morphology is embedded in both neuronal progenitors and postmitotic neurons.

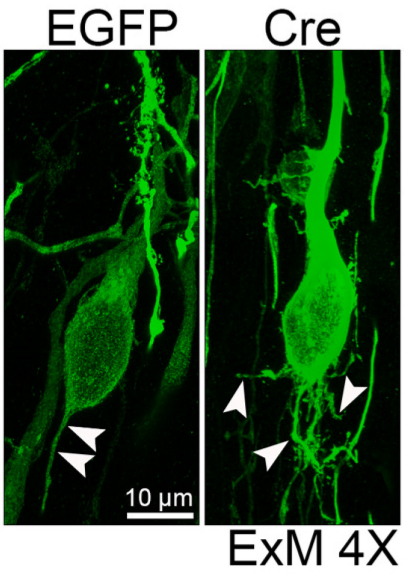

Fig. 11. Ire1α controls the formation of bipolar neuronal morphology. Representative pictures of the coronal section from E18.5 brains after IUE at E14.5 with EGFP or with EGFP and Cre were obtained with expansion microscopy. Sections were stained against EGFP.

Because we observed that *Ire1α* KO neurons are multipolar with multiple trailing processes, that is why we hypothesized that the process of the axon-dendrite specification is affected. In order to study the mechanism of axon-dendrite specification in neurons, we used a cell culture method combined with *ex utero* electroporation. This method allows us to modify gene expression at the stage of neuronal progenitors and use these cells for culturing. According to the literature, *in vitro* neuronal polarization of cortical neurons from stage E14.5 goes through several stages: stage of lamellipodial and filopodial protrusive activity (DIV0); stage of multiple immature neurites (DIV1-2); stage of symmetry break, axon and dendrites specification (DIV2-4); stage of axonal and dendritic outgrowth (DIV4-15); stage of synaptogenesis (DIV15-25) [Polleux F. and Snider W., 2010]. We have previously shown that axon specification occurs in cell culture at the DIV4 stage in our model (Ambrozkiewicz M. et al., 2018).

We transfected neuronal progenitors in the *Ire1α*$^{f/f}$ line at stage E14.5 using EGFP and EGFP with Cre simultaneously using the EUE method, then prepared a primary cortical cell culture and cultivated it till stage DIV4. Control neurons had a single

long neurite at this stage, whereas *Ire1α* KO cells were symmetrical and lacked a single distinct long neurite (Fig. 12).

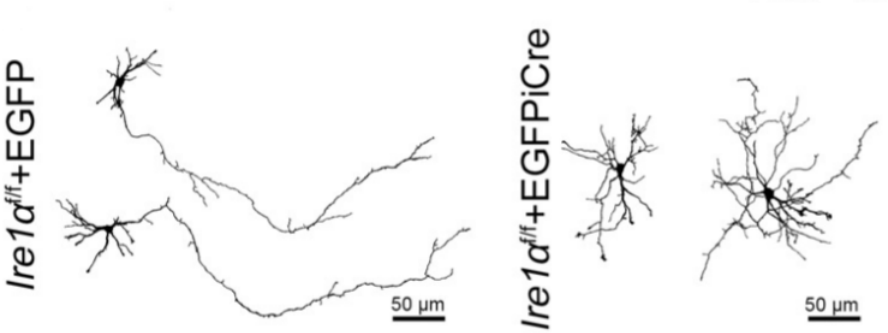

Fig. 12. Representative tracings based on EGFP-signal of DIV4 neurons transfected with EGFP and EGFP with Cre simultaneously.

To differentiate between dendrites and axons, we performed immunocytochemistry using the axonal marker Tau-1 and the dendritic marker MAP2. We assumed a neurite with enriched Tau-1 staining and an absence of MAP2 staining as an axon. The number of axons projected from a single neuron in *Ire1α* KO and control was analyzed (Fig. 13). We demonstrated that a big fraction of *Ire1α* KO neurons projects multiple axons or – interestingly – no specialized axon at all, in contrast with control neurons (EGFP: 0 axons – 4%, one axon – 92%, multiple axons – 4%; Cre: 0 axons – 37%, one axon – 32%, multiple axons – 30%) [Fig. 13b]. In neurons with specialized axons, axon length and the number of primary branches were analyzed (Fig. 13c,d). We demonstrated that axons in *Ire1α* KO are shorter (EGFP – 350,4 ± 206,6; Cre – 106,9 ± 79,58 µm) and more branched in comparison with control (EGFP – 0,066 ± 0,037; Cre – 0,094 ± 0,07 branches/µm). That highlights the essential role of Ire1α in the process of axon specification.

In the next step, we characterized the dendritic tree in *Ire1α* KO and control neurons using Scholl analysis, from which the axon and all its branches were removed; in the case of multiple axons, all axons were removed (Fig. 13e,f). *Ire1α* KO neurons with an axon have the same dendritic tree morphology as control neurons. At the same time, *Ire1α* KO neurons lacking a specialized axon were characterized by a more branched dendritic tree (EGFP – 210,2 ± 68,55; Cre One – 243,8 ± 92,88; Cre No – 427,1 ± 184,5; Cre Multiple – 207,5 ± 53,46 crossing dendrites/neuron). These findings suggest that the lack of *Ire1α* leads to changes in the axonal-dendritic specification of the neurite. In the case of *Ire1α* KO neurons with multiple axons, the formation of redundant axons rather than the replacement of dendrites by axons occurs.

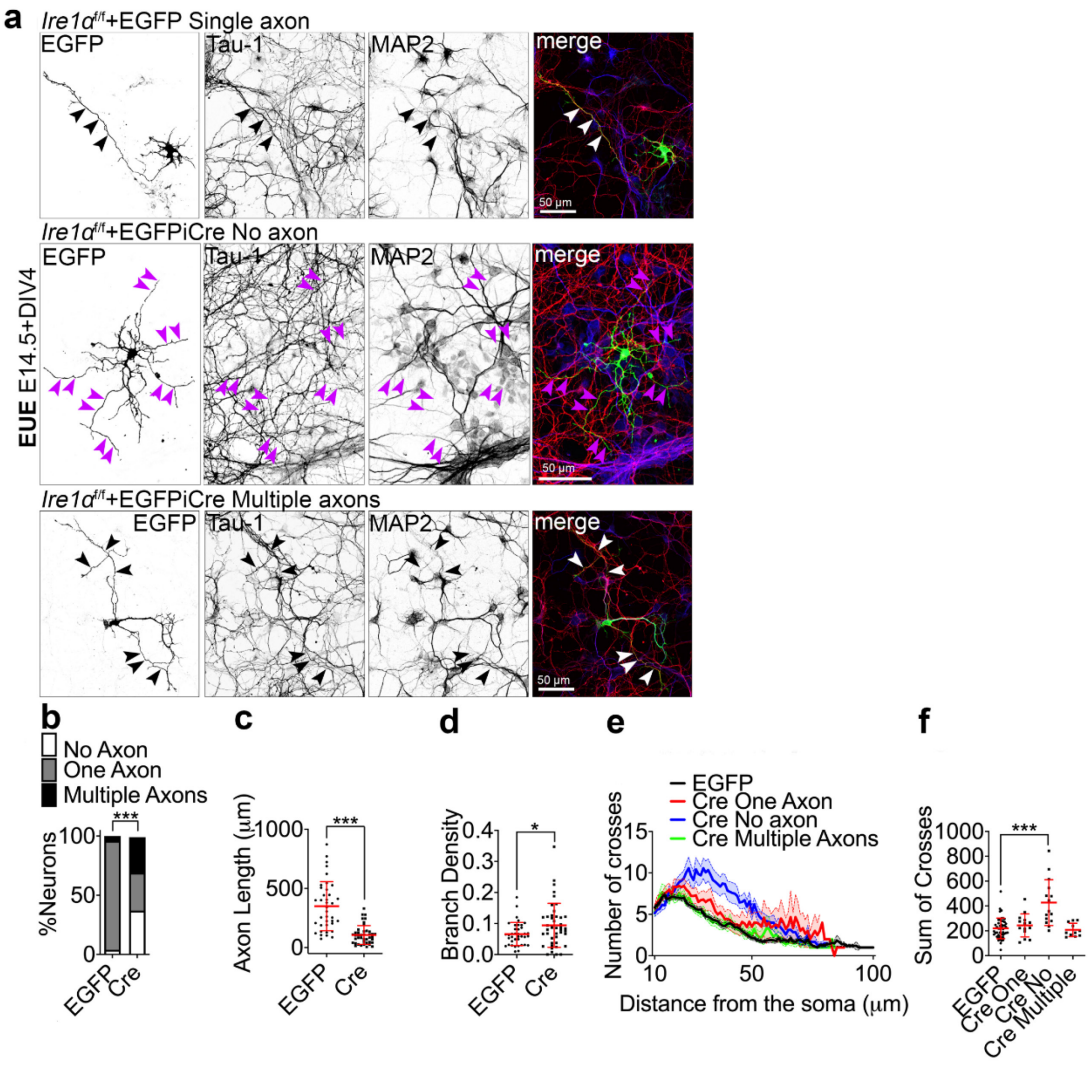

Fig. 13. Ire1α is indispensable for axon specialisation. (a) Representative images of DIV4 cortical cell culture stained with EGFP, axonal marker Tau-1 and dendritic marker Map2. (b) The number of axons projected from a single neuron. (c) The averaged axon length. (d) Axon branch density per µm. (e) Sholl analysis graph in EGFP and Cre expressing neurons with one axon, multiple axons and absence of axons. (f) Averaged sum of crossing dendrites. (c,d,f) Line and error bars indicate average ± S.D. (e) Graphs represent averages ± S.E.M. Statistics: (b) Chi-square test; (c,d) D'Agostino and Pearson normality test, Mann-Whitney test; (f) Kruskal Wallis test with Dunn's multiple comparisons test. 0,01< * p<0,05; *** p <0,001.

The interaction between microtubules and ER has been shown in the literature to be necessary for the formation of neuron polarity. ER is involved in the organization and stabilization of axonal microtubules, and these microtubules, in turn, stabilize ER tubules that enter the axon. Directing the ER tubules into one of the neurites initiates its specification as an axon (Farías G.G. et al., 2019).

Therefore, we decided to characterize the ER status in *Ire1α* KO neurons and compare it with control. We used the EGFP-Sec61β expression vector to nucleofect neurons and visualize ER tubules (Fig. 14). *Ire1α* KO neurons with morphological defects were characterized by somatic ER localization (somatic - 80%; polarized – 20%), in contrast to control neurons, in which ER localization was polar and ER tubules entered the axon (somatic – 20%; polarized – 80%). We can hypothesize that the changes in neuronal polarity in *Ire1α* KO neurons are related to changes in ER.

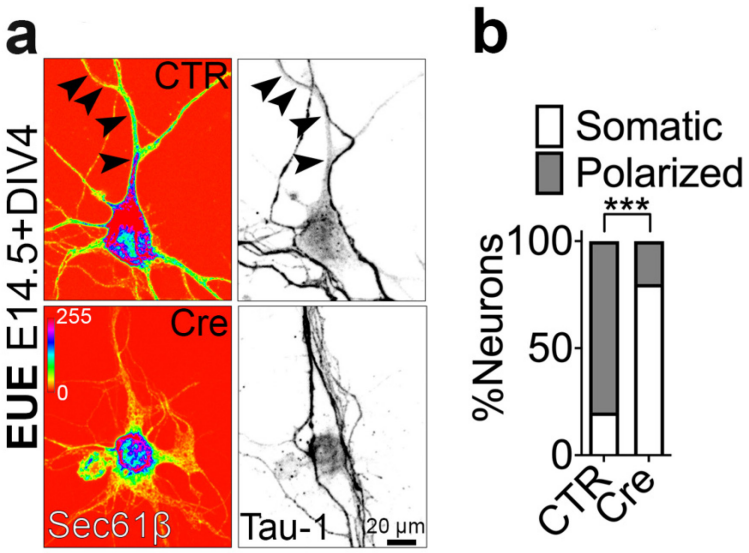

Fig. 14. Mislocalisation of ER in *Ire1α* KO. (a) Representative images of DIV4 control and *Ire1α* KO neurons transfected with EGFP-Sec61β. (b) Quantification of EGFP-Sec61β localization in the cell. Statistics: Fisher's test. *** p <0,001.

Since we detected alterations in axon specification in *Ire1α* KO, we performed immunohistochemical staining of cell culture at DIV6 for axonal markers Tau-1, Ankyrin-G and voltage-gated Na^+ channels (Fig. 15). In control neurons, we observed staining in the initial segments of the axon (AIS). In contrast to *Ire1α* KO neurons, which showed perinuclear somatic localization of these markers (Tau-1: EGFP Neurite – 91%, Soma – 9%; Cre Neurite – 56%, Soma – 44%; Ankyrin-G: EGFP Neurite – 84%, Soma – 16%; Cre Neurite – 59%, Soma – 41%; pan-Na: EGFP Neurite – 92%, Soma – 8%; Cre Neurite – 68%, Soma – 32%).

According to the literature, Ankyrin-G plays a crucial role in AIS formation and maturation. The AIS is the site of electrogeneration in neurons and a large number of voltage-gated Na+ channels are located in this area. The AIS is a critical part of the axon and is involved in action potential generation (Salzer J.L., 2019). Therefore, impaired axon specification in *Ire1α* KO may be associated with impaired AIS formation and maturation.

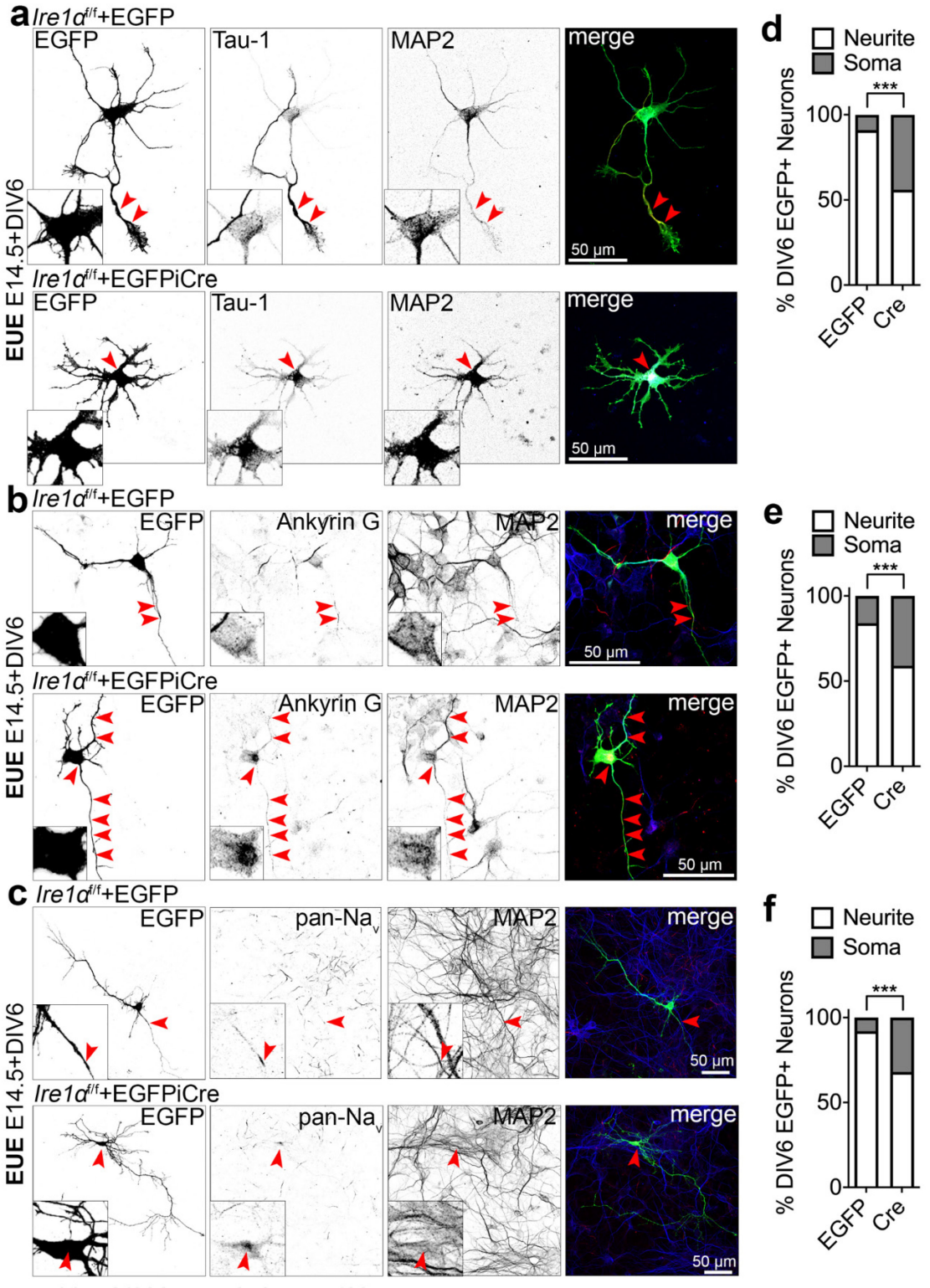

Fig. 15. Ire1α-dependent axon specification is connected with the specification and maturation of AIS. (a,b,c) Representative images of DIV6 neurons after EUE at E14.5 with EGFP or EGFP and Cre simultaneously stained with Tau-1, Ankyrin G,

pan-Na and MAP2. (d,e,f) Quantification of cellular distribution of axonal markers. Red arrowheads indicate enrichment of corresponding markers. Statistics: Fisher's test. *** p <0,001.

We suggested that the morphological alterations found in *Ire1α* KO neurons could cause abnormalities in neurophysiology. To test this hypothesis, our collaborator Marisa Brockmann infected the culture of hippocampal neurons from the *Ire1α*$^{f/f}$ line with lentiviruses encoding EGFP or EGFP and Cre (Fig. 16). Current clamp recordings were subsequently carried out. It was shown that *Ire1α* KO neurons generate more action potentials generated by smaller current injections (Fig.16b). This result could be explained because some *Ire1α* KO neurons have a greater number of AIS, which could entail the generation of action potentials at lower current injections. The overall conductance of *Ire1α* KO neurons is not different from that of control neurons, nor is the membrane integrity compromised (Input resistance: EGFP – 122,3 ± 16,78, Cre – 119,7 ± 15,43 MΩ; Average holding potential: EGFP – 54,87 ± 6,42, Cre – 54,08 ± 7,12 mV) [Fig. 16c,d]. To summarize our discoveries, Ire1α is essential for the formation of a bipolar neuronal morphology. In contrast, loss of *Ire1α* is associated with defects of axonal specification, mislocalization of axonal markers and increased current sensitivity.

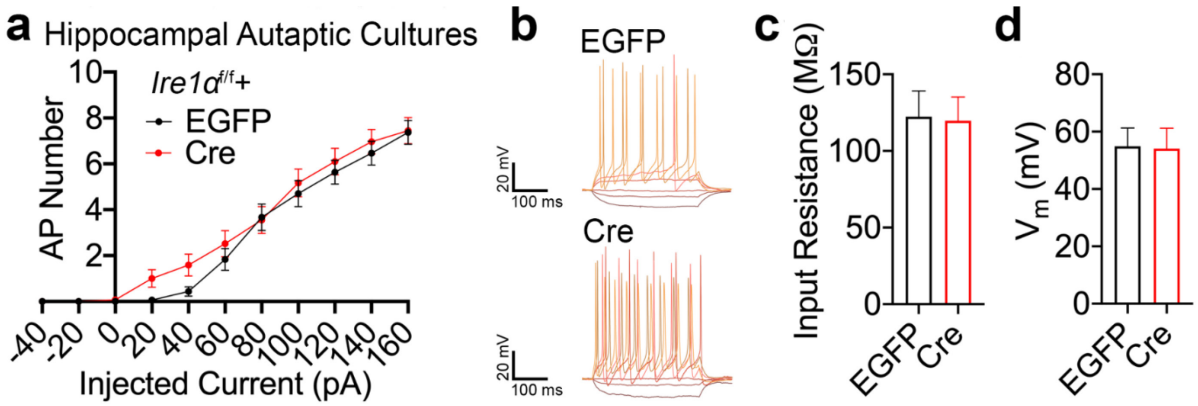

Fig. 16. Loss of *Ire1a* disrupts current sensitivity. Electrophysiological recordings from autaptic hippocampal cultures were obtained from P0 *Ire1α*$^{f/f}$ pups infected with lentiviruses encoding for EGFP or Cre. (a) Quantification of the number of action potentials generated after administration of an increasing amount of current. (b) Representative traces of recordings are described in (a). (c) Average input resistance. (d) Average holding potential. (a) Data points and error bars indicate mean ± S.E.M. (c,d). Bar graphs represent mean ± S.D. Statistics: (d) one-way ANOVA; (c,d) Mann-Whitney test.

5.3. Ire1α regulates cell fate acquisition and bipolar morphology formation by controlling the expression of translation initiation and elongation factors.

It has been shown that activation of Ire1α by cellular stress and unfolded proteins is accompanied by suppression of the overall level of translation (Di Prisco G.V. et al., 2014). Based on these data and previous findings, we hypothesized that Ire1α could regulate the translation of key proteins necessary for cell fate acquisition, axon specification, and neuronal polarity. Together with our collaborator Matthew Kraushar, we compared ribosome profiles in *Ire1α* cKO and wild-type P0 cortexes to test this hypothesis. First, using a sucrose density gradient, active-translating ribosomes (polysomes) were purified *ex vivo* from the cortex of *Ire1α* cKO at stage E18.5. Previously, polysomes have been reported to predominate at the early stages of neocortex development E12.5 – E14 and have a lower steady state from E15 to P0 (Kraushar M.L. et al., 2021). Since it is impractical to collect the required amount of material in early embryogenesis, we settled on stage E18.5. *Ire1α* cKO cortex was characterized by a higher level of actively translated ribosomes (Fig. 17).

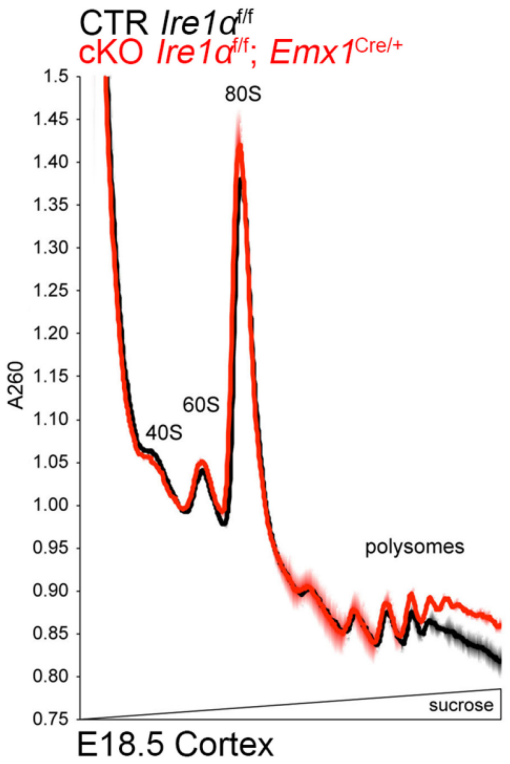

Fig. 17. *Ire1α* loss leads to the accumulation of actively translated ribosomes on mRNA. Analytic density gradient fractionation of A260-normalized E18.5 cortical lysates. The graph represents measuring the relative abundance of ribosomal

subunits 40S and 60S, 80S ribosomes and polysomes. A260 curves indicate mean ± S.D. across replicate fractionations (n = 2, each including 7-8 brains per condition), baseline (1.0) centered at the onset of 40S peak.

Since elevated levels of polysomes were found in *Ire1α* cKO, we hypothesized that ribosomes are stalled on mRNA, which may indicate that some proteins are not being translated in our mutant that is why our next step was to investigate the RNA that is localized in this fraction. We performed bulk RNA sequencing of both total RNA isolated from the cortex in the control and *Ire1α* cKO and individually the polysome fraction. Comparing the entire transcriptome, we found no significant differences between the two conditions (Fig. 18). In *Ire1α* cKO, RNAs associated with polysomes encode ribosomal proteins and proteins involved in translation regulation. We can deduct from this that Ire1α influences the translation of proteins involved in translation regulation and ribosomal assembly. Bioinformatic analyses were conducted by Andrew Newman.

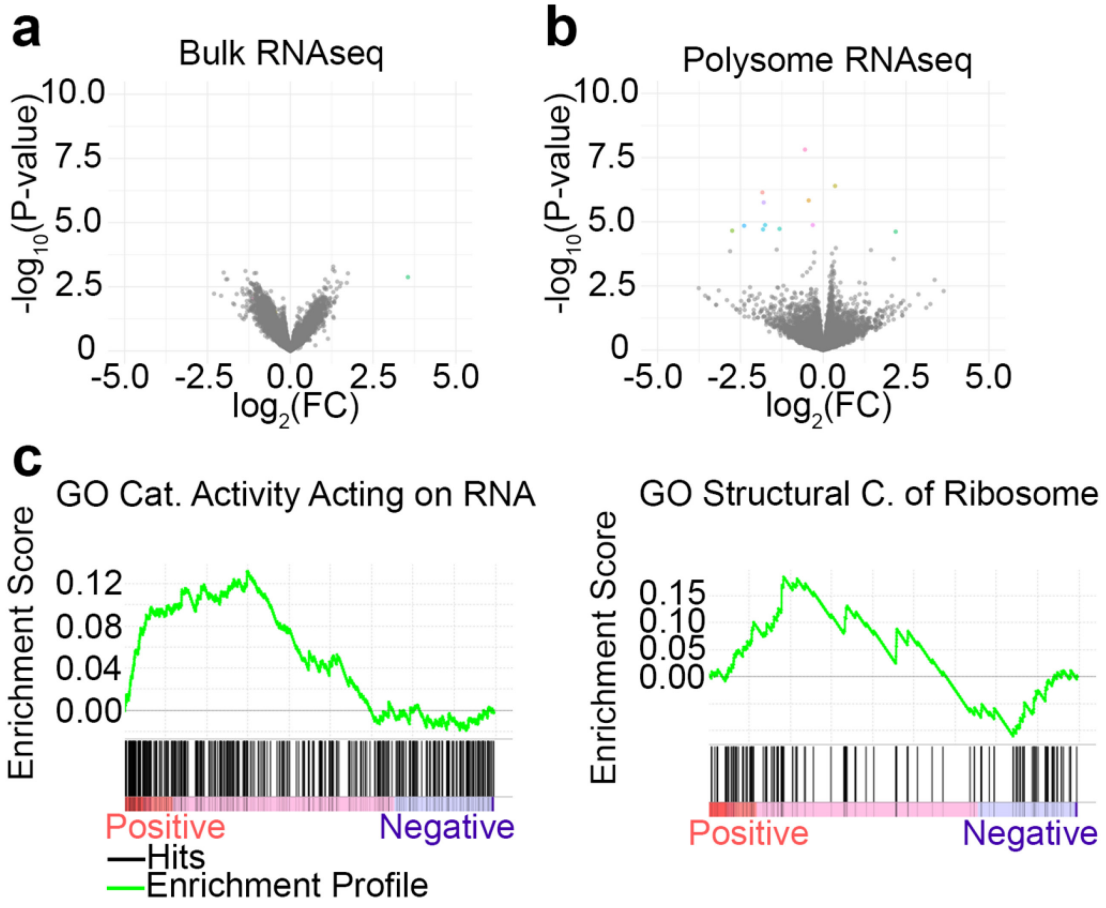

Fig. 18. Ire1α affects the translation of proteins involved in the translation regulation and ribosome assembly. (a) Volcano plot for RNAseq from *Ire1α* cKO bulk tissue. (b) Volcano plot for RNA enriched in polysome fraction. Colored dots indicate significantly regulated genes. FC – fold change. All P-values are Benjamini-Hochburg adjusted p-values. (c) Enrichment plots for control polysome RNA fraction

versus *Ire1α* cKO polysome RNA, Catalytic Activity Acting on RNA and Structural Component of Ribosome.

Since we previously found the ribosome stalling in *Ire1α* KO, we hypothesized that this might be due to changes in the initiation machinery. To characterise the role of translation regulation in corticogenesis the expression levels of the main translation regulators: phosphorylated ribosomal protein S6 (S6-P); Fragile X Mental Retardation Protein (FMRP); translation initiation factors and their phosphorelated forms: eIF2α, eIF2αP^{Ser51}, eIF4A1, eIF4BP^{Ser422}, eIF4E, eIF4G, eIF4G^{Ser1108}, eIF4H; translation elongation factor and its phosphorelated form: eEF-2, eEF-2P^{Thr56} were examined with the help of Rike Danneberg. We performed western blotting of E18.5 cortical lysates from *Ire1α*$^{f/f}$*Emx1*$^{Cre/+}$ (WT and cKO). We detected decreased level of eukaryotic initiation factor 4A1 (eIF4A1) and phosphorylated eukaryotic elongation factor 2 (eEF-2 on Thr56) and increased level of eEF2 (Fig. 19) [eEF-2: CTR – 1 ± 0,47, cKO – 2,5 ± 0,27; eEF-2_P: CTR – 1 ± 0,29, cKO – 0,45 ± 0,16; eIF4A1: CTR – 1 ± 0,33, cKO – 0,52 ± 0,11]. Moreover, no alteration in the levels of other regulators of translation were found (Xbp1S: CTR – 1 ± 0,21, cKO – 0,86 ± 0,28; eIF4H: CTR – 1 ± 0,09, cKO – 0,97 ± 0,06; eIF4G-P: CTR – 1 ± 0,27, cKO – 0,91 ± 0,29; eIF4G: CTR – 1 ± 0,24, cKO – 0,96 ± 0,22; eIF4E: CTR – 1 ± 0,18, cKO – 1,08 ± 0,33; eIF4B-P: CTR – 1 ± 0,13, cKO – 0,82 ± 0,26; eIF2α-P: CTR – 1 ± 0,39, cKO – 1,04 ± 0,38; FMRP: CTR – 1 ± 0,08, cKO – 0,95 ± 0,30; S6-P: CTR – 1 ± 0,15, cKO – 0,94 ± 0,07).

Since the alterations were detected only at the protein level but no changes at the RNA level, we conclude that regulation occurs at the translation level.

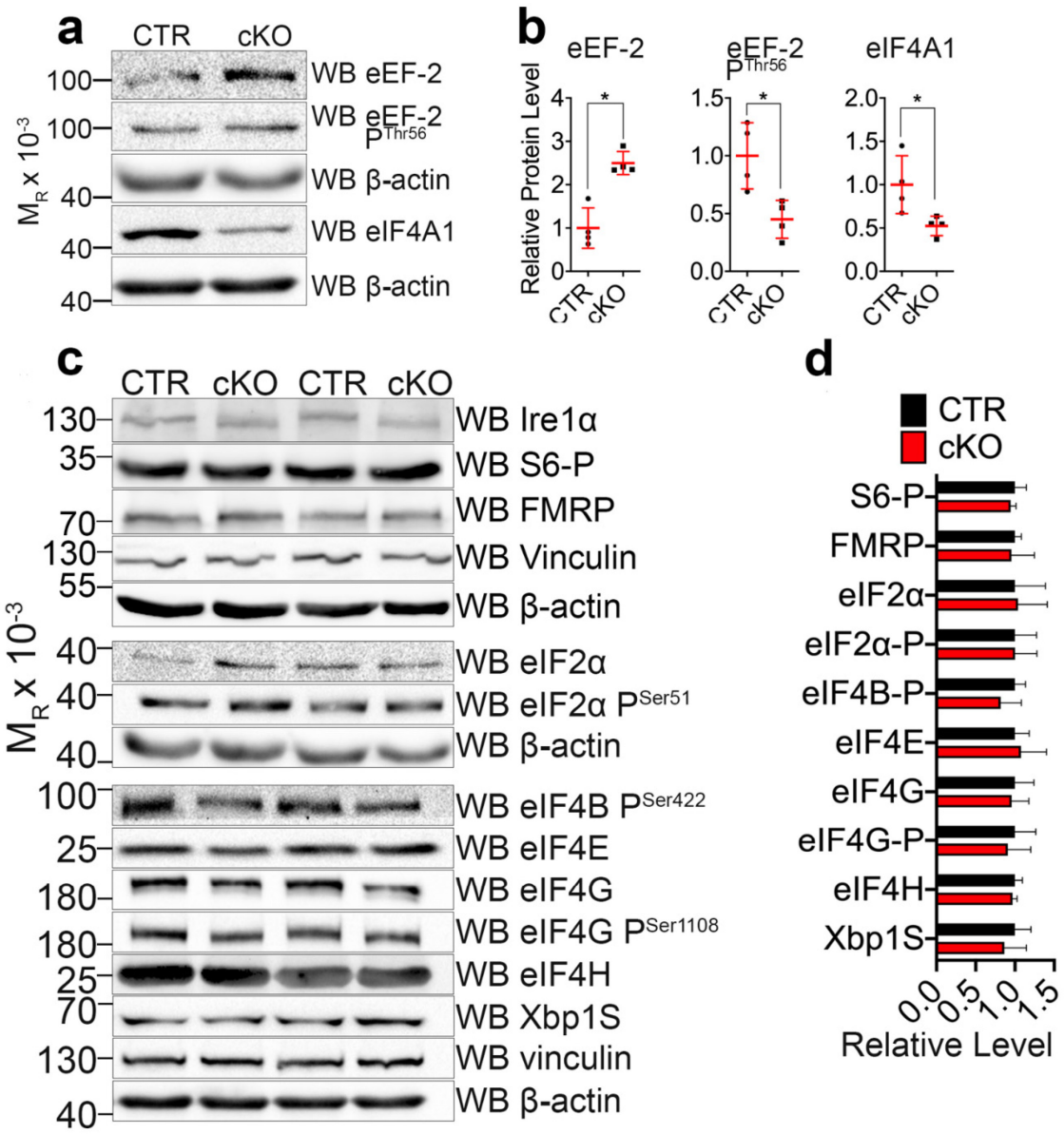

Fig. 19. Ire1α modulates the protein level of translation initiation and elongation factors. (a,c) Representative images of Western blotting results using control and *Ire1α* cKO E18.5 cortical lysates and indicated antibodies. (b,d) Quantification of the expression level of designated proteins normalized to the amount of β-actin in the sample. (b) Line and error bars show mean ± S.D. (d) Bar graphs indicate average ± S.D. Statistics: (b,d) D'Agostino and Pearson normality test, Mann-Whitney test.

Furthermore, no alteration in the level of the spliced isoform of X-box binding protein 1 (Xbp1S), which is produced by unconventional RNA splicing during UPR, indicates a noncanonical role of Ire1α in the regulation of polysome level (Fig. 19c).

To mimic the molecular scenario found in *Ire1α* KO, the constructs for overexpression of eEF-2 and a CRISPR-Cas9 construct for inactivation of *eIF4A1*

were designed. CRISPR-Cas9 technology combines CRISPR-associated (Cas) nuclease and single guide RNA (sgRNA), which consists of a target specific crRNA sequence that is complementary to the targeting DNA and a track DNA that acts as a binding scaffold for the Cas nuclease. The sgRNA targets the nuclease to a specific DNA locus, where the enzyme carries out double-strand breaks (Xiang X. et al., 2021).

These constructs were used for *in vivo* and *in vitro* approaches. First, we transfected wild-type progenitors at E14.5 using EUE method, thereby overexpressing eEF-2, inactivating eIF4A1 or eEF-2 OE and *eIF4A1* KO simultaneously, plated them in cortical cell culture, and then after 4 days we evaluated changes in neuronal morphology (Fig. 20). We showed that in all three conditions there are alterations in neuronal polarity, and found a large percentage of cells with no specialized axons, due to the lack of Tau-1 enrichment in one neurite. The highest percentage of neurons without axons were found in the condition with combination of eEF-2 OE and *eIF4A1* KO (EGFP: 0 axons – 11,1%; single axon – 88,9%; multiple axons – 0%; EGFP+eEF-2 OE: 0 axons – 23,3%; single axon – 74,4%; multiple axons – 2,3%; EGFP+*eIF4A1* KO: 0 axons – 20,0%; single axon – 80,0%; multiple axons – 0,0%; EGFP+eEF-2 OE+*eIF4A1* KO: 0 axons – 36,4%; single axon – 60,0%; multiple axons – 3,6%). The axon length in those cases where it was specialized was measured and we found no statistically significant difference between conditions (EGFP – 134,8 ± 58,69; EGFP+eEF-2 OE – 136,0 ± 56,15; EGFP+*eIF4A1* KO – 155,3 ± 71,25; EGFP+eEF-2+*eIF4A1* KO – 132,2 ± 51,41 μm).

To assess the effect of eEF-2 OE and *eIF4A1* KO on dendritogenesis, we also characterized the complexity of the dendritic tree using Scholl analysis. For this purpose, concentric circles with an initial radius of 7 μm and 1 μm intervals between them were drawn on GFP signal thresholded images of individual neurons. The number of intersections with each of the circles was counted. We showed that all conditions had a similar dendritic tree structure. The total number of intersections with concentric circles was also calculated for an individual neuron and found no differences between the experimental conditions and the control (EGFP – 153,8 ± 112,4; EGFP+eEF-2 OE – 184,0 ± 108,9; EGFP+*eIF4A1* KO – 157,3 ± 96,89; EGFP+eEF-2 OE+*eIF4A1* KO – 160,7 ± 100,1intersections/neuron). Importantly, the combination of *eIF4A1* KO and eEF-2 OE results in the highest proportion of neurons without a specialized axon. The same proportion of neurons without an axon we found in *Ire1α* KO. Therefore, both of these factors are most likely involved in the axon specification pathway and Ire1α-dependent polarity regulation is not linear, but involves several downstream targets.

Therefore, we can conclude that the eEF-2 and eIF4A1 factors are involved in axon specification while not affecting dendrite formation and branching.

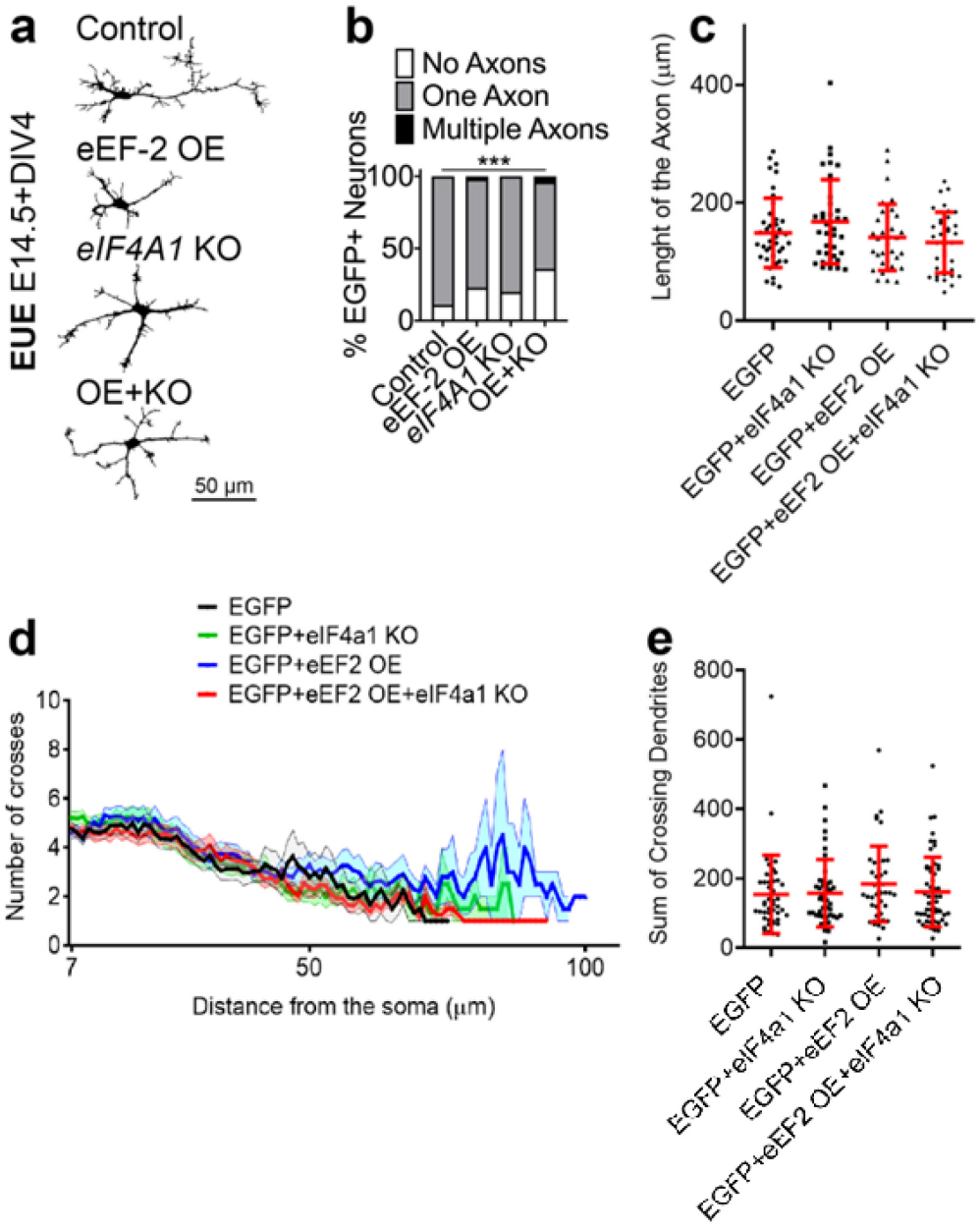

Fig. 20. Translation factors eEF-2 and eIF4A1 affects the axon specification. (a) Representative tracings based on EGFP-signal of DIV4 neurons transfected using EUE with indicated conditions. OE+KO – a simultaneous expression of eEF-2 OE and eIF4A1 KO. (b) The number of axons projected from a single DIV4 neuron after EUE from (a). (c) Averaged length of the axon from the experiment (a). (d) Sholl analysis graph in neurons with corresponding conditions. (e) Averaged sum of crossing dendrites. (c,e) Line and error bars show mean ± S.D. (d) Graphs represent averages ± S.E.M. Statistics: (b) Chi-square test; (c,e) D'Agostino and Pearson normality test, Mann-Whitney test. All conditions were compared to the control. * $p < 0.05$.

In the following step, the expression of eEF-2 and eIF4A1 factors in the cortex at stages E12.5 and E14.5 was characterized by immunohistochemical staining with appropriate antibodies, and Draq5 was used as a nuclear marker (Fig. 21). Both factors were highly and homogeneously expressed at the early stage of E12.5, while expression was reduced at the later stage of E14.5. Therefore, the eEF-2 and eIF4A1 expression patterns are similar to the expression pattern of Ire1α that was shown above.

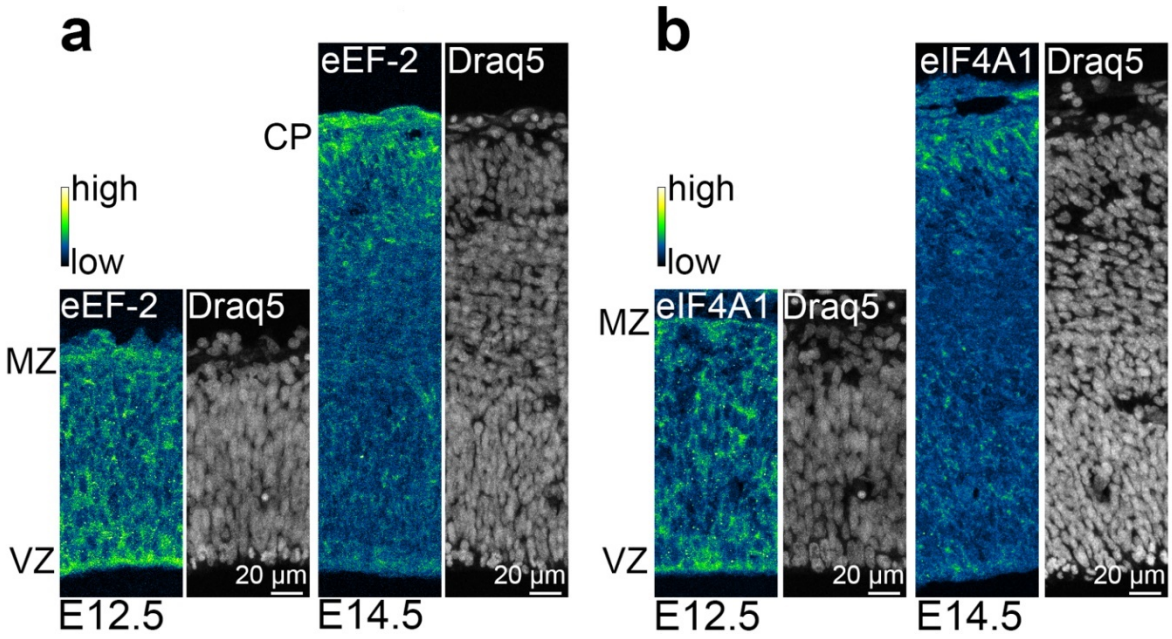

Fig. 21. Expression pattern of eEF-2 and eIF4A1 factors. (a,b) Representative images of E12.5 and E14.5 coronal sections immunostained against eEF-2 (a), eIF4A1 (b) and Draq5 as a nuclear marker. MZ – marginal zone; VZ – ventricular zone; CP – cortical plate.

We next overexpressed eEF-2 together with EGFP in wild-type progenitors at stages E12.5 and E14.5 using IUE and assayed at 18.5 (Fig. 22c,e). Coronal sections at stage E18.5 were stained for GFP to mark all transfected cells and cell fate markers: Satb2 for upper layers and CTIP2 for deeper layers. The percentage of GFP-positive neurons positive for Satb2 or CTIP2 was then counted. There were no alterations in cell fate determination at both stages when eEF-2 was overexpressed compared to controls (E12.5-E18.5: Satb2 CTR – 66,27 ± 5,74%; Satb2 eEF-2 OE – 68,65 ± 14,54%; E14.5-E18.5: Satb2 CTR – 89,31 ± 6,19%; Satb2 eEF-2 OE – 95,02 ± 1,67%; CTIP2 CTR – 0,88 ± 0,96%; CTIP2 eEF-2OE – 0 ± 0%) [Fig. 22b,g]. Further, a laminar positioning analysis of GFP-positive cells was performed and showed a defect in the distribution of cells in the cortex after eEF-2 OE at stage E14.5 (Fig. 22f). Compared to the control at EF-2 OE, more

neurons were located in the SVZ rather than in the upper part of the cortical plate, which would be consistent with our quantification of their fate. A similar phenotype was detected by us earlier in *Ire1α* KO.

We further inactivated *eIF4A1* using the CRISPR-Cas9 system in wild-type progenitors at E12.5 and E14.5 by IUE and analyzed the laminar distribution and cell fate identity at E18.5 (Fig. 22a,e). Loss of *eIF4A1* at stage E12.5 from progenitors with mixed neuronal identity reduced the number of Satb2-expressing neurons by increasing the number of CTIP2-expressing cells, which replicates the phenotype found at the loss of *Ire1α* at the same stage (Satb2 CTR – 49,76 ± 5,25%; *eIF4A1* KO – 30,18 ± 10,15%; CTIP2 CTR – 25,89 ± 9,41%; *eIF4A1* KO – 38,97 ± 7,17%) [Fig. 22b]. Moreover, there were no differences in the fate of neurons when *eIF4A1* was inactivated from the progenitors of upper-layer neurons as compared to the control (Satb2 CTR – 89,31 ± 6,19%; *eIF4A1* KO – 98,41 ± 1,69%; CTIP2 CTR – 0,88 ± 0,96%; *eIF4A1* KO – 2,95 ± 2,34%) [Fig. 22g]. The *eIF4A1* KO knockout at both stages produced no changes in the laminar distribution of neurons.

From the findings, we can assume that eIF4A1 plays an essential role at the early stages of corticogenesis (E12.5) in the determination of neuronal identity, whereas eEF-2 is not involved in the process of cell fate acquisition, but at later stages (E14.5) is involved in the process of neuronal migration.

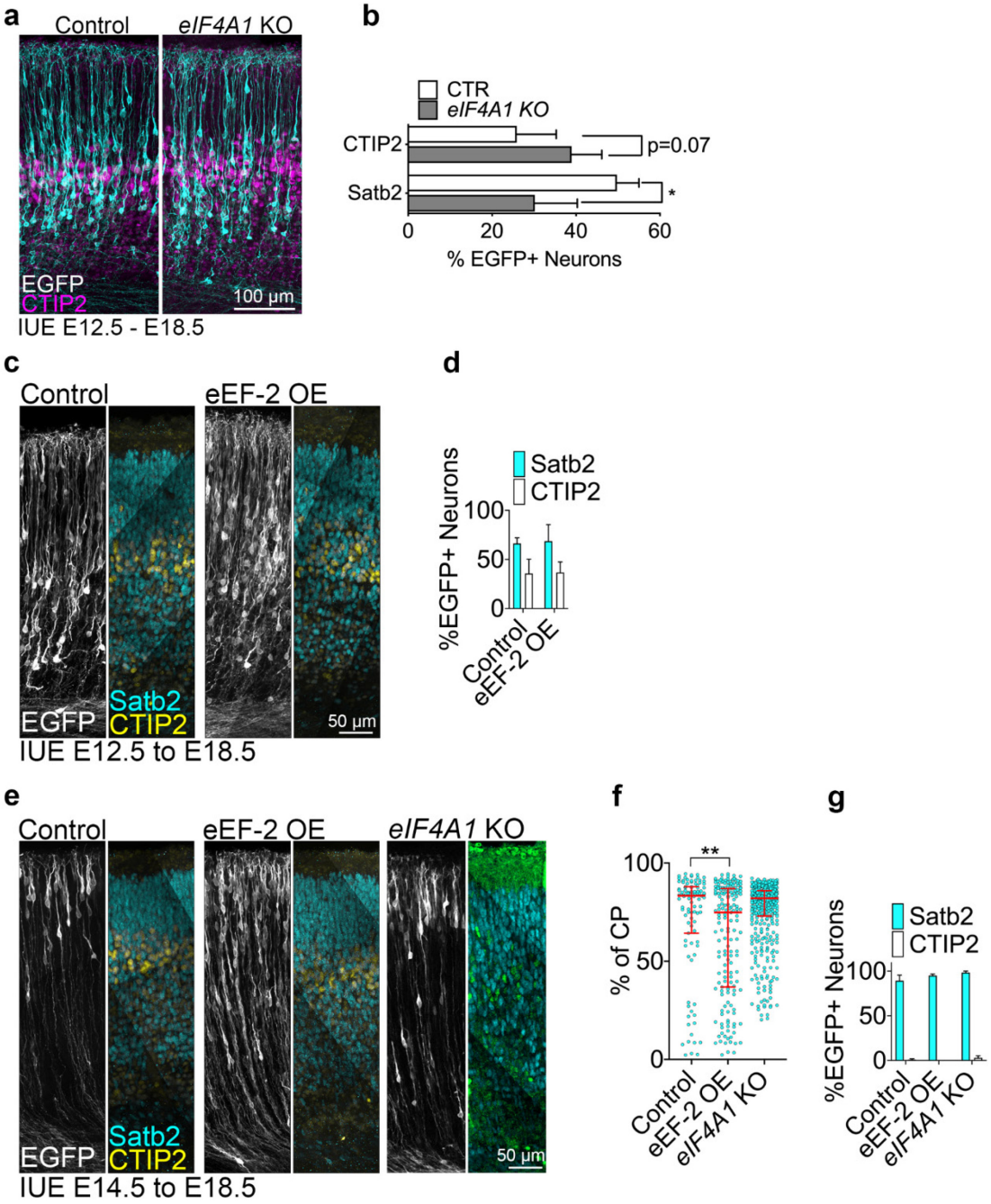

Fig. 22. Ire1α regulates cell fate acquisition of upper layer neurons via eIF4A1. (a,c,e) Representative images of coronal cortical sections at E18.5 stained against EGFP, Satb2 and CTIP2 after IUE at E12.5 (a,c) or E14.5 (e) with indicated plasmids. (b,d,g) Quantification of neuronal cell identity. (f) Laminar distribution of EGFP-positive neurons after IUE from (e). 0% CP – bottom of the CP, 100% - pia. (b,d,g) Bar graphs indicate mean ± S.D. (f). Line and error bars show median and interquartile ranges. Statistics: (b,d) D'Agostino and Pearson normality test, Mann-Whitney test; (f,g) Kruskal-Wallis test with Dunn's multiple comparisons.

We demonstrated an increased level of polysomes in *Ire1α* KO. The explanation for this could be a decrease in the elongation rate or ribosome stalling, which leads to their accumulation in this fraction (Eshraghi M. et al., 2021). Features of the internal mRNA sequence can cause ribosome stalling, the effect of external factors on mRNA, as well as structural features of the ribosomes themselves (Gutierrez E. et al., 2013; Koutmou K.S. et al., 2015; Richter J.D. and Coller J., 2015).

Based on these data, we hypothesized the possibility of an interaction between Ire1α and the ribosome during corticogenesis. To test this hypothesis, the expression level of ribosomal proteins was characterized by immunoprecipitation from cortical protein lysates at E12.5 and E14.5 followed by Western blotting. We performed immunoprecipitation of protein samples obtained from wild-type cortical homogenate at E12.5 and E14.5 using sepharose beads bounded with antibodies specific to the protein of small ribosomal subunit Ribosomal protein S6 (RPS6), large ribosomal subunit Ribosomal protein L7 (RPL7) and poly(A)-tail interactor Poly(A) Binding Protein Cytoplasmic 4 (PABPC4) [Fig. 23a]. These proteins are the main players of ribosome assembly machinery (Klinge S. and Woolford Jr. J.L., 2018).

Interestingly, an increase in the level of interaction between endogenous Ire1α and RPS6 at stage E12.5 was observed (E12.5 – 1 ± 0,20; E14.5 – 0,33 ± 0,05). The level of binding of Ire1α with RPL7 and PABPC4 does not change during development (RPL7 E12.5 – 1 ± 0,14; E14.5 – 1,13 ± 0,24; PABPC4 E12.5 – 1 ± 0,27; E14.5 – 1,10 ± 0,62) [Fig. 23b]. Thus, binding to the small ribosome subunit is regulated during development, whereas binding to the large ribosome subunit and mRNA poly(A) tail interactors does not change during corticogenesis. It also suggests a specific requirement for the interaction of Ire1α with the small subunit of the ribosome at the early stages of corticogenesis in multipotent progenitors.

Altogether, this shows that Ire1α-associated regulation of translation is mediated through ribosomes and the expression level of the regulators of transcription initiation and elongation.

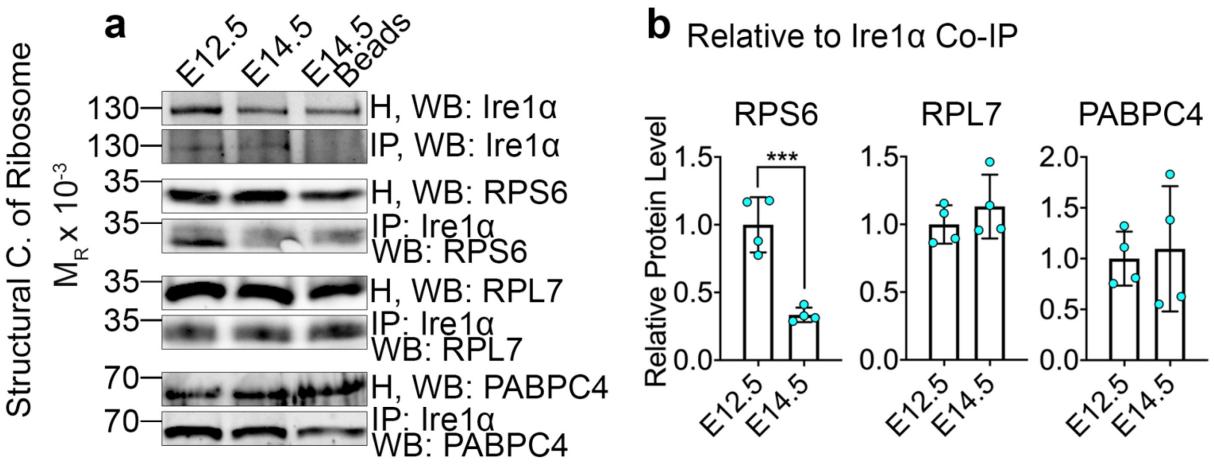

Fig. 23. Translation regulation by Ire1α is regulated mediated through ribosomes. (a) Representative images of Western blotting of endogenous Ire1α co-immunoprecipitation from E12.5 and E14.5 with indicated antibodies. (b) The interaction strength between Ire1α and ribosomal proteins was quantified relative to the amount of immunoprecipitated Ire1α. Bar graphs show mean ± S.D. Statistics: Shapiro-Wilk normality test and unpaired t-test. *** p<0,001.

5.4. Ire1α regulates translation rates during cortical development

The increase in polysome levels detected in the case of *Ire1α* loss may indicate a ribosomal arrest or a slowing of the elongation rate. Elongation is one of the essential steps in translation, during which the ribosome scans the mRNA sequence and adds new amino acids to the nascent polypeptide chain. Ribosome stalling can cause changes in protein expression, conformational changes of proteins, mRNA degradation, and pathological changes (Buchan J.R. and Stansfield I., 2007; Tsai C.J. et al., 2008; Tuller T. et al., 2010; Ishimura R. et al., 2014).

To further understand the consequences of the increased level of polysomes in the cKO, we then assayed the process of protein translation in our mutant. Using fluorescent noncanonical amino acid tagging (FUNCAT) and primary cortical cell cultures, the protein synthesis rates in the developing cortex were measured.

The method is based on metabolic labeling by replacing L-methionine with a bioorthogonal reactive group, which is the alkyne-containing methionine surrogate homopropargylglycine (HPG). In the next step, HPG is attached to the azide-bound fluorophore. When introduced into the methionine-free growth medium, the amino acid analog is taken up by the cell and incorporated into the nascent polypeptide chain (Beatty K.E. and Tirrell D.A., 2008; Dieterich D.C. et al., 2010; Dieck T.S. et al., 2012). After fixation of the cell culture, chemoselective attachment of the fluorophore to the introduced functional groups occurs during the "Click reaction". This is an azide-alkyne cycloaddition that is catalyzed by copper. This method can

be combined with other immunohistochemical methods. We used azide-bound Alexa-647 and evaluated the fluorescence intensity proportional to the amount of HPG incorporated into the newly synthesized proteins to estimate the translation rate in an individual cell in the allotted time interval. The translation rates study was performed on a homogeneous cell population to exclude the influence of the synthesis rate of different cell types on each other.

To investigate the translation rates in early neuronal progenitors at stage E12.5, we used FUNCAT on cell culture from the *Ire1α*$^{f/f}$ line after EUE transfection with EGFP and EGFP together with Cre to induce *Ire1α* loss (Fig. 24). On DIV1, cells were incubated with a medium containing HPG for 360 minutes, then fixed followed by click reaction and immunocytology against GFP to label all transfected cells and against the proliferative marker Ki67 to label progenitors. At DIV1 *Ire1α* KO Ki67-positive cells showed a decreased translation rate (162,6 ± 73,98) compared with EGFP-expressing Ki67-positive progenitors in control (294,6 ± 162,8). The findings emphasize the involvement of Ire1α in the translation regulation.

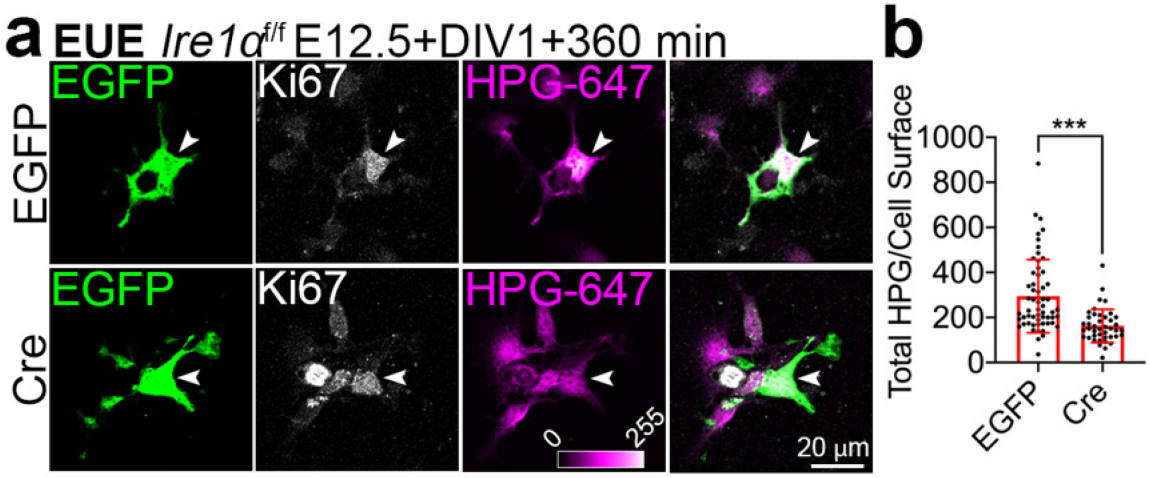

Fig. 24. Ire1α-associated regulation of translation rates. (a) Representative images of primary cortical cell culture prepared from *Ire1α*$^{f/f}$ cortices after EUE at E12.5 with EGFP or EGFP with Cre expressing plasmids. Cells were treated at DIV1 with HPG for 360 min. HPG was labeled with Sulfo-Cyanine5 azide. (b) Quantification of HPG incorporation in the cells. Bar graphs indicate average ± S.D. Statistics: D'Agostino and Pearson normality test, Mann-Whitney test. *** p <0,001.

Subsequently, to evaluate the effect of the *eIF4A1* loss observed in *Ire1α* KO, we performed a comparable experiment using FUNCAT. At stage E12.5 in the wild type, progenitors were transfected using EUE with EGFP and EGFP together with the CRISPR-Cas9 construct for eIF4A1 (Fig. 25). At the DIV1 stage, cells were incubated for 360 minutes with HPG, then fixed, clicked and immunostained, followed by an evaluation of Alexa-647 fluorescence intensity, which is proportional

to the intensity of translation over a particular time interval. We showed that mitotic progenitors on E12.5 with *eIF4A1* KO (172,3 ± 73,78) have reduced translation rates compared to controls (264 ± 157,9). The same changes in *Ire1α* KO were observed, suggesting the involvement of the eIF4A1 in the Ire1α-mediated regulation of translation.

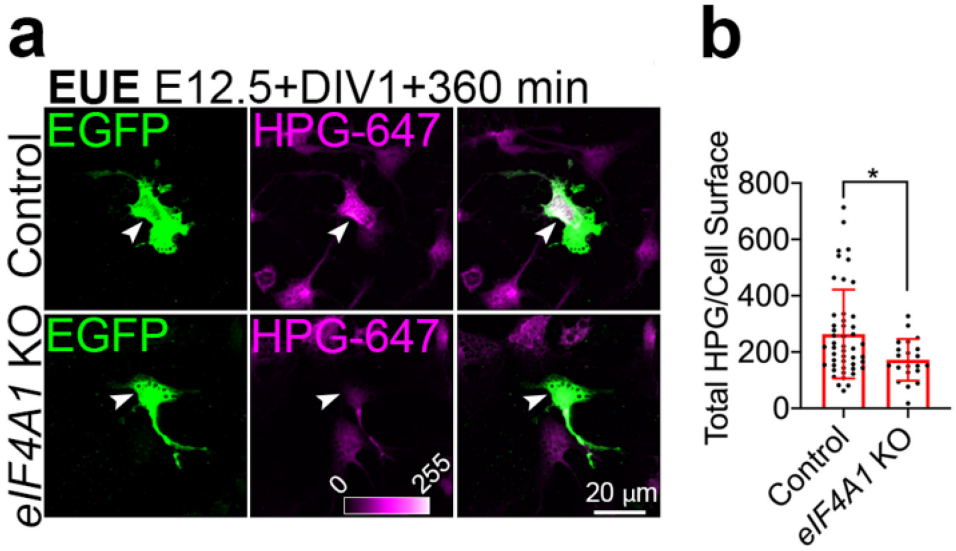

Fig. 25. eIF4A1 is involved in the Ire1α-mediated regulation of translation. (a) Representative images of primary cortical cell culture prepared from wild type cortices after EUE at E12.5 with EGFP or EGFP with *eIF4A1* KO expressing constructs. Cells were fed at DIV1 with HPG for 360 min. HPG was labeled with Sulfo-Cyanine5 azide. (b) Quantification of HPG incorporation in the cells. Bar graphs show average ± S.D. Statistics: D'Agostino and Pearson normality test, Mann-Whitney test. 0,01< * p <0,05.

During the next step, we investigated the translation rates in late progenitors with limited potency at E14.5 with FUNCAT. Using EUE, progenitors were transfected in *Ire1α* cKO (*Ire1α*$^{f/f}$*Emx*$^{Cre/+}$) and control (*Ire1α*$^{f/f}$) with EGFP construct (Fig. 26). By incubating the cells in an HPG medium and subsequent click-reaction, we showed that *Ire1α* cKO neurons at the DIV4 stage were characterized by lower synthesis rates (474,7 ± 212,5) than control neurons (906,5 ± 648,7). Consequently, irrespective of the developmental stage, the loss of *Ire1α* leads to lower translation rates. Together with the fact that the polysome fraction increases in *Ire1α* loss, these findings support our theory of ribosomal arrest and stalling.

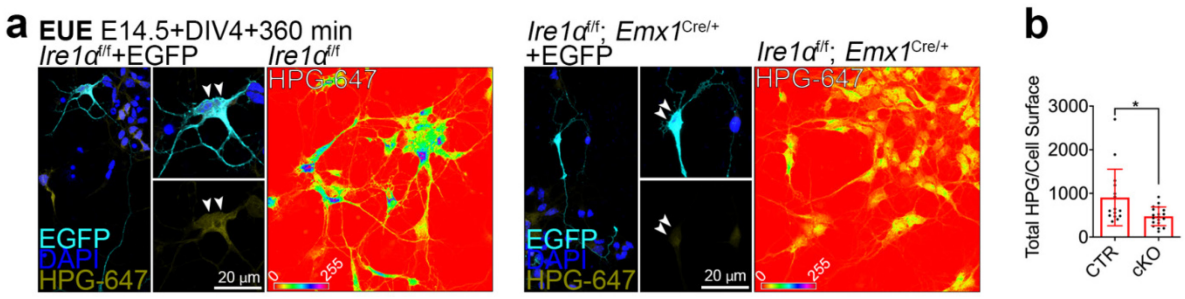

Fig. 26. Ire1α regulates the translation of upper layer neurons. (a) Representative images of primary cortical cell culture prepared from control and *Ire1α* cKO cortices after EUE at E12.5 with EGFP-expressing plasmid. Cells were treated at DIV1 with HPG for 360 min. HPG was labeled with Sulfo-Cyanine5 azide. (b) Quantification of HPG incorporation in the cells. Bar graphs show average ± S.D. Statistics: D'Agostino and Pearson normality test, Mann-Whitney test. 0,01< * p <0,05.

Since primary culture models are characterized by heterogeneity of cell types present and hence may influence the translation rate measurement for the following experiments, mouse embryonic fibroblasts (MEFs) obtained from *Ire1α*$^{f/f}$ mouse embryos at stage E13.5 were used. The experiments with this cell type were performed by technical assistant Rike Danneberg. The embryo body was chopped up with a blade, subjected to trypsinization and subsequent trituration, and then incubated in the medium in T75 flasks. In the fifth passage, the cells were cryopreserved until further processing.

To induce *Ire1α* inactivation, cells were infected with an adeno-associated virus (AAV) encoding Cre recombinase. The loss of *Ire1α* in AAV-infected cells was confirmed by Western blot using antibodies against Ire1α (Fig. 27). Control cells infected with the EGFP-expressing virus had a band of 132 kDa, which corresponds to the size of a functional Ire1α isoform. In contrast, cells infected with the Cre-expressing virus showed the presence of a nonfunctional isoform with a lower molecular weight.

In the first step, a surface sensing of translation (SUnSET) assay was used to estimate global protein synthesis. The method is based on the use of puromycin, which is a structural analog of aminoacyl-tRNA that allows it to be incorporated into the nascent protein chain, and this incorporation prevents further elongation. Using immunochemistry and antibodies to puromycin, it is possible to monitor translation (Lelouard H. et al., 2007; Schmidt E.K. et al., 2009).

At the DIV0 stage, MEFs were infected with EGFP-expressing virus and EGFP- and Cre-expressing AAV simultaneously. At the DIV5 stage, cells were metabolically labeled with puromycin and then lysed. Protein lysates were used for Western blot using antibodies against puromycin. Cells in *Ire1α* KO were characterized by

decreased incorporation of puromycin (0,7043 ± 0,07), and hence a reduced level of synthesis from mRNA compared to control (1 ± 0,03).

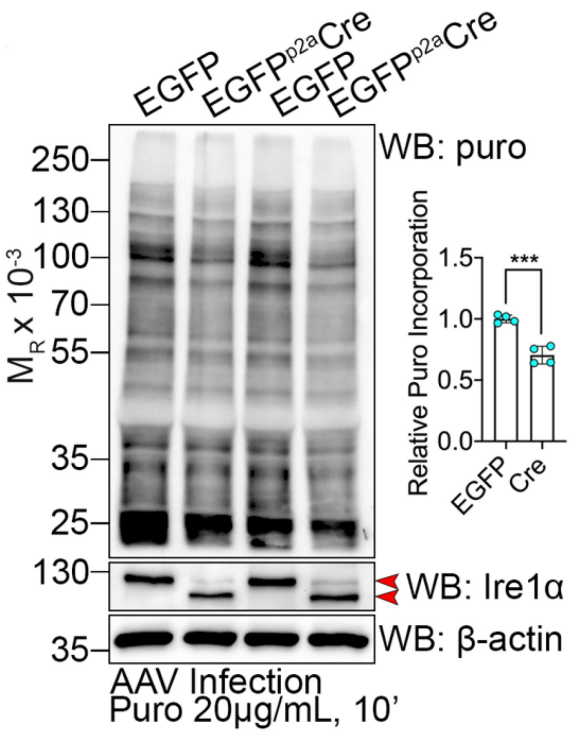

Fig. 27. *Ire1α* KO in the homogeneous cell population of MEFs. Representative images of Western blotting using DIV5 lysates from *Ire1αf/f* MEFs infected with control or Cre-expressing AVVs. Cells were metabolically labeled with puromycin. The graph shows the quantification of the puromycin incorporation. Red arrowheads indicate wild-type and KO isoforms of Ire1α. It is important to note that the KO isoform of Ire1α is characterized by the absence of a cytoplasmic active site, while the remaining part of the protein is still expressed. Bar graphs represent average ± S.D. Statistics: Shapiro-Wilk and unpaired t-test. *** p<0,001.

To characterize the elongation rate, a ribosome run-off experiment with harringtonine was conducted. Harringtonine is an alkaloid isolated from *Cephalotaxus herringtonina*. This alkaloid is a specific inhibitor of translation initiation, causing disintegration of polysomes on ribosomes, blocking the formation of new peptide bonds and aminoacyl-tRNA binding while not affecting ribosomes downstream of the mRNA chain (Fresno M. et al., 1977; Lee S. et al., 2012; Yan X., 2016).

For the ribosome run-off assay MEFs at DIV0 were infected with AAVs encoding EGFP (control) and EGFP^{p2a}Cre (*Ire1α* KO). On DIV5, cells were incubated with 3 µg/ml of harringtonine to block translation for 1, 4, 8 and 10 minutes, followed by

another 10 minutes with 20 µg/ml of harringtonine (Fig. 28). As ribosomes already bound to mRNA complete translation and descend, under both conditions attenuation of signal intensity was observed. It is important to note that *Ire1α* KO cells are characterized by a slower decay in signal intensity, suggesting a slowly elongating ribosomes (EGFP: 1 min – 1 ± 0; 4 min – 0,62 ± 0,06; 8 min – 0,19 ± 0,11; 10 min – 0,13 ± 0,08; Cre: 1 min – 0,78 ± 0,05; 4 min – 0,43 ± 0,07; 8 min – 0,09 ± 0,03; 10 min – 0,06 ± 0,03).

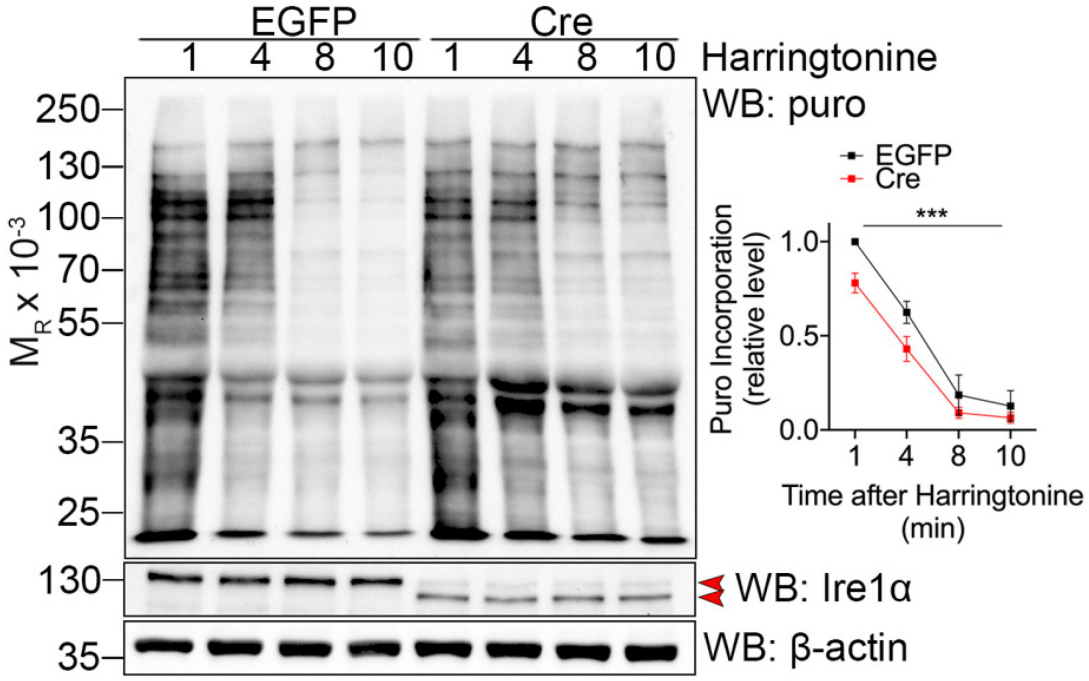

Fig. 28. *Ire1α* KO cells are characterized by a slower ribosomal decay. Representative Western blotting images using control and *Ire1α* KO MEFs after ribosome run-off assay using harringtonine treatment after indicated timepoints. Red arrowheads indicate wild-type and KO isoforms of Ire1α. Quantification of puromycin incorporation. Data points and error bars indicate average ± S.E.M. from three separated experiments. Statistics: two-way ANOVA. *** p <0,001.

In order to label single mRNAs and nascent proteins in cells, the SunTag method was used. This method is based on the multimerization of proteins, such as fluorescent proteins, on the target protein scaffold and is applicable for long-term visualization of individual mRNAs in living cells without affecting the synthesis rate (Tanenbaum M.E. et al., 2014; Yan X. et al., 2016).

At DIV4 after infection with empty virus (control) and with Cre-encoding virus (*Ire1α* KO), MEFs were transfected with plasmids for SunTag labeling (pcDNA4TO-24xGCN4_v4-BFP-24xPP7; pHR-scFv-GCN4-sfGFP-GB1-NLS; pHR-tdPP7-

3xmCherry). 20 hours after transfection, reporter expression was induced with 1 µg/ml doxycycline. Consequently, nascent proteins would be stained green (GFP), while mRNA would be fluorescently labeled red (mCherry) (Fig. 29). A lower number of colocalized red and green puncta in *Ire1α* loss was observed (5,59 ± 4,78) compared to the control (12,6 ± 9,92). Thus, *Ire1α* KO cells are characterized by a smaller number of active translation sites.

Altogether, the decrease in translation rates in the loss of *Ire1α* is associated with a decrease in the number of active translation sites and a slower rate of ribosome elongation.

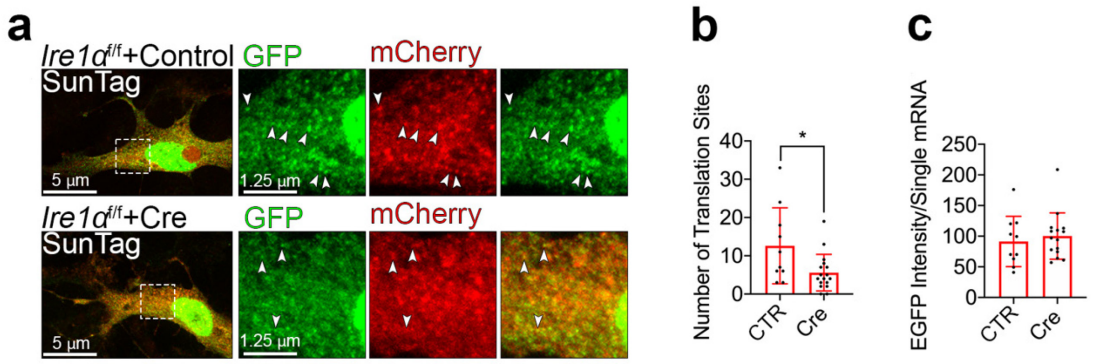

Fig. 29. Ire1α loss leads to decreased amount of active translation sites. (a) Representative images of MEFs infected with control and Cre-encoding AVVs and transfected with SunTag24x-BFP-PP7 reporter plasmid. Insets showed enlarged fragments of cytoplasm. White arrowheads indicate active translation sites. (b) Quantification of translation site number. (c) Quantification of the intensity of scFv-GFP per single mRNA. Bar graphs represent average ± S.D. Statistics: D'Agostino and Pearson normality test, Mann-Whitney test. 0,01< * p <0,05.

5.5. Deeper layer neurons of the cortex are characterized by higher translation rates than upper layer neurons.

Previously, we showed that loss of *Ire1α* leads to a decreased translation rate; and demonstrated that Ire1α is involved in determining cell fate during corticogenesis. Based on these findings, we hypothesized that differences in translation levels might be a characteristic feature of neurons of different layers.

To test this hypothesis, a pooled cell culture consisting of E12 primary cortical cells and E14 primary cortical cells was cultured with plasmids encoding dsRed and EGFP, respectively. For cell culture, the two cell populations were mixed in equal proportions and cultured together to assess the effect of the microenvironment. We first analyzed the cellular identity of neurons at the DIV5 stage obtained from cortex

E12 and E14. For this purpose, the cell culture was fixed at DIV5 and immunocytochemically stained with layer VI postmitotic projecting neurons marker (Tbr1), deeper layer postmitotic neurons marker (FoxP2) and upper layer postmitotic neurons marker (Satb2) [Fig. 30]. We demonstrated that neurons derived from the E12 cortex in the combined cortical cell culture are enriched with deeper layer marker-expressing cells (Tbr1 55,83 ± 18,92%; FoxP2 68,24 ± 10,46%; Satb2 33,47 ± 17,57%), whereas neurons derived from the E14 cortex are dominated by the expression of Satb2 (Tbr1 41,85 ± 5,97%; FoxP2 44,57 ± 2,16; Satb2 66,39 ± 7,04). Cells were also stained for proliferative marker Ki67 and radial progenitor marker Pax6 at the DIV1 stage. We showed that only a small number of cyclic cells or progenitors at both E12 and E14 stages were present at DIV1 (E12: Ki67 8,96 ± 4,31%; Pax6 6,85 ± 8,59 %; E14: Ki67 4,38 ± 3,81 %; Pax6 3,09 ± 4,26 %).

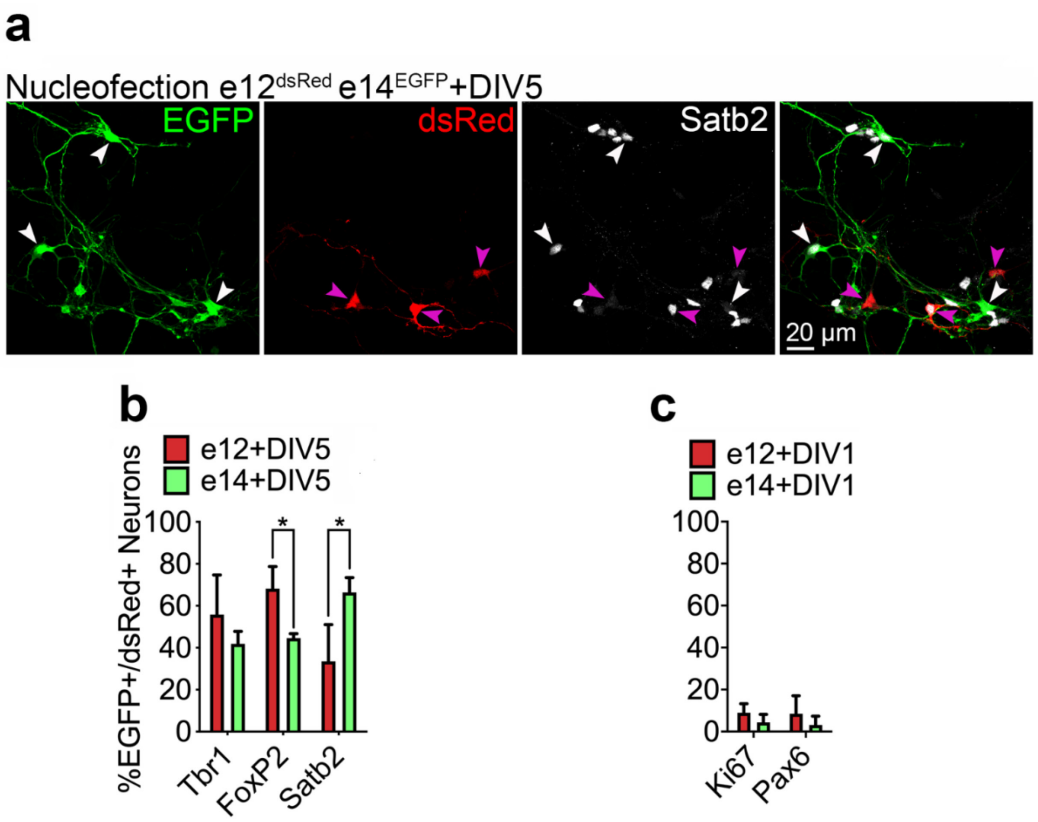

Fig. 30. In combined cortical cell culture neurons derived from E12.5 have enrichment of deeper layer markers, whereas neurons derived from E14.5 have enrichment of upper layer markers. (a) Representative images of DIV5 neurons after nucleofection at E12.5 with dsRed (purple arrowheads) and E14.5 with EGFP (white arrowheads). Cells from different populations were mixed and plated together on a single coverslip. (b) Quantification of cell identity of EGFP- or dsRed-positive neurons with indicated markers at DIV5. (c) The proportion of EGFP- or dsRed-positive primary cells with depicted markers at DIV1. Bar graphs show mean ± S.D.

Statistics: D'Agostino-Pearson normality test and Mann-Whitney test. 0,01< * p <0,05.

To evaluate the translation rates, neurons were incubated in a methionine-free medium with the addition of HPG for 60, 120, and 240 minutes at DIV1 and DIV5 stages (Fig. 31). Immediately after HPG pulse, the medium was removed, and cells were gently washed with 1x PBS and then fixed. After click-reaction, the fluorescence intensity in the far-red spectrum was evaluated, which is proportional to the translation efficiency. We showed that E12 cells were characterized by higher translation rates on DIV1 (60 min – 282,66 ± 22,55; 120 min – 638,19 ± 52,33; 240 min – 998,32 ± 65,61) compared to E14 cells (60 min – 187,94 ± 12,86; 120 min – 417,77 ± 33,09; 240 min – 617,96 ± 43,19). At the DIV5 stage, we also found a tendency for a higher level of HPG incorporation into E12 cells (60 min – 56,57 ± 4,61; 120 min – 295,99 ± 47,26; 240 min – 608,42 ± 51,42) than into E14 cells (52,79 ± 3,79; 120 min – 221,02 ± 20,89; 240 min – 478,45 ± 48,59), with the difference between the two stages being less distinct than at DIV1 (Fig. 31b). At the same time, cells on DIV1 were generally characterized by higher translation rates than those on DIV5 regardless of the embryonic stage (Fig. 31d). To confirm that these results were specifically related to translation as a negative control, the translation inhibitor cycloheximide (CHX) was added to the medium simultaneously with HPG (Fig. 31e). When CHX was supplemented to the media, a significant decrease in HPG incorporation to an undetectable level was observed. Thus, this confirms that the observed changes are specifically related to translation.

Altogether, we demonstrated that deep layer-fated neurons exhibit higher translation rates than upper layer neurons.

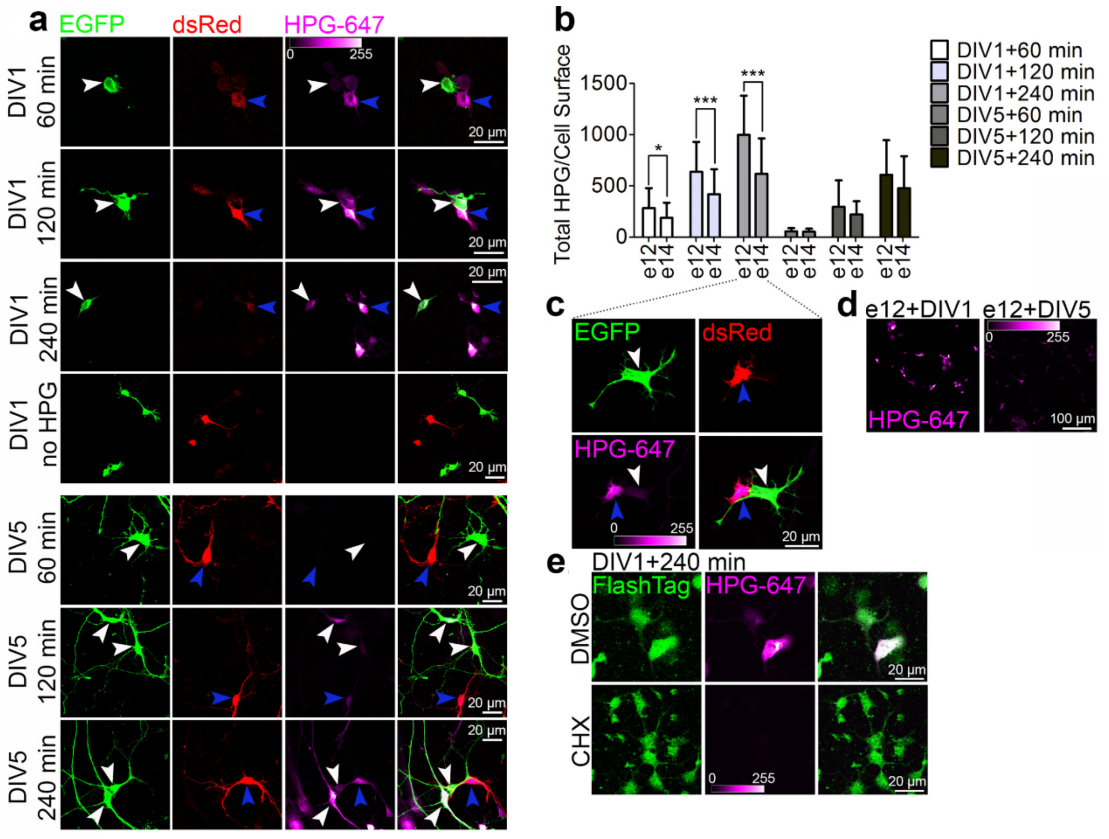

Fig. 31. Deep layer-fated neurons are characterized by higher translation rates than upper layer neurons. (a) Representative images of combined primary cell culture with cells transfected at E12.5 with dsRed (blue arrowheads) and at E14.5 with EGFP (white arrowheads). Cells were pulsed with HPG for the indicated time period before fixation. HPG was detected after click-reaction with far-red fluorophore-coupled azide. (b) Quantification of the level of HPG-incorporation. (c) DIV1 primary cells from the experiment (a) were treated with HPG for 240 minutes. (d) DIV1 primary cells and DIV5 neurons derived from E12.5. (e) DIV1 primary cells from E14.5 cortex were fed with HPG for 240 minutes and treated with DMSO and CHX. Bar graphs represent mean ± S.D. Statistics: two-way ANOVA with Bonferroni post-tests. 0,01< * p <0,05; *** p <0,001.

5.6. During corticogenesis, the transition from multipotent deeper layer progenitors to upper layer progenitors with limited potency is accompanied by a dramatic increase in translation rates

In the following experiment, we addressed the question about the difference in translation rates between cycling progenitors and neurons representing their direct progeny. Since the nucleofection method remained a small number of progenitors in culture, cells were transfected using EUE, allowing to label this cell population

and study the incorporation of HPG in progenitors. Using EUE, ventricular progenitors were transfected at E12 and E14 with plasmids encoding dsRed and EGFP, respectively. The cells were then triturated, mixed, and plated together on glass coverslips. At DIV1 and DIV5 stages, cells were incubated in a methionine-free medium with HPG for 240 min. Subsequently, after click-reaction, cells were stained at DIV1 with the progenitor marker Ki67 and at DIV5 with the postmitotic upper layer neuronal marker Satb2 (Fig. 32a). Then HPG incorporation into cells was analyzed by measuring fluorescence intensity in the far-red spectrum (Alexa-647). We showed that multipotent Ki67-positive E12 progenitors are characterized by a significant decrease in the level of HPG incorporation (271,4 ± 122,6) compared to Ki67-positive E14 progenitors with limited potency (585,8 ± 261,3) [Fig. 32b].

We demonstrated that neurons derived from E12 progenitors are characterized by higher translation rates (204,7 ± 119,5) than neurons derived from E14 progenitors (55,12 ± 37,65), which is consistent with our previous results. We also assessed cell fate in neurons derived from E12 and E14 progenitors at DIV5 by staining with the upper layer marker Satb2 and deeper layer marker CTIP2 (Fig. 32c). Most neurons from E12 progenitors co-expressed Satb2 (86%) and CTIP2 (91%), whereas neurons from E14 were characterized by predominant expression of Satb2 (56%) and almost complete absence of CTIP2 (4%) [Fig. 32d].

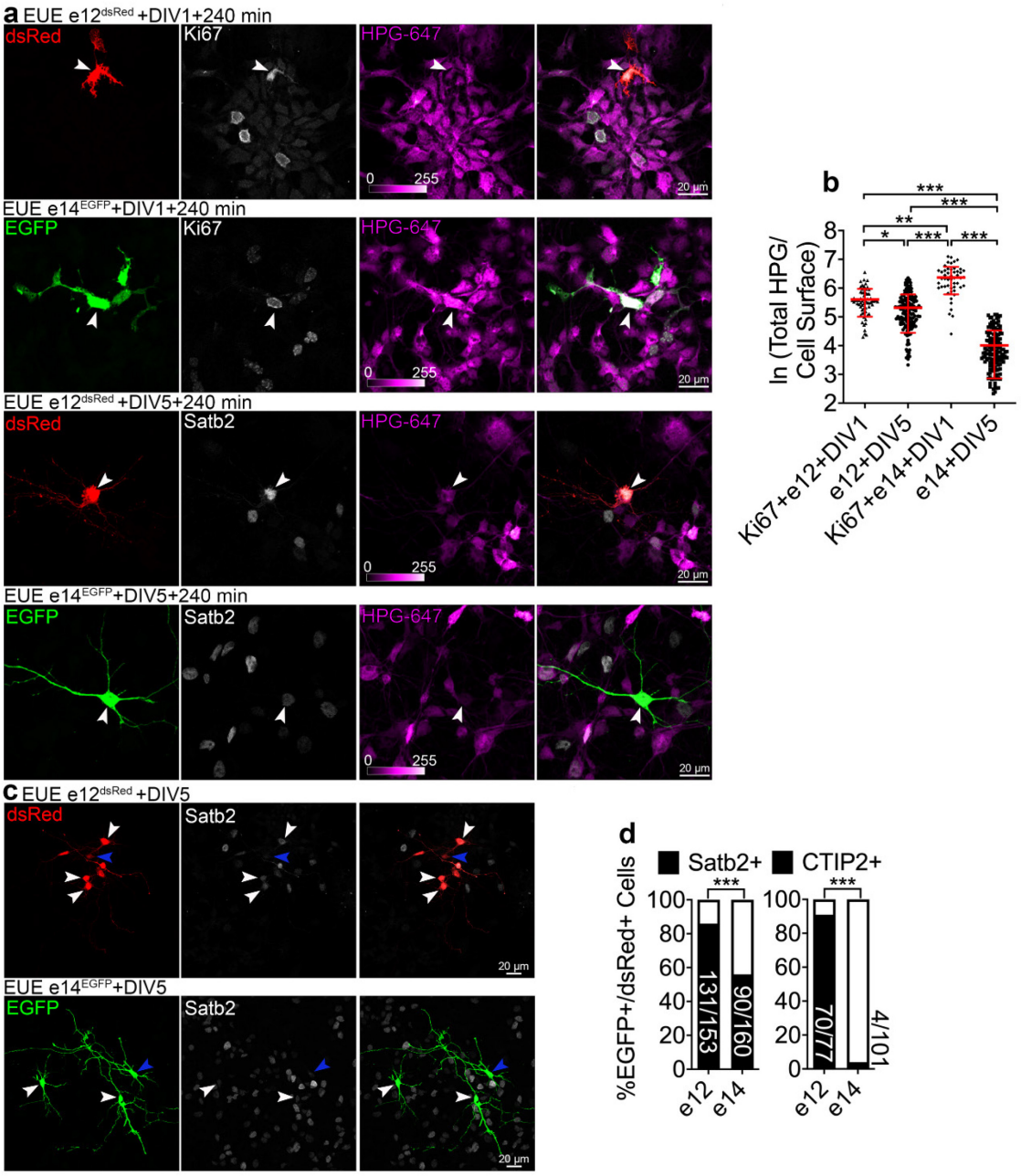

Fig. 32. During the developmental progression of progenitors, a dramatic decrease in translation rates occurs. (a) Representative images of combined cortical cell culture at DIV1 and DIV5 stained with EGFP, dsREd, Ki67 and Satb2. Cells were plated after EUE with dsRed-expressing plasmid at E12.5 and EGFP-expressing construct at E14.5. Primary cells and neurons were fed with HPG for 240 minutes. (b) HPG incorporation at different stages is depicted on the graph (natural logarithm scale). (c) Representative pictures of DIV5 neurons stained with Satb2. White arrowheads indicate neurons with a high level of Satb2 expression; blue arrowheads demonstrate neurons with a low level of Satb2. (d) Quantification of the proportion of neurons with indicated cell fate markers. Line and error bars (b) show mean ±

S.D. Statistics: (b) D'Agostino-Pearson normality test and Kruskal-Wallis test with Dunn's multiple comparisons test; (d) Fisher's test. 0,01< * p <0,05; 0,001< ** p <0,01; *** p <0,001.

Altogether, translation rate is a dynamic characteristic of cells during corticogenesis. Translation rates increase with the course of cortical progenitor development from E12 to E14. During differentiation of progenitors into neurons, a reduction in translation rates occurs; it is also important to mention that this reduction is dramatic in the case of upper-layer neurons (Fig. 33). This can be explained by the different requirements for the composition of cellular proteins at different stages of development.

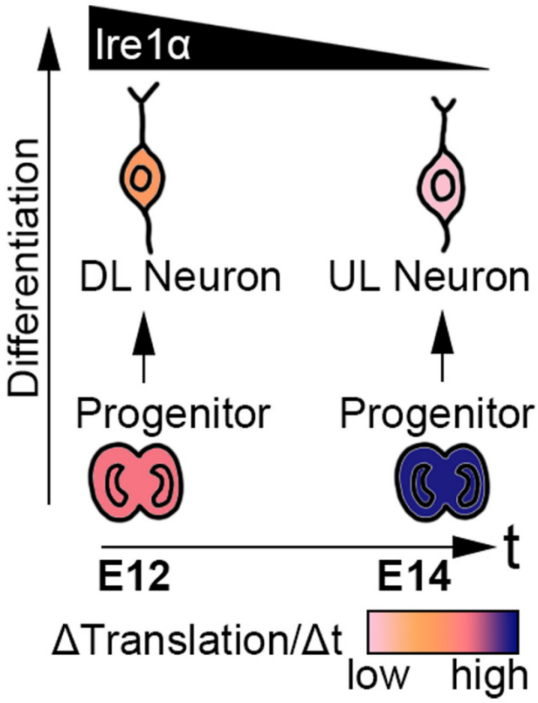

Fig. 33. Translation rates are dynamic characteristic of the cells during corticogenesis. Scheme of the translation rates (ΔTranslation/Δt) in progenitors and their derived progeny at E12 and E14. DL – deeper layers; UL – upper layers.

5.7. Temporary inhibition in translation elongation results in a loss of bipolar morphology and identity of upper layer neurons

Since we showed a difference in translation rates between E12- and E14-derived neurons, we questioned the possibility of using a pharmacological agent to slow

down the translation rates and thereby affect the specification of upper layer neurons. We used the nucleofection method described above for cell transfection, at E12 with a plasmid encoding dsRed and at E14 with EGFP-encoding plasmid. Subsequently, cells were plated together on a glass coverslip. Two hours after when the cells were attached to the surface, the medium was supplemented with translation inhibitor cycloheximide (CHX) and DMSO as a negative control for 24 hours. After the treatment, the medium containing CHX or DMSO was removed and replaced with a normal medium for cell culture. Neurons were cultured in the medium until DIV5, and after they were fixed and immunocytochemically stained for the upper layer marker Satb2 and the deeper layer marker CTIP2 (Fig. 34a). We found a significant reduction in the number of Satb2-positive neurons obtained from E12 and E14 after the CHX treatment (E12+DMSO – 14,45 ± 13,95%; E12+CHX – 0%; E14+DMSO – 52,97 ± 18,59%; E14+CHX – 22,8 ± 18,6%) [Fig. 34b]. It is important to note that no Satb2-positive neurons were detected in E12 neurons after suppressing protein synthesis. At the same time, translation suppression had no effect on CTIP2 expression at both stages (E12+DMSO – 72,52 ± 13,25%; E12+CHX – 73,59 ± 26,88%; E14+DMSO – 51,24 ± 17,82%; E14+CHX – 53,33 ± 18,11%).

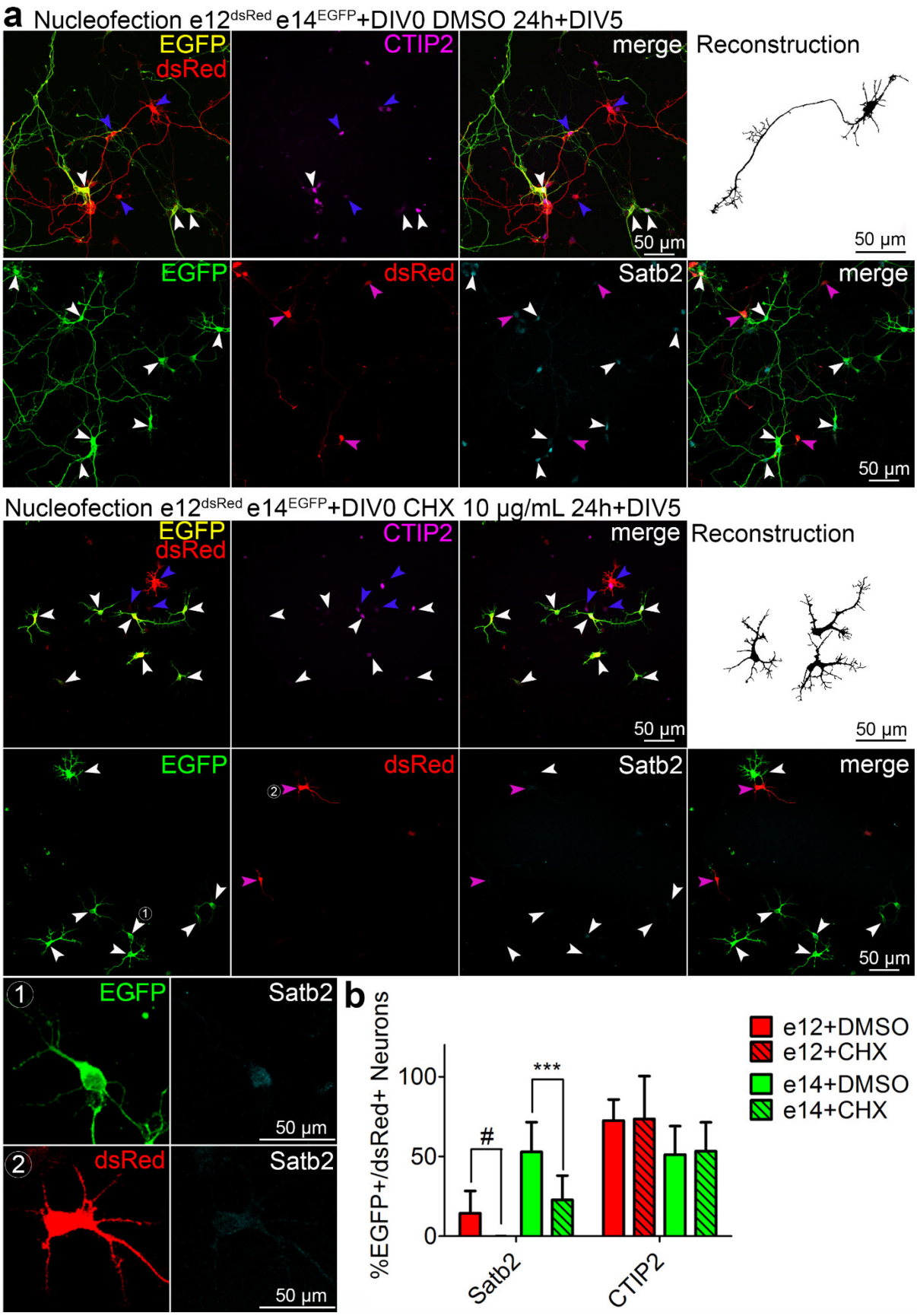
a
Nucleofection e12dsRed e14EGFP+DIV0 DMSO 24h+DIV5
EGFP
dsRed
CTIP2
merge
Reconstruction
50 µm
EGFP
dsRed
Satb2
merge
50 µm
Nucleofection e12dsRed e14EGFP+DIV0 CHX 10 µg/mL 24h+DIV5
EGFP
dsRed
CTIP2
merge
Reconstruction
50 µm
EGFP
dsRed
Satb2
merge
50 µm
1
EGFP
Satb2
50 µm
2
dsRed
Satb2
50 µm
b
%EGFP+/dsRed+ Neurons
100
50
0
#
***
Satb2
CTIP2
e12+DMSO
e12+CHX
e14+DMSO
e14+CHX

Fig. 34. Inhibition of translation leads to loss of upper layer neuronal identity and disrupts axon specification. (a) Representative images of combined cortical cell culture nucleofected before plating with dsRed-expressing plasmid (E12.5) and EGFP-expressing construct (E14.5). At DIV0 cells were treated with DMSO and CHX for 24h, then the medium was exchanged for a normal one. Cells were fixed at DIV5 and stained against EGFP, dsRed and Satb2. The blue arrowheads are E12-derived cells; the white arrowheads are E14-derived cells. Reconstructions of DIV5 neurons based on dsRed and EGFP signal. (b) Quantification of cell fate identity of DIV5 neurons. Bar graphs represent mean ± S.D. Statistics: two-way ANOVA with Bonferroni's multiple comparisons test. # - comparison between E12-derived neurons treated and untreated with CHX. *** p <0,001.

The effect of translation suppression on neuronal polarity was also investigated. For this purpose, the fixed cells were stained with antibodies against Tau-1 and evaluated its enrichment in neurites (Fig. 35a). We demonstrated that CHX treatment affects the ability of the neuron to form a bipolar morphology with a single axon, and Tau-1 mislocalization in the perinuclear region of the soma (CHX 10 µg/ml: 0 axons – 92,9%; 1 axon – 7,1%). This alteration in neuronal morphology has a dose-dependent effect (CHX 20 µg/ml: 0 axons – 100%) [Fig. 35b]. We observed the same localization of Tau-1 in the cell in *Ire1α* KO (Fig. 14). Control neurons incubated with DMSO overwhelmingly (87.5%) had a single axon with pronounced enrichment of Tau-1 staining and a small number of neurons with Tau-1 staining in several neurites (12.5%).

The effect of translation inhibition on dendritic tree formation was assessed by evaluating dendritic tree branching using Scholl analysis with a starting radius of 10 µm and concentric circles every 1 µm (Fig. 35c,d). Neurons were characterized by a decrease in the total number of intersections with concentric circles after the CHX treatment, indicating less complexity of dendritic tree branching and these changes are dose-dependent (DMSO – 287,80 ± 95,84; CHX 10 µg/ml – 172,90 ± 71,81; CHX 20 µg/ml – 124,50 ± 38,37 crossing dendrites/cell).

Altogether, temporary inhibition of translation at early stages of neuronal development engenders loss of bipolar morphology and the ability of neurons to form a single axon, as well as acquiring of Satb2 identity. Thus, we identified a time window critical for both the formation of correct morphology and the determination of cell identity.

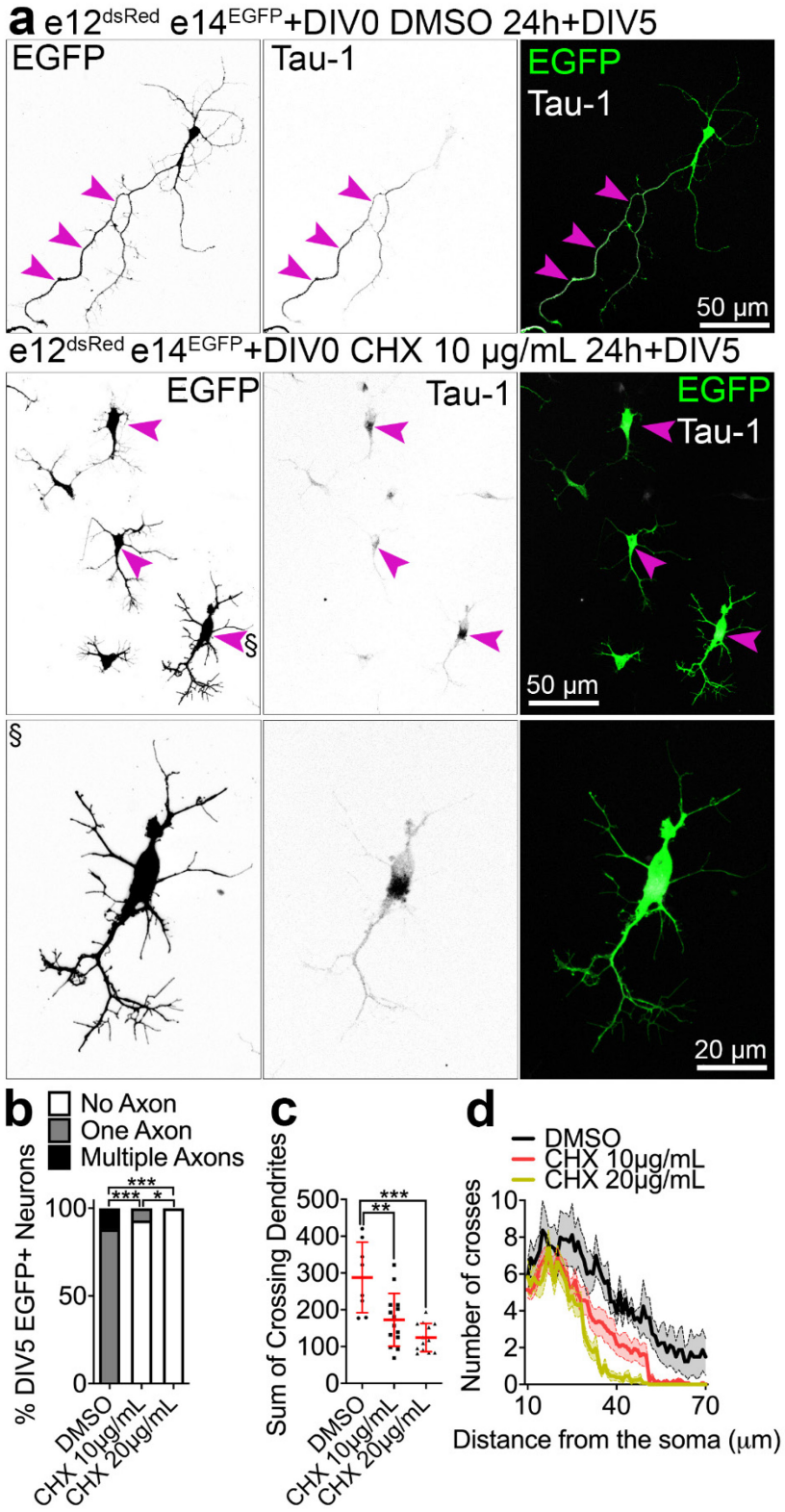

Fig. 35. Temporary inhibition of translation in the early stages during neuronal development leads to loss of bipolar morphology with a single axon. (a) Representative images of combined cortical culture nucleofected before plating with

dsRed- (E12.5) and EGFP-expressing plasmids (E14.5). At DIV0 primary cells were treated with DMSO and CHX for 24 hours, followed by the medium exchange. At DIV5 neurons were stained against axonal marker Tau-1. (b) Quantification of the proportion of cells with 0, one and multiple axons. (c,d) Quantification of dendritic tree complexity using Sholl analysis. Line and error bars indicate mean ± S.D (c). Data points and error bars represent average ± S.E.M (d). Statistics: (b) Chi-square test; (c) D'Agostino and Pearson normality test and one-way ANOVA with Bonferroni post-hoc test. 0,01< * p <0,05; 0,001< ** p <0,01; *** p <0,001.

5.8. Ire1α and eIF4A1 regulate the translation initiation of transcription factors Satb2 and CTIP2, based on the secondary structure of 5'UTR of mRNA

We demonstrated earlier that it is critical for the development of upper layer neurons that their progenitors have high translation rates; also, Ire1α-mediated regulation of translation through eIF4A1 was shown. Therefore, the next question is how Ire1α regulates the translation of Satb2, which globally determines the acquisition of the fate of upper layer neurons.

One of the known functions of the eIF4A1 helicase is the unwinding of secondary 5'UTR structures during translation initiation, which makes recruitment of the 40S ribosomal complex possible (Svitkin Y.V. et al., 2001; Marintchev A. et al., 2009; Raza F. et al., 2015). According to the literature, ribosomal footprinting has shown that the 12-mer guanine quartet $(CGG)_4$ motif that forms G-quadruplex (G4s) structures is the hallmark for eIF4A1-dependent transcripts (Wolfe A.L. et al., 2014). Guanine (G)-rich nucleic acids can form noncanonical four-chain guanine-quadruplex structures (Kharel P. et al., 2020). Based on these data, the 5'UTR mRNA of Satb2 and CTIP2 was examined using bioinformatic prediction of mRNA secondary structures (Fig. 36a). 5'UTR of Satb2 has a greater number of G4s structures (7), which are arranged with greater density than in 5'UTR of CTIP2 (2) [Fig. 36b,c]. Another mRNA structural element that plays a role in mRNA processing is R-loops. eIF4A1 has also been shown to unwind RNA/DNA such as R-loops (Rogers G.W. et al., 2001). We also found that 5'UTR of Satb2 has two R-loops structures (Fig. 36d).

Therefore, we hypothesized that the presence of G4s structures in 5'UTR of Satb2 makes the translation of its mRNA heavily eIF4A1-dependent, downstream of Ire1α.

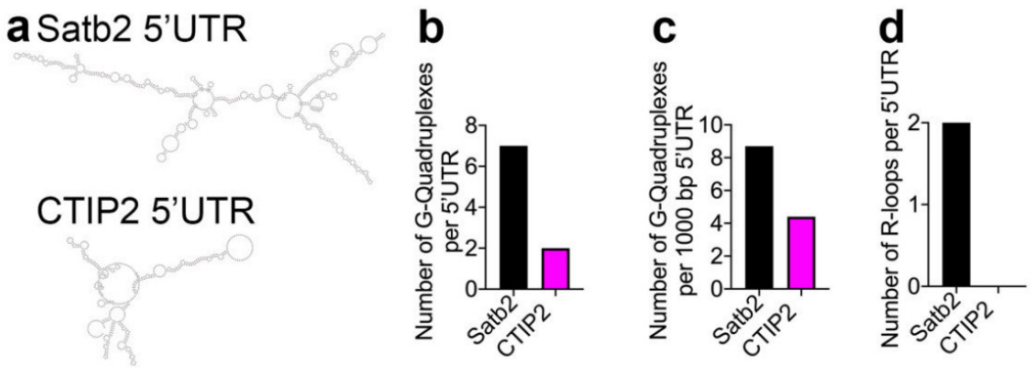

Fig. 36. Translation of transcription factors Satb2 and CTIP2 depends on the presence of G4s structures in 5'UTR. (a) Schematic model of 5'UTR mRNA structures of Satb2 and CTIP2. (b) The total number of G4s structures in the 5'UTR. (c) The density of G4s structures in 5'UTR. (d) Number of R-loops in the 5'UTR.

The constructs in which 5'UTR of Satb2 and CTIP2 were fused with EGFP were created by our collaborator Theres Schaub to test this hypothesis. Using these plasmids, we can evaluate the efficiency of 5'UTR-dependent translation in cells based on the estimation of GFP fluorescence intensity.

Using IUE in the wild type, the translational reporter construct (control) and the reporter construct together with the CRISPR-Cas construct were expressed to inactivate *eIF4A1* at E12.5. The concentration of the reporter plasmids for both conditions was the same 500 ng/μL. Four days after transfection, the brains were fixed, sectioned and stained against GFP, and the fluorescence intensity of GFP signal was measured (Fig. 37a,c). We found a decrease in GFP signal intensity in *eIF4A1* KO in the case of Satb2 reporter (75106 ± 65719) compared with the control (256262 ± 138432), indicating a decrease in translation efficiency (Fig. 37b,d). At the same time, when *eIF4A1* was inactivated in the case of the CTIP2 reporter, the intensity of GFP fluorescence was increased (179968 ± 116879) compared to the control (27794 ± 16777). This suggests a redistribution of ribosomes during translation between these mRNAs, leading to a decrease or increase in translation efficiency. Therefore, G4s located in the 5'UTR of cell fate determinants Satb2 and CTIP2 affect the intensity of their translation, which explains the phenotype of reduction of Satb2-positive neurons in the loss of *eIF4A1*.

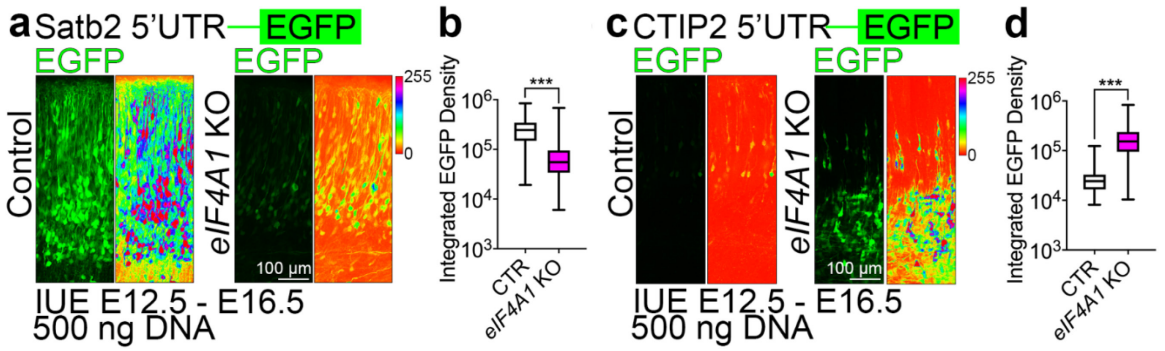

Fig. 37. Translation of fate determinants having G4s structures in 5'UTR depends on eIF4A1 on the early stages of development. (a,c) Representative images of E16.5 coronal sections after IUE in the wild type at E12.5 with empty and CRISPR-Cas9 plasmid for *eIF4A1* KO and Satb2 5'UTR (a) or CTIP2 5'UTR (c) reporter constructs. The right panels show the intensity encoding signal. (b,d) Quantification of the EGFP fluorescent intensity after IUE from (a,c) with Satb2 5'UTR (b) or CTIP2 5'UTR (d) reporters. Violin plots indicate median, interquartile range (box) and minimum and maximum value (whiskers). Statistics: D'Agostino and Pearson normality test and Mann-Whitney test. *** p <0,001.

The same experiment with the Satb2 and CTIP2 reporter constructs at stage E14.5 was performed in wild type and evaluated the GFP fluorescence intensity two days later (Fig. 38a,c). We found no significant differences in translation efficiency with either the Satb2 reporter (EGFP – 115349 ± 100090; *eIF4A1* KO – 147010 ± 127670) or the CTIP2 reporter (EGFP – 106365 ± 83885; *eIF4A1* KO – 126992 ± 129430) [Fig. 38b,d].

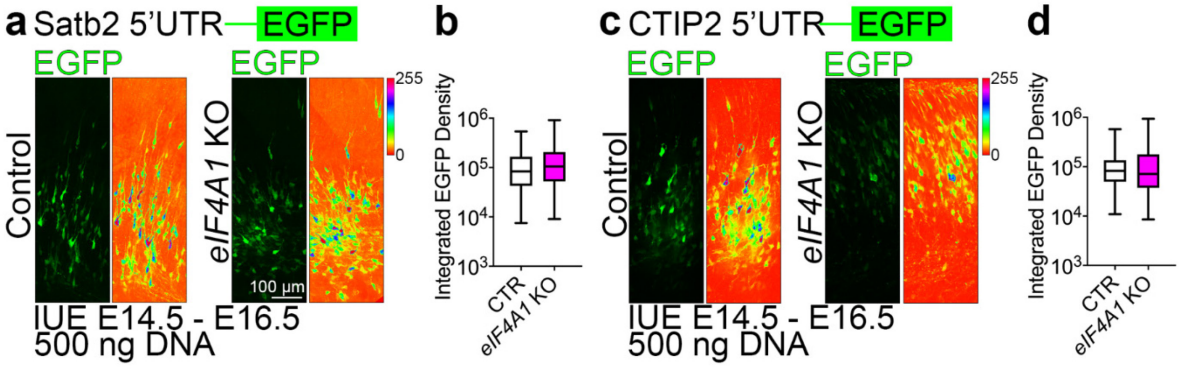

Fig. 38. Translation of fate determinants having G4s structures in 5'UTR is independent of eIF4A1 on later stages of development. (a,c) Representative images of E16.5 coronal sections after IUE in the wild type at E14.5 with empty and CRISPR-Cas9 plasmid for *eIF4A1* KO and Satb2 5'UTR (a) or CTIP2 5'UTR (c) reporter constructs. The right panels show the intensity encoding signal. (b,d)

Quantification of integrated EGFP fluorescent intensity after IUE from (a,c) with Satb2 5'UTR (b) or CTIP2 5'UTR (d) reporters. Violin plots indicate median, interquartile range (box) and minimum and maximum value (whiskers). Statistics: D'Agostino and Pearson normality test and Mann-Whitney test.

The translation efficiency of Satb2 and CTIP2 in the condition of *Ire1α* loss was studied on MEFs, because of poor breading of *Ire1α*$^{f/f}$ mouse line. The same approach we used to study the kinetics of translation. On DIV0, MEFs were infected with AAVs with an empty virus (control) and with Cre-encoding virus (*Ire1α* KO). Then, on DIV5, cells were transfected with the reporter constructs of Satb2 and CTIP2; a day later, the cells were fixed and immunostained (Fig. 39).

In *Ire1α* KO, the changes in translation efficiency similar to those in *eIF4A1* KO were identified. In the case of the Satb2 reporter, we observed a decrease in GFP signal intensity (0,65 ± 0,56) compared to control (1 ± 0,68). In the case of the CTIP2 reporter, the intensity of the GFP signal was higher (1,48 ± 0,84) than in control (1 ± 0,61). The intensity of endogenous expression of Satb2 and CTIP2 markers was also quantified. A decrease in the translation efficiency of Satb2 in *Ire1α* KO was accompanied by a decrease in endogenous expression of Satb2 (0,73 ± 0,22) compared to control cells (1 ± 0,27). Opposite to this, with an increase in the efficiency of translation of CTIP2 in the loss of *Ire1α*, the intensity of CTIP2 expression was increased (1,11 ± 0,20) compared to control cells (1 ± 0,13).

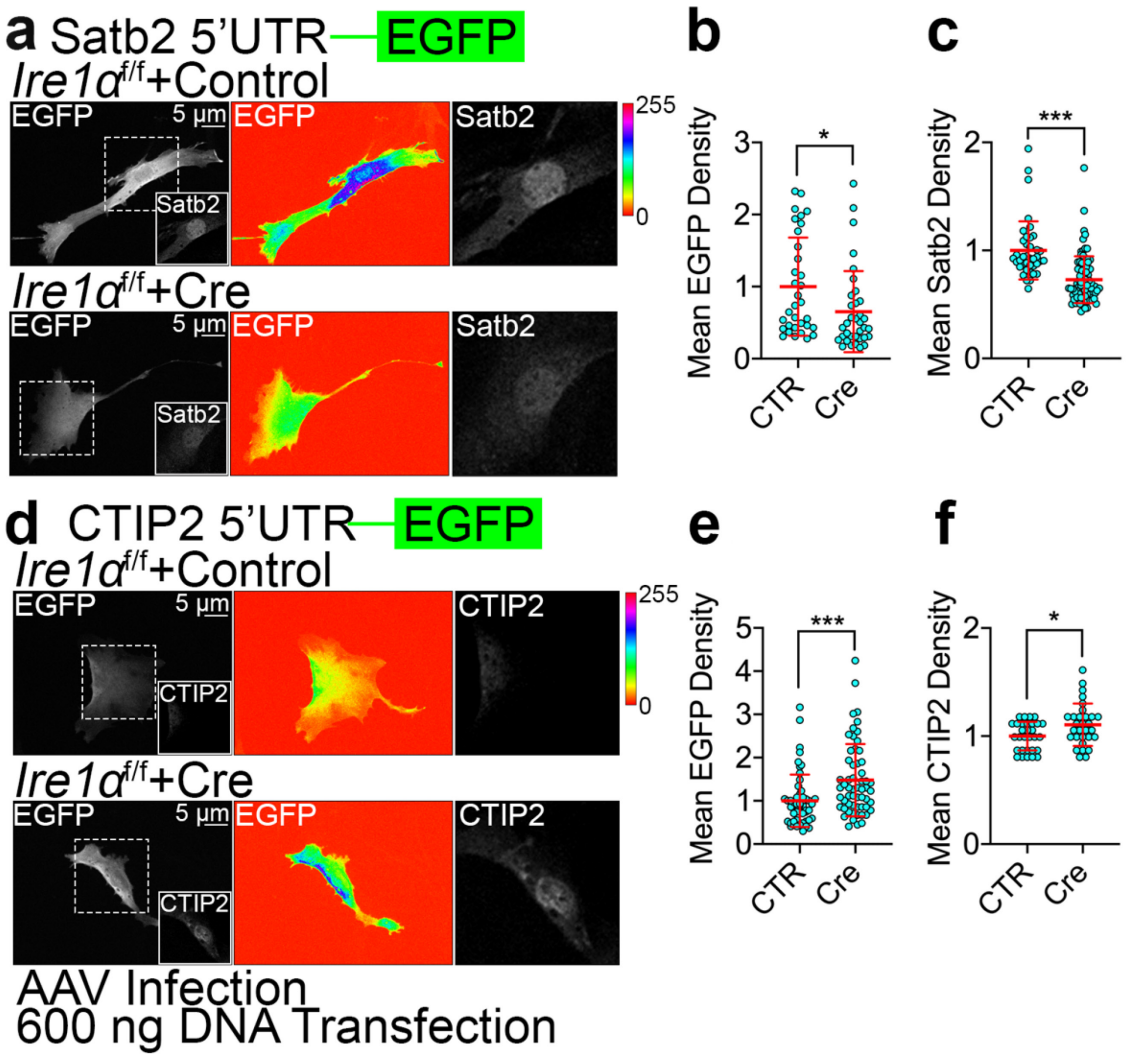

Fig. 39. Regulation of Ire1α-dependent translation is embedded in Satb2 and CTIP2 5'UTR. (a,d) Representative images of MEFs infected with control and Cre-encoding AVVs at DIV0, transfected at DIV5 with Satb2 5'UTR (a) or CTIP2 5'UTR (d) reporter constructs, stained at DIV6 against Satb2 and CTIP2. (b,e) Quantification of EFGP fluorescent intensity. (c,f) Quantification of signal intensity after staining with Satb2 (c) and CTIP2 (f). Lines and error bars indicate mean ± S.D. Statistics: D'Agostino and Pearson normality test and Mann-Whitney test. 0,01< * p <0,05; *** p <0,001.

We also transfected reporter constructs at E14.5 in the *Ire1α*$^{f/f}$ line together with an empty vector (control) and Cre-expressing plasmid (*Ire1α* KO) using IUE (Fig. 40a,c). GFP fluorescence intensity was measured two days after the IUE. No alterations in translation efficiency were found between conditions using both Satb2 (CTR – 90282 ± 75142; Cre – 111678 ± 88106) and CTIP2 reporters (CTR – 29852 ± 21219; Cre – 21721 ± 16668) [Fig. 40b,d].

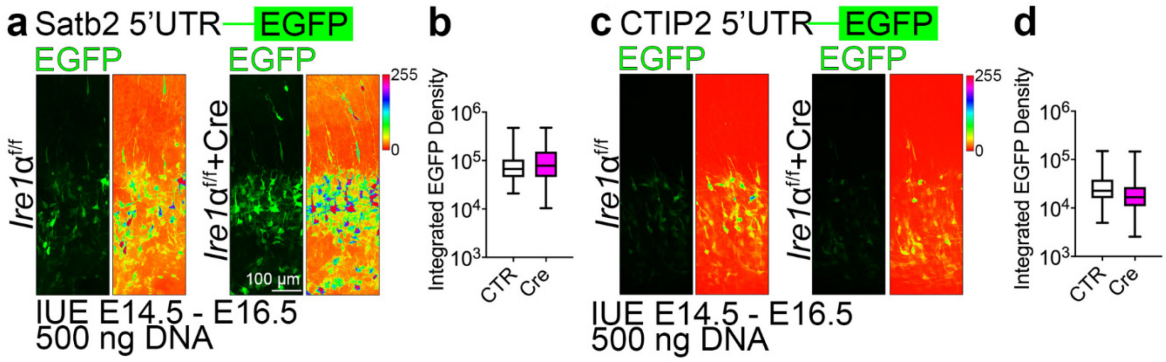

Fig. 40. Ire1α-dependent regulation of translation is absent at later stages of cortical development. (a,c) Representative images of E16.5 coronal sections after IUE in *Ire1α*$^{f/f}$ at E14.5 with empty and Cre-encoding plasmid and Satb2 5'UTR (a) or CTIP2 5'UTR (c) reporter constructs. The right panels show the intensity encoding signal. (b,d) Quantification of integrated EGFP fluorescent intensity after IUE from (a,c) with Satb2 5'UTR (b) or CTIP2 5'UTR (d) reporters. Violin plots indicate median, interquartile range (box) and minimum and maximum value (whiskers). Statistics: D'Agostino and Pearson normality test and Mann-Whitney test.

Altogether, these results demonstrate that Ire1α regulates translation in the early stages of cortical development through downstream eIF4A1, which is involved in the preferential selection of cell fate determinants mRNAs to the conformation of their 5'UTRs (Fig. 41).

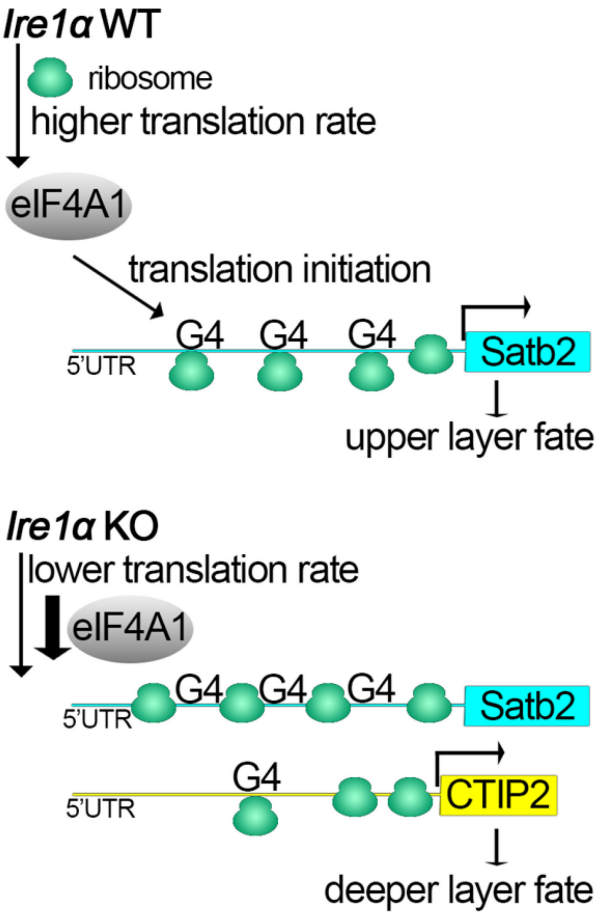

Fig. 41. Ire1α-dependent translation regulation and upper layer cell fate establishment are implemented by helicase eIF4A1 via controlling translation initiation through RNA secondary structural elements embedded in 5'UTR of Satb2.

These findings provide an alternative outlook on the fundamental principles orchestrating the neocortex development. This work is the first demonstration that neuronal progenitors exhibit a unique requirement for ribosome-driven translation rates in order to specify neurons of a given type.

5.9. ENU mutagenesis is an effective tool for screening to identify new gene mutations responsible for epilepsy

To screen for mutations responsible for epilepsy, six series of ENU mutagen injections were performed according to the protocol described above. A total of 280 males from the C3H/HeN line were injected intraperitoneally with 80 μg/kg of ENU at 8-weeks-age. After mutagen injection, mice exhibited a period of sterility due to

depletion of spermatogonial stem cells in the testes (Kennedy C.L. and O'Bryan M.K., 2006). The average sterility period was 27-28 weeks.

To obtain recessive mutations in the third generation (G3), mice were bred according to the three-generation crossing scheme described above (Fig. 1). The screening was performed on G3 mice.

Seizures in response to sound stimulation are among the most common models of generalized epilepsy in humans (Jobe P.C. and Browning R.A., 2006). For screening on audiogenic epilepsy, we created a system for generation AGS and recording. With AGS assay, we tested the offspring of 67 founders and identified mouse lines that are sensitive to the epileptogenic action of sound: S1-3, S2-3, S3-2, S5-1, S8-3, S9-4, S32-1, S34-1, S63-1.

5.10. Increased number of interneurons and astrocytes as a cause of E/I imbalance

For mutation mapping and phenotype description, we chose the S8-3 line, which was detected first. Alteration in the excitatory/inhibitory balance of the neuronal network is considered as an underlying mechanism for epileptogenesis (Reid C.A. et al., 2009, Huberfeld G. et al., 2011, Ye H. and Kaszuba S., 2017). To estimate the number of interneurons, we performed immunohistochemical staining of P21 brain slices using GABA antibodies and Draq5 as a nuclear marker (Fig. 42a,c). Staining demonstrated that the number of interneurons was increased in the S8-3 line both in the cortex (Control – 52,83 ± 5,6; S8-3 – 108,0 ± 10,52 neurons/selected area) and dentate gyrus (DG) (Control – 9,5 ± 4,89; S8-3 – 18 ± 0,82 neurons/selected area) compared to controls (Fig. 42b,d). These findings suggest an alteration in the inhibitory part, leading to E/I imbalance.

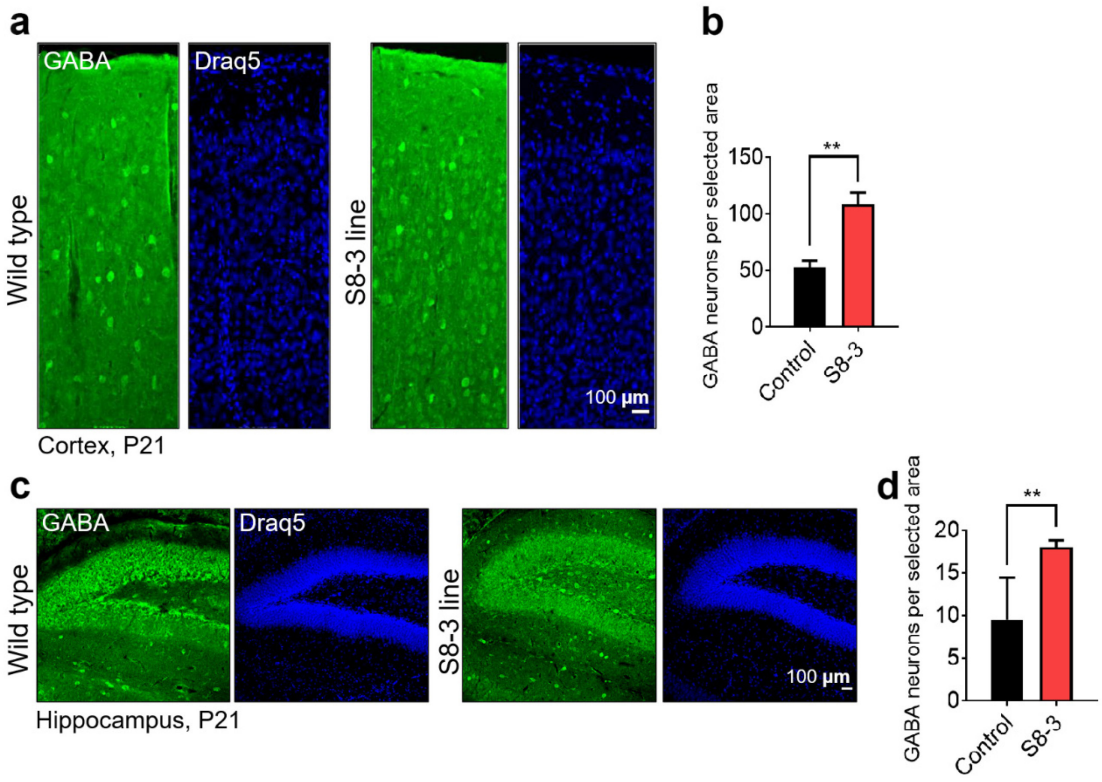

Fig. 42. S8-3 line is characterized by an increased level of interneurons. (a,c) Representative images of P21 coronal sections stained against GABA and Draq5 as a nuclear marker in different brain regions: cortex (a) and dentate gyrus (c). (b) Quantification of the number of interneurons in the cortex. (d) Quantification of the number of GABA-positive neurons in the dentate gyrus. Bar graphs show mean ± S.D. Statistics: D'Agostino-Pearson normality test and Mann-Whitney test. 0,001< ** p <0,01.

Astrocytes play an important role in neuronal circuit physiology. They express ion channels, transmitter receptors and transporters, and participate in redistributing K^+ concentration, which is directly linked to epileptogenesis. Astrocytes are also considered as possible targets for antiepileptic therapy (Araque A. et al., 2014; Coulter D.A. and Steinhäuser C., 2015). To assess astrocytic status in the S8-3 line and the control, the S100β astrocytic marker was used. Brain slices at P21 were stained, and then the number of astrocytes in the cortex and different regions of the hippocampus (CA1 and dentate gyrus) was quantified (Fig. 43a). Staining showed that the number of astrocytes in the cortex and dentate gyrus and CA1 of the hippocampus did not differ in the mutant and control (Cortex: Control – 13,17 ± 0,88%; S8-3 – 13,26 ± 0,08%; Dentate gyrus: Control – 39,42 ± 4,23%; S8-3 – 32,56 ± 2,28%; CA1: Control – 51,23 ± 5,38%; S8-3 – 33,75 ± 2,10%) [Fig. 43b]. Additionally, the CA1 hippocampal region was divided into zones (stratum oriens [SO], stratum pyramidale [SP], stratum radiatum [SR], stratum lacunosum

moleculare [SLM]), and the number of astrocytes in them was quantified (Fig. 43c). We showed a significant increase in the number of astrocytes in the SML zone of the S8-3 mutants (SO: Control – 0,00037 ± 0,0001, S8-3 – 0,0002 ± 0,0001; SP: Control – 0,0002 ± 0,0001, S8-3 – 0,0003 ± 0,0002; SR: Control – 0,0006 ± 0,0002, S8-3 – 0,0003 ± 0,00001; SLM: Control – 0,0005 ± 0,00001, S8-3 – 0,0011 ± 0,0004 astrocytes/μm^2) [Fig. 43d].

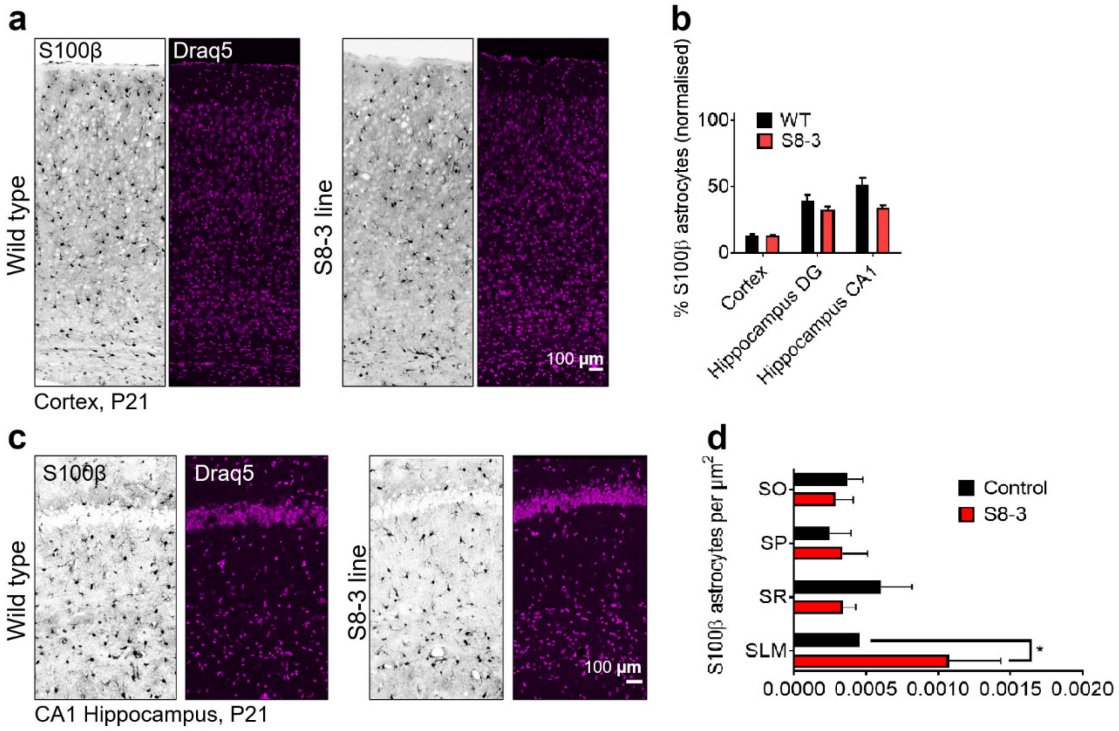

Fig. 43. S8-3 line characterized by increased amount of S100β astrocytes in stratum lacunosum moleculare (SLM) CA1 region of the hippocampus. (a,c) Representative images of P21 coronal sections from control and S8-3 line stained with astrocytic marker S100β and Draq5 for nuclear labeling in the cortex (a) and in the CA1 region of the hippocampus (c). (b) Quantification of the proportion of S100β astrocytes in different brain regions labeled on the graph. (d) Quantification of the proportion of S100β astrocytes in a different zone of CA1 is depicted on the graph. Bar graphs represent mean ± S.D. Statistics: D'Agostino-Pearson normality test and Mann-Whitney test. 0,01< * p <0,05.

Therefore, we demonstrated that our mutant is characterized by gliosis, which can affect the E/I balance. In the future, these pathways will be studied in more detail.

For coarse mapping of the S8-3 mutation, we used a method based on single-nucleotide substitutions (SNP). We created the SNP panel to identify the loci of C3H homozygosity and map the mutations after ENU-induced mutagenesis. This panel consisted of 114 SNPs (6 on each chromosome), which were evenly spaced along the chromosome and necessarily affected the terminal regions. 23 samples of genomic DNA from the S8-3 mouse line and control samples of C3H/HeN and C57Bl6 lines were tested using the created SNP panel (Fig. 44). Using ARMS-PCR, we identify the locus of mutation in the S8-3 mouse line on the 8th chromosome (8:28057473-32291828).

a

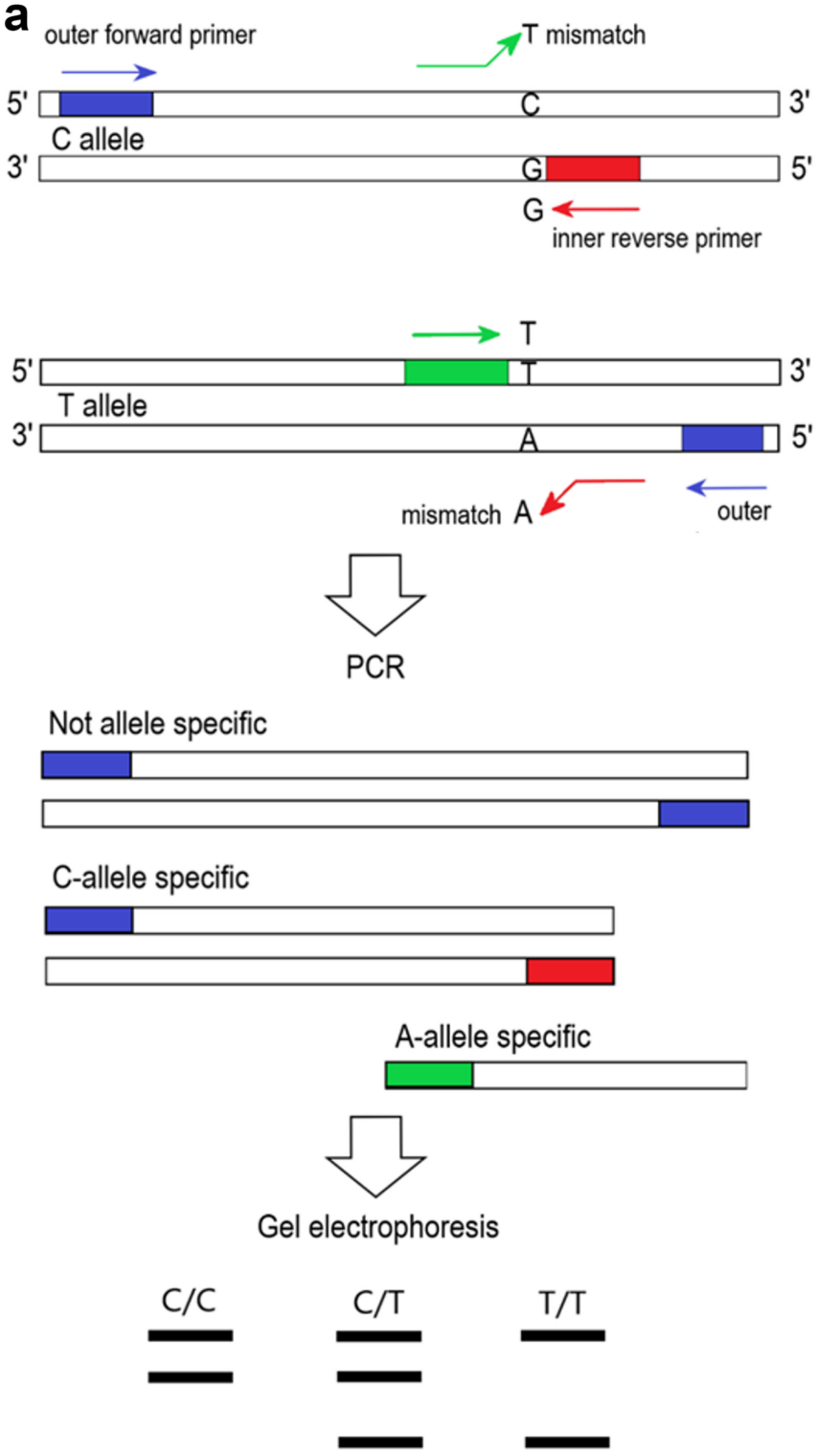

b

Samples	C3H/HeN	C57Bl6	1	2	3	4	11	12	17	18	19	22	23	24	25	26	27	34	35	37	39	40	42	44	47	SNP position
																										8:4471753
																										8:12602140
																										8:18906266
																										8:28057473
																										8:32291828
																										8:125410102

Fig. 44. Identification of the mutated locus on the 8th chromosome. (a) Scheme of tetra-primer ARMS-PCR method. (b) Results of SNP analysis on the 8th chromosome of samples from the S8-3 mouse line. The blue color indicates C3H/HeN homozygote, yellow – C57Bl6 homozygote and green – C3H/HeN/C57Bl6 heterozygote.

To more precisely map the S8-3 mutation, our collaborators performed DNA sequencing. A single-nucleotide substitution from thymine to adenine (8:29288964) was detected in the gene of netrin receptor D (Unc5d). This substitution is located at the homozygosity locus we detected previously with the SNP panel. According to the literature, patients with focal epilepsy were found to have a deletion in the UNC5D gene (Vlaskamp D.R.M. et al., 2017). It was also previously shown that Unc5d is implicated in p53-dependent apoptosis in neuroblastoma cells (Wang H. et al., 2014) and is also involved in corticogenesis (Sasaki S. et al., 2008). Altogether, Unc5d can be considered by us as a candidate gene. However, we have to confirm that the dysfunction of this particular gene is causing the previously detected phenotype with audiogenic epilepsy and knocked out this gene in wild type using, for example, the CRISPR-Cas9 system and test mice for susceptibility to audiogenic stimulation-induced seizures.

In summary, ENU-induced mutagenesis is an effective tool for screening for novel mutations in genes involved in epileptogenesis. This approach can also be successfully applied to the creation of mouse models of epilepsy, which can be used to characterize the molecular cascades involved in the development of this disease and to test anti-epileptic drugs.

6. Discussion

6.1. Translation in cortical development and pathology

One of the main findings of this project is that Ire1α plays a non-canonical role as a regulator of progenitor-embedded cell fate acquisition during cortical development by regulation of translation initiation and elongation. Neuronal cell fate requires specific protein synthesis rates in progenitor cells. Surprisingly, we observed that distinct progenitors and differentiated neurons are characterized by their unique requirements for protein synthesis rates.

We quantitatively evaluated translation rates using HPG-labeling of newly synthesized proteins in the cell and showed Ire1α-dependent control of protein synthesis during cortical development (Fig. 24,26). This control is exerted through the stimulation of expression of translation regulators. In the case of Ire1α loss, the decrease in translation rates is due to slower elongation and translocation of ribosomes, as well as a decrease in the number of translation sites (Fig. 28,29).

On top of Ire1α action as a classical regulator of UPR, the molecule has an Xbp1-dependent role in pathways associated with energy metabolism, angiogenesis and cell differentiation (Hetz C. et al., 2015). In our study, we demonstrated that the role of Ire1α in the regulation of protein synthesis is Xbp1-independent (Fig. 19). Therefore, we can hypothesize that the role of Ire1 in the cell is more extensive than previously assumed and is associated not only with the regulation of UPR.

Urra H. et al. demonstrated non-canonical UPR-independent role of Ire1α in cortical development (Urra H. et al., 2018). Filamin A has been identified as an essential partner of Ire1α. Ire1α recruits filamin A, thereby controlling cell migration. Ire1α was previously shown to regulate cytoskeletal dynamics and cell movement in zebrafish and Drosophila, suggesting that this mechanism is conservative. In IRE1α(Ern1)-null animals the radial migration of neurons during cortical development was disrupted, which imitates periventricular nodular heterotopia. This syndrome is characterized by clusters of neurons ectopically positioned along the wall of the lateral ventricles, and associated with the loss of filamin A. Upon dimerization of Ire1 on the ER membrane, it acts as a scaffold to incorporate filamin A signaling to control the actin cytoskeleton dynamics. In our study, we similarly showed a UPR-independent role of Ire1α in neuronal migration and cell fate determination.

Furthermore, we showed that *Ire1α* KO leads to a delay in neuronal migration, but we also demonstrated that this delay only takes place at later developmental stages in Satb2-positive neurons. Importantly, we demonstrated a new molecule eEF-2, which is involved in Ire1α-dependent regulation of migration (Fig. 22). Therefore, we showed an entirely new mechanism of neuronal migration regulation that involves Ire1α-dependent translation regulation. For Ire1α OE in the early stages of

development (E12.5), we observed impaired cell migration as well as an increase in the number of Satb2-positive cells (Fig. 6). These data also support the idea that impaired migration occurs in Satb2-positive neurons. Also, based on the data that Ire1α acts as a scaffold for filamin A only when it is in the dimer state. We can assume that in the case of Ire1α OE an excessive amount of protein is located on the ER membrane, which may cause spontaneous dimerization and disruption of clustering. These changes can lead to alteration of cytoskeleton remodeling and, due to autophosphorylation through the cytoplasmic kinase domain, induce activation of the UPR.

By analyzing the interactome of Ire1α, its close interaction with the translation machinery and protein targeting mechanism was shown. In particular, it was demonstrated to interact with the components of the translational mechanism: translocon, SRP proteins and ribosomal proteins, which suggests that Ire1α is located in close proximity to ribosomes integrated into the ER membrane via translocon. Analysis of the crystal structure showed that cytosolic domains of Ire1α interact with 80S ribosomes with high affinity (Acosta-Alvear D. et al., 2018). Altogether, Ire1α is found to affect protein synthesis during corticogenesis with a high probability. We also showed an enhanced interaction of Ire1α with the small subunit of the ribosome at E12.5 stage, when neuronal progenitors have multipotency to generate neurons of different layers and when neuronal fate can be regulated. Thereby, we showed that the strength of the interaction between Ire1α and RPS6 is dynamically regulated during development. The stronger association between Ire1α and the ribosome in the early stages of development may indicate that translation regulation occurs to the most extent at this stage (E12.5). Since we showed the interaction of Ire1α with RPS6, which is part of the 40S initiating complex during translation, and the interaction of Ire1α with the translocon was also demonstrated (Sundaram A. et al., 2017), we can hypothesize that Ire1α is involved in the recruitment of ribosomes from the cytoplasm for further synthesis on the ER membrane via the translocon.

Moreover, it was shown that both BiP and Sec61 translocons are required to stabilize Ire1α in the inactive state as an activator of UPR. However, BiP is released under stress conditions (Aragón T. et al., 2009), whereas Sec61 remains bound even during stress (Sundaram A. et al., 2017). We can suggest that through the interaction of Ire1α with the translocon the regulation of UPR also occurs, for instance, there may be a decrease in the recruitment of ribosomes from the cytoplasm to the ER membrane, thereby reducing ER loading.

Factor eEF-2 is an essential participant in the elongation stage of translation and mediates ribosome translocation. In the case of Ire1α loss, we observed increased levels of active eEF-2 and decreased levels of inactive phosphorylated eEF-2PThr56. However, we also observed an accumulation of actively translating ribosomes on mRNA and decreased elongation rates, which may indicate the presence of another mechanism regulating ribosome translocation involving Ire1α.

Alteration or modification of individual components of translation machinery in the cell can lead to the development of serious diseases. For example, the RNA-binding protein TDP-43 is associated with the development of neurodegenerative diseases such as Amyotrophic Lateral Sclerosis and Frontotemporal Dementia. It has been shown that TDP-43 in motor neurons binds directly to ribosomes as well as to mRNA, causing an intensification of their translation. TDP-43 acts as a specific activator of mRNA translation, including mRNA of genes associated with neurodegeneration (Neelagandan N. et al., 2019). Ire1 and TDP-43 have similar phenotypes: both proteins are characterized by interaction with ribosomes and translation regulation factors, thereby affecting the intensity of translation.

In Rett syndrome, which is characterized by cerebral hypoplasia and progressive cerebellar atrophy, there is a global reduction in protein synthesis, by inhibition at the initiation stage (Rodrigues D.C. et al., 2020). In Alzheimer's disease was observed a decrease in mRNA translation due to increased levels of phosphorylated initiation factor eIF2α, which inhibits the global protein synthesis (Meyer K. et al., 2019). We demonstrated in this study that the levels of active eIF2α as well as inactive phosphorylated eIF2α (eIF2αPSer51) were not different in control and *Ire1α* KO (Fig. 19). This indicates that this factor is not involved in Ire1α-dependent translation regulation. At the same time, phosphorylation of eIF2α and thereby inhibition of its activity is a characteristic of another UPR regulator, PERK (Samuel C.E., 1979). Moreover, homozygous mutations in any of the EIF2B subunits cause leukoencephalopathy, a syndrome characterized by loss of astrocytes, oligodendrocytes, and axons (Bugiani M. et al., 2010). Studies in mouse models of disease suggest that chemicals that enhance eIF2 activity can be used to treat taupathy and Alzheimer's disease (Halliday M. et al., 2017). According to the literature, IRE1 deficiency completely restores memory and learning ability in AD mice by reducing protein expression and improving synaptic function (Duran-Aniotz C. et al., 2017). Taking into account the lack of alterations in the level of eIF2α expression in *Ire1α* KO compared to controls and the ER stress condition observed in AD, we can conclude that in the pathogenesis of AD the role of Ire1α is not related to the regulation of translation in particular through eIF2α, but rather mediated by the regulation of UPR.

The dysregulation of ribosome stalling during elongation can lead to neurological diseases. For example, using screening after ENU mutagenesis was identified GTP-binding protein 2 (GTPBP2) that regulates ribosome stalling at the AGA codon and is associated with a spontaneous ataxia-like neurodegenerative syndrome (Ishimura R. et al., 2014). Mutations in mRNA-binding proteins can also lead to pathological changes: in survival motor neuron (SMN) to spinal muscular atrophy (Gabanella F. et al., 2016); in fused in sarcoma (FUS) to motor and cognitive deficits (López-Erauskin J. et al., 2018); in ataxin-2 to spinocerebellar ataxia type 2 and amyotrophic lateral sclerosis (Fittschen M. et al., 2015). Fragile X mental retardation 1 (FMR1) regulates ribosome stalling, and loss of this gene is the cause of mental

retardation in fragile X syndrome (FXS) [Willemsen R. et al., 2011]. Huntingtin (mHTT) has been shown to promote ribosome stalling during elongation in striatum neurons. Loss of chantingtin leads to defects in corticostriatal development and age-dependent neurodegeneration (Eshraghi M. et al., 2021).

Altogether, dysregulation of translation at different levels may be a common mechanism for various neurological diseases.

6.2. Ire1α and polarity of the neuron

The endoplasmic reticulum has been shown to be involved in the formation of neuronal morphology by interacting with microtubules in addition to protein synthesis. The axon contains ER tubules, which are stabilized by microtubules, while ER cisterns are localized in the somatosensory region of the cell. During the establishment of bipolar neuron morphology, ER tubules translocate into a single neurite, which initiates its specification as an axon. Therefore, the existence of feedback between ER and microtubules regulates neuronal morphology (Farías G.G. et al., 2019). In the case of Ire1α loss, mislocalization of ER relative to the axon was shown (Fig. 14). We also showed that in *Ire1α* KO axonal markers have somatic localization, which may indicate the absence of crosstalk between ER and microtubules.

We can hypothesize that the loss of *Ire1α* initially results in the mislocalization of ER. Therefore, in the case of *Ire1α* KO, the protein lacks a cytoplasmic domain, which prevents it from acting as a scaffold for microtubules. Since microtubules have been shown to be a major determinant in the formation and maintenance of neuronal polarity, the polarized microtubule network acts as a foundation for selective axonal and dendritic transport (van Beuningen S.F.B. and Hoogenraad C.C., 2016). Hence, in the absence of control of microtubule organization by Ire1α, no basis for selective transport of proteins, such as for Tau-1, Ankyrin G, and Pan, is formed; because of the mislocalization of these markers, the axon initiating segment and subsequent axon specification do not occur. Since one of the neurites does not specialize as an axon, the other neurites do not get a dendritic identity either. How to call such neurites, which are actually neither axons nor dendrites, remains an open question.

We have shown that translation blocking with CHX leads to the same changes as in *Ire1α* KO and *eIF4A1* KO (loss of *Satb2* expression and mislocalization of axonal markers). The effects detected were more pronounced as a global synthesis blockade occurred (Fig. 34, 35). The findings suggest that the involvement of Ire1α and the presence of high translation rates in neuronal progenitors are necessary for the formation of upper layer neurons.

Cycloheximide (CHX) is an inhibitor of protein synthesis; it blocks translation at the elongation stage by binding to the ribosome and inhibiting eEF-2-mediated

translocation (Schneider-Poetsch T. et al., 2010). Initially, we assumed that such global inhibition of translation by CHX would lead to neuronal death. However, instead we observed a phenotype similar to *Ire1α* KO: neurons became unpolarized and lost Satb2 identity. Inhibition of translation by CHX, as well as loss of *Ire1α* leads to ribosome accumulation on mRNA, in the case of CHX at the start codon region (Ingolia N.T. et al., 2011). Therefore, we can once again emphasize the importance of a high translation rate for the acquisition of Satb2-identity by the neuron. We can also assume that when translation is inhibited by CHX or Ire1α loss, ER invasion into the axon does not occur, which affects protein sorting and prevents the factors required for axon initiation from being directed into a single neurite. This is also confirmed by the accumulation of Tau-1 in the soma of the neurons, and explains the phenotype with the absence of a specialized axon.

Prokaryotes have no cell compartmentalization and protein translation occurs in the cytoplasm. Protein synthesis is carried out in eukaryotes mainly by ribosomes attached to the ER membrane. We have shown that Ire1α is involved in the control of translation in neurons during development. According to the literature, Ire1α-dependent activation of UPR appeared first during evolution and is highly conserved. Based on these data, we can assume that Ire1α appeared as an evolutionary buildup in eukaryotes and participates in the comprehensive regulation of protein synthesis: at the initiation stage via eIF4A1, at the recruitment of ribosomes to the ER membrane, at the elongation stage via eEF-2, monitoring ER stress state and UPR activation.

6.3. Regulation of Satb2 in the cortex

During cortical development, there is a requirement for rapid and efficient protein synthesis and rearrangement of the proteome, which leads proteostasis to a state close to the stress state. Therefore, it can be assumed that the same factors are involved in the regulation of these processes as those involved in the activation of the stress state. During corticogenesis, Ire1α regulates translation processes by providing high translation rates in multipotent progenitors of upper-layer neurons, initiating the translation program of Satb2 in their progeny.

We have shown that the phenotype associated with the fate in *Ire1a* cKO coincides with the phenotype of *Satb2* KO (Britanova O. et al., 2008). In both cases, there is a decrease in the number of Satb2-positive neurons due to an increase in the number of deeper layer neurons (Figs. 5, 9). Satb2 serves as a postmitotic determinant of upper layer neuronal cell fate, and genetic deletion of *Satb2* disturbs the formation of upper layers and results in the absence of the *corpus callosum*. In the case of *Satb2* loss, the neurons had shorter axons, but nevertheless, the cells

were polarized. Therefore, we can assume that the acquisition of the determinants of neuronal fate and its morphology are independent processes but implicated in one general process - the determination of neuron fate, which also includes the concept of connectivity. The absence of such connection is also confirmed by the experiment with *Ire1α* KO at stage E14.5 using IUE (Fig. 10). There was no change in the aquisition of cell fate determinants in this case, but we observed an altered neuronal morphology.

Early neuronal progenitors are multipotent and capable of generating neurons of upper and deeper layers; as the cells develop, they lose the ability to generate cells of different layers and give rise to progeny expressing Satb2. When Ire1α is lost, we did not observe such a switch (Fig. 9). Examination of the molecular signature of IRE1 activity showed that activation of IRE1 leads to a decrease in the expression of such transcription factors typical for stem cells as SOX2, SALL2, POU3F2 and OLIG2 (Doultsinos D. et al., 2019).

6.4. eIF4A1 interplay with Satb2

We found that during cortical development, a dramatic jump in translation rates occurs during the transition from early multipotent progenitors to late progenitors. We hypothesized that this creates the necessary molecular background for eIF4A1 to preferentially unwind the secondary structures of the 5'UTR of the transcription factor Satb2.

Previously, it has been shown that an elegant multistep regulation of transcription factors takes place during cortical development (Nowakowski T.J. et al., 2017; Telley L. et al., 2019). The structure of 5'UTR has also been shown to play a critical role in translation efficiency and proteome formation. This structure is responsible for recruiting ribosomes to mRNA and also determines the choice of the start codon (Hinnebusch A.G. et al., 2016).

During translation initiation, ribosomes have a weak ability to unfold secondary mRNA structures (Takyar S. et al., 2005), whereas eIF4A1 is able to unfold even stable secondary structures in 5'UTR during mRNA scanning (Svitkin Y.V. et al., 2001; Pestova T.V. and Kolupaeva V.G., 2002; Sonenberg N. and Hinnebusch A.G., 2009). Given the fact that we have shown that the loss of both Ire1α and eIF4A results in the loss of Satb2 identity, but an increase in the number of cells expressing CTIP2 (Fig. 5, 22). Therefore, we can hypothesize that there is a redistribution of ribosomes during translation based on the structure of their 5'UTRs, and that this process is regulated by eIF4A.

Using bioinformatic analysis, we showed that 5'UTR of Satb2 has a more complex secondary structure compared to CTIP2 (Fig. 36). It has been shown that the

distinctive features of eIF4A-dependent transcripts are the presence of G-quadruplexes in the 5'UTR (Wolfe A.L. et al., 2014).

Altogether, eIF4A1 performs time-limited regulation of translation of cell fate determinants based on the structure of their 5'UTR, acting downstream of Ire1α.

6.5. ENU mutagenesis as a tool for identifying novel genes involved in epileptogenesis

Recent studies demonstrated that genomic screening after ENU mutagenesis in mice is an effective tool to investigate the function of mammalian genes under normal and pathological conditions. In this study, we showed the effectiveness of the screening method that was developed to be effective in detecting the propensity for seizures induced by an audiogenic stimulus. ENU is an effective chemical mutagen causing point mutations in the coding or splice regions. ENU causes a wide range of effects on the mutated gene. The combination of mutagenesis and relevant selection based on phenotypic traits makes ENU mutagenesis an effective tool for identifying genes involved in the formation of a pathological condition and creating mouse models based on this. We found nine mouse lines with epileptiform activity after screening using the AGS assay.

The Amplification Refractory Mutation System PCR (ARMS-PCR) has been shown to be one of the most accurate tools in genetic disease diagnosis and mutation mapping (Caruana G. et al., 2013; Ehnert S. et al., 2019). Using ARMS-PCR and SNP panel we created, the homozygosity locus on chromosome 8 was determined (Fig. 44). By DNA sequencing, we detected a point mutation in the Unk5d gene in this region. Based on genome analysis of patients with focal epilepsy, it was previously shown that UNK5D is a potential candidate involved in epileptogenesis (Vlaskamp D. et al., 2017).

GABA is the main inhibitory neurotransmitter in the brain, which balances the excitatory component. When an excitation/inhibition imbalance occurs, seizures develop. According to the literature, GABA plays an important role in epileptogenesis and is also used in the treatment of epilepsy. Many animal models of epilepsy show impaired GABAergic function (Horton R.W. et al., 1982; Olsen R.W. et al., 1986). In studies of brain tissue of patients with epilepsy, a decrease in GABA in the cerebrospinal fluid and a decrease in GABA-mediated inhibition were found (Johnson E.W. et al., 1992). GABA antagonists cause seizures, while GABA agonists are powerful anticonvulsants (Macdonald R.L., 1983). In our study, we found an increased number of GABAergic neurons, which can lead to the E/I imbalance and cause seizures (Fig. 42).

The neurotrophic cytokine S100β, produced by astrocytes, causes an increase in intracellular calcium in neurons and promotes neurite growth. At the same time, in epilepsy there is a disruption of calcium homeostasis and sprouting of neurites. In patients with epilepsy, an increase in S100β has been shown in specific brain regions (Griffin W.S.T. et al., 1995). In the S8-3 mouse line we found an increase in the number of S100β astrocytes in the area receiving afferent inputs from layer III neurons of the cerebral cortex – SLM region of the hippocampus (Fig. 43). These data suggest the involvement of cytokine S100β in epileptogenesis.

7. References

Acosta-Alvear D., Karagöz G.E., Fröhlich F., Li H., Walther T.C., Walter P. The unfolded protein response and endoplasmic reticulum protein targeting machineries converge on the stress sensor IRE1. 2018. eLife. Vol. 7.

Adams C.J., Kopp M.C., Larburu N., Nowak P.R., Ali M.M.U. Structure and Molecular Mechanism of ER Stress Signaling by the Unfolded Protein Responce Signal Activator IRE1. 2019. Front Mol. Biosci. Vol. 6:11.

Ambrozkiewicz M.C., Bessa P., Salazar-Lázaro A., Salina V., Tarabykin V. Satb2(Cre/+) mouse as a tool to investigate cell fate determination in the developing neocortex. 2017. J. Neurosci. Methods. Vol. 291. P. 113–121.

Ambrozkiewicz M.C., Borisova E., Schwark M., Ripamonti S., Schaub T., et al. The murine ortholog of Kaufman oculocerebrofacial syndrome protein Ube3b regulates synapse number by ubiquitinating Ppp3cc. Molecular Psychiatry. 2020. Vol. 26. P. 1980–1995.

Ambrozkiewicz M.C., Schwark M., Kishimoto-Suga M., Borisova E., et al. Polarity Acquisition in Cortical Neurons Is Driven by Synergistic Action of Sox9-Regulated Wwp1 and Wwp2 E3 Ubiquitin Ligases and Intronic miR-140. Neuron. 2018. Vol. 5. P. 1097-1115.

Andreou A.Z., Harms U., Klostermeier D. Single-stranded regions modulate conformational dynamics and ATPase activity of eIF4A to optimize 5'-UTR inwinding. 2019. Nucleic Acids Res. Vol. 47(10). P. 5260-5275.

Aragón T., van Anken E., Pincus D., Serafimova I.M., Korennykh A.V., Rubio C.A., Walter P. Messenger RNA targeting to endoplasmic reticulum stress signalling sites. 2009. Nature. Vol. 457(7230). P. 736-740.

Araque A., Carmignoto G., Haydon P.G., Oliet S.H., Robitaille R., Volterra A. Gliotransmitters travel in time and space. 2014. Neuron. Vol. 81. P. 728–739.

Asano S.M., Gao R., Wassie A.T., Tillberg P.W., Chen F. and Boyden E.S. Expansion Microscopy: Protocols for Imaging Proteins and RNA in Cell and Tissue. Current Protocols in Cell Biology. 2018; 80.

Ayala R., Shu T., Tsai L.-H. Trekking across the Brain: The Journey of Neuronal Migration. 2007. Cell. Vol. 128(1). P.29-43.

Badawy R.A.B., Freestone D.R., Lai A., Cool M.J. Epilepsy: Ever-changing states of cortical excitability. 2012. Neuroscience. Vol. 222. P. 89-99.

Bandler R.C., Vitali I., Delgado R.N., Ho M.C., Dvoretskova E., Molinas J.S.I., Frazel P.W., Mohammadkhani M., Machold R., Maedler S., Liddelow S.A., Nowakowski T.J., Fishell G., Mayer C. Single-cell delineation of lineage and genetic identity in the mouse brain. 2021. Nature. Vol. 601. P. 404-409.

Barbosa C., Peixeiro I., Romão L. Gene expression regulation by upstream open reading frames and human disease. 2013. PLoS Genet. Vol. 9.

Barkovich A.J., Guerrini R., Kuzniecky R.I., Jackson G.D., Dobyns W.B. A developmental and genetic classification for malformations of cortical development: update 2012. 2012. Brain. Vol. 135. P. 1348-1369.

Barnes A.P. and Polleux F. Establishment of axon-dendrite polarity in developing. 1010 neurons. 2009. Annu. Rev. Neurosci. Vol. 32. P. 347–381.

Beatty K.E. and Tirrell D.A. Two-color labeling of temporally defined protein populations in mammalian cells. 2008. Bioorg Med Chem Lett. Vol. 18. P. 5995–5999.

Biever A., Glock C., Tushev G., Ciirdaeva E., Dalmay T., Langer J.D. and Schuman E.M. Monosomes actively translate synaptic mRNAs in neuronal processes. 2020. Science. Vol. 367.

Bochman M.L., Paeschke K., Zakian V.A. DNA secondary structures: stability and function of G-quadruplex structures. 2012. Nat Rev Genet. Vol. 13. P. 770-780.

Boitard M., Bocchi R., Egevari K., Petrenko V., Viale B., Gremaund E., Salmon P., Kiss J.Z. Wnt Signaling Regulates Multipolar-to-Bipolar Transition of Migrating Neurons in the Cerebral Cortex. 2015. Cell Reports. Vol. 10(8). P. 1349-1361.

Bonnefont J. and Vanderhaeghen P. Neuronal fate acquisition and specification: time for a change. 2021. Curr Opin Neurobiol. Vol. 66. P. 195-204.

Borisova E.V., Epifanova E.A., Tutukova S.A., Belousova I.I., Zhidkova N.M., Rusanova A.M., Salina V.A., Turovsky E.A., Turovskaya M.V., Tarabykin V.S., Babaev A.A. Identification of novel mutations controlling cerebral cortex malformations caused by ENU-induced mutagenesis in the mouse. 2018. Modern technologies in medicine. Vol. 10(3). P. 70-76.

Borisova E.V., Turovsky E.A., Turovskaya M.V., Tomilin A.N., Nedospasov S.A., Tarabykin V.S. ENU mutagenesis as a tool for identifying novel mouse models of epilepsy. 2021. Opera Medica et Physiologica. Vol. 8(1). P. 5-11.

Bozzi Y., Casarosa S., Caleo M. Epilepsy as a Neurodevelopmental Disorder. 2012. Front Psychiatry. Vol. 3. P. 1-14.

Braakman I., Hebert D.N. Protein folding in the endoplasmic reticulum. 2013. Cold Spring Harb Perspect Biol. Vol. 5(5).

Brandman O. and Hegde R.S. Ribosome-associated protein quality control. 2016. Nat. Struct. Mol. Biol. Vol. 23. P. 7–15.

Britanova O., de Juan Romero C., Cheung A., Kwan K.Y., Schwark M., Gyorgy A., Vogel T., Akopov S., Mitkovski M., Agoston D., et al. Satb2 is a postmitotic determinant for upper-layer neuron specification in the neocortex. 2008. Neuron. Vol. 57. P. 378–392.

Buchan J.R. and Stansfield I. Halting a cellular production line: responses to ribosomal pausing during translation. 2007. Biol. Cell. Vol. 99. P. 475-487.

Bugiani M., Boor I., Powers J.M., Scheper G.C., van der Knaap M.S. Leukoencephalopathy with vanishing white matter: A review. 2010. J. Neuropathol. Exp. Neurol. Vol. 69. P. 987-996.

Busquets Garcia A., Soria-Gomez E., Bellocchio L., Marsicano G. Cannabinoid Receptor Type-1: Breaking the Dogmas. 2016. F1000Res. Vol. 5.

Cardenas A. and Borrell V. Molecular and cellular evolution of corticogenesis in amniotes. 2019. Cell. Mol. Life Sci. Vol. 77. P. 1435-1460.

Carlberg U., Nilsson A. and Nygård O. Functional Properties of Phosphorylated Elongation Factor 2. 1990. Eur. J. Biochem. Vol. 191. P. 639–645.

Caruana G., Farlie P.G., Hart A.H., Bagheri-Fam S., Wallace M.J., Dobbie M.S., Gordon C.T., Miller K.A., Whittle B., Abud H.E., Arkell R.M., Cole T.J., Harley V.R., Smyth I.M., Bertram J.F. Genome-Wide ENU Mutagenesis in Combination with High Density SNP Analysis and Exome Sequencing Provides Rapid Identification of Novel Mouse Models of Developmental Disease. 2013. PLoS One. Vol. 8(3).

Caviness V.S. and Takahashi T. Proliferative events in the cerebral ventricular zone. 1995. Brain Dev. Vol. 17. P. 159–163.

Chen Q., Zhu Y.-C., Yu J., Miao S., Zheng J., Xu L., Zhou Y., Li D., Zhang C., Tao J., Xiong Z.-Q. CDKL5, a Protein Associated with Rett Syndrome, Regulates Neuronal Morphogenesis via Rac1 Signaling. 2010. J. Neurosci. Vol. 30(38). P. 12777-12786.

Clapham D.E. Calcium signaling. 2007. Cell. Vol. 131(6). P. 1047–1058.

Coelho D.S. and Domingos P.M. Physiological roles of regulated Ire1 dependent decay. 2014. Front Genet. Vol. 5.

Colasante G., Collombat P., Raimondi V., Bonanomi D., Ferrari C., Maira M., Yoshikawa K., Mansouri A., Valtorta F., Rubenstein J.L., Broccoli V. Arx Is a Direct Target of Dlx2 and Thereby Contributes to the Tangential Migration of GABAergic Interneurons. 2008. J Neurosci. Vol. 28(42). P. 10674-10868.

Cooper J.A. Mechanisms of cell migration in the nervous system. 2013. Cell Biology in Neuroscience. Vol. 202 (5). P. 725-734.

Cooper J.A. Molecules and mechanisms that regulate multipolar migration in the intermediate zone. 2014. Front Cell Neurosci. Vol. 8. P. 1-11.

Corazzari M., Gagliardi M., Fimia G.M., Piacentini M. Endoplasmic Reticulum Stress, Unfolded Protein Response, and Cancer Cell Fate. 2017. Front. Oncol. Vol. 7(78).

Coulter D.A. and Steinhäuser C. Role of Astrocytes in Epilepsy. 2015. Cold Spring Harb Perspect Med. Vol. 5(3).

Covan L. The epidemiology of the epilepsies in children. Ment Retard Dev Disabil Res Rev. 2002. Vol. 8(3). P. 171-181.

Cox J.S. and Walter P. A novel mechanism for regulating activity of a transcription factor that controls the unfolded protein response. 1996. Cell. Vol. 87. P. 391-404.

Dalic L. and Cook M.J. Managing drug-resistant epilepsy: challenges and solutions. 2016. Neuropsychiatr Dis Treat. Vol. 12. P. 2605-2616.

De Anda F.C., Meletis K., Ge X., Rei D., Tsai L.H. Centrosome motility is essential for initial axon formation in the neocortex. 2010. J. Neurosci. Vol. 30(31). P. 10391-10406.

DeBoer E.M., Kraushar M.L., Hart R.P. and Rasin M.-R. Posttranscriptional regulatory elements and spatiotemporal specification of neocortical stem cells and projection neurons. 2013. Neuroscience. Vol. 248. P. 499-528.

Dehay C. and Kennedy H. Cell-cycle control and cortical development. 2007. Nat. Rev. Neurosci. Vol. 8. P. 438–450.

Desai A.R. and McConnel S.K. Progressive restriction in fate potential by neural progenitors during cerebral cortical development. 2000. Development. Vol. 127(13). P. 2863-2872.

Deshaies R.J., Sanders S.L., Feldheim D.A., Schekman R. Assembly of yeast Sec proteins involved in translocation into the endoplasmic reticulum into a membrane-bound multisubunit complex.1991. Nature. Vol. 349(6312). P. 806–808.

Dever T.E. and Green R. The elongation, termination, and recycling phases of translation in eukaryotes. 2012. Cold Spring Harb. Perspect. Vol. 4.

Di Prisco G.V., Huang W., Buffington S.A., Hsu C.-C., Bonnen P.E., Placzek A.N., Sidrauski C., Krnjević K., Kaufman R.J., Walter P. et al. Translational control of mGluR-dependent long-term depression and object-place learning by eIF2α. 2014. Nat Neurosci. Vol. 17. P. 1073–1082.

Dieck T.S., Muller A., Nebring A., Hinz F.I., Bartnik I., Schuman E.M. and Dieterich D.C. Metabolic labeling with noncanonical amino acid and visualization by chemoselective fluorescent tagging. Curr Protoc Cell Biol. 2012; Chapter 7, Unit 7.11.

Dieterich D.C., Hodas J.J.L., Gouzer G., Shadrin I.Y., Ngo J.T., Triller A., Tirrell D.A., Schuman E.M. In situ visualization and dynamics of newly synthesized proteins in rat hippocampal neurons. 2010. Nat Neurosci. Vol. 13. P. 897–905.

Doultsinos D., McMahon M., Voutetakis K., Obacz J., Pineau R., Jouan F., Le Reste P., Obiedat A., Samal J., Patterson J.B., Zheng Q., Samali A., Pandit A., Tirosh B., Chatziioannou A., Chevet E., Avril T. Constitutive IRE1α signaling maintains glioblastoma cell differentiation. 2019. bioRxiv.

Duncan J.S., Sander J.W., Sisodiya S.M., Walker M.C. Adult epilepsy. 2006. Lancet. Vol. 367(9516). P. 1087-1100.

Duran-Aniotz C., Cornejo V.H., Espinoza S., Ardiles A.O., Medinas D.B., Salazar C., Foley A., Gajardo I., Thielen P., Iwawaki T., Scheper W., Soto C., Palacios A.G., Hoozemans J.J.M., Hetz C. IRE1 signaling exacerbates Alzheimer's disease pathogenesis. 2017. Acta Neuropathol. Vol. 134(3). P. 489-506.

Dwyer N.D., Chen B., Chou S.-J., Hippenmeyer S., Nguyen L., Ghashghaei H.T. Neural Stem Cells to Cerebral Cortex: Emerging Mechanisms Regulating Progenitor Behavior and Productivity. 2016. The Journal of Neuroscience. Vol. 36(45). P. 11394-11401.

Ehnert S., Linnemann C., Braun B., Botsch J., Leibiger K., Hemmann P., Nussler A.K. One-Step ARMS-PCR for the Detection of SNPs-Using the Example of the PADI4 Gene. 2019. Methods Protoc. Vol. 2(3):63.

Eid L., Lachance M., Hickson G., Rassignol E. Ex Utero Electroporation and Organotypic Slice Cultures of Embryonic Mouse Brains for Live-Imaging of Migrating GABAergic Interneurons. 2018. J Vis Exp. Vol. 134.

Endersby R. and Baker S.J. PTEN signaling in brain: neuropathology and tumorigenesis. 2008. Oncogene. Vol. 27. P. 5416-5430.

Eshraghi M., Karunadharma P.P., Blin J., Shahani N., Ricci E.P., Michel A., Urban N.T., Galli N., Sharma M., Ramírez-Jarquín U.N. et al. Mutant Huntingtin stalls ribosomes and represses protein synthesis in a cellular model of Huntington disease. 2021. Nat Commun. Vol. 12. P. 1461.

Evans A.J., Gurung S., Henley J.M., Nakamura Y., Wilkinson K.A. Exciting times: new advances towards understanding the regulation and roles of kainate receptors. 2017. Neurochem Res. Vol. 44(3). P. 572-584.

Fagone P. and Jackowski S. Membrane phospholipid synthesis and endoplasmic reticulum function. 2009. J Lipid Res. Vol. 50. P. 311–316.

Farías G.G., Fréal A., Tortosa E., Stucchi R., Pan X., Portegies S., Will L., Altelaar M., Hoogenraad C.C. Feedback-Driven Mechanisms between Microtubules and the Endoplasmic Reticulum Instruct Neuronal Polarity. 2019. Vol. 102(1). P. 184-201.

Fattorusso A., Matricardi S., Mencaroni E., DellÍsola G.B., Di Cara G., Striano P., Verrotti A. The Pharmacoresistant Epilepsy: An Overview on Existant and New Emerging Therapies. 2021. Front. Neurol. Vol. 12.

Finlay B.L. and Darlington R.B. Linked regularities in the development and evolution of mammalian brains. 1995. Science. Vol. 268. P. 1578–1584.

Fishell G. and Hanashima C. Pyramidal neurons grow up and change their mind. 2008. Neuron. Vol. 57. P. 333–338.

Fittschen M., Lastres-Becker I., Halbach M.V., Damrath E., Gispert S., Azizov M., Walter M., Müller S., Auburger G. Genetic ablation of ataxin-2 increases several global translation factors in their transcript abundance but decreases translation rate. 2015. Neurogenetics. Vol. 16. P. 181–192.

Fresno M., Jimenez A., Vazquez D. Inhibition of Translation in Eukaryotic Systems by Harringtonine. 1977. Eur. J. Biochem. Vol. 72. P. 323-330.

Gabanella F., Pisani C., Borreca A., Farioli-Vecchioli S., Ciotti M.T., Ingegnere T., Onori A., Ammassari-Teule M., Corbi N., Canu N., Monaco L., Passananti C., Di Certo M.G. SMN affects membrane remodelling and anchoring of the protein synthesis machinery. 2016. J Cell Sci. Vol. 129 (4). P. 804–816.

Gelman D.M. and Marín O. Generation of interneuron diversity in the mouse cerebral cortex: Interneuron diversity in cerebral cortex. 2010. Eur. J. Neurosci. Vol. 31. P. 2136–2141.

Gilmore R., Blobel G., Walter P. Protein translocation across the endoplasmic reticulum. Detection in the microsomal membrane of a receptor for the signal recognition particle. 1982. J Cell Biol. Vol. 95(2 Pt 1). P. 463–469.

Ginhoux F. and Guilliams M. Tissue-resident macrophage ontogeny and homeostasis. 2016. Immunity. Vol. 44. P. 439-449.

Ginhoux F., Greter M., Lebouef M., Nandi S., See P., Gokhan S., Mehler M.F., Conway S.J., Ng L.G., Stanley E.R., Samokhvalov I.M., Merad M. Fate mapping analysis reveals that adult microglia derive from primitive macrophages. 2010. Vol. 330. P. 841-845.

Gorski J.A., Talley T., Qiu M., Puelles L., Rubenstein J.L.R., Jones K.R. Cortical Excitatory Neurons and Glia, But Not GABAergic Neurons, Are Produced in the Exm1-Expressing Lineage. Journal of Neuroscience. 2002. Vol. 22(15). P. 6309-6314.

Götz M. and Huttner W.B. The cell biology of neurogenesis. 2005. Nat. Rev. Mol. Cell Biol. Vol. 6. P. 777-788.

Green M.R. and Sambrook J. Isolation of DNA from Mouse Tails without Extraction by Organic Solvents. 2018. Cold Spring Harb Protoc.

Greig L.C., Woodworth M.B., Galazo M.J., Padmanabhan H. and Macklis J.D. Molecular logic of neocortical projection neuron specification, development and diversity. 2013. Nat. Rev. Neurosci. Vol. 14. P. 755–769.

Griffin W.S.T., Yeralan O., Sheng J.G., Boop F.A., Mrak R.E., Rovnaghi C.R., Burnett B.A., Feoktistova A., Van Eldik L.J. Overexpression of the Neurotrophic Cytokine S100β in Human Temporal Lobe Epilepsy. 1995. J Neurochem. Vol. 65(1). P. 228–233.

Grinshtein N., Rioseco C.C., Marcellus R., Uehling D., Aman A., Lun X., Muto O., Podmore L., Lever J., Shen Y. et al. Small molecule epigenetic screen identifies novel EZH2 and HDAC inhibitors that target glioblastoma brain tumor-initiating cells. 2016. Oncotarget. Vol. 7. P. 59360–59376.

Guarnieri F.C., Chevigny A., Falace A., Cardoso C. Disorders of neurogenesis and cortical development. 2018. Dialogues Clin Neurosci. Vol. 20(4). P. 255-266.

Guerrini R. and Dobyns W.B. Malformations of cortical development: clinical features and genetic causes. 2014. Lancet Neurol. Vol. 13. P. 710-726.

Guerrini R. and Parrini E. Neuronal migration disorders. 2010. Neurobiol Dis. Vol. 38(2). P. 154-166.

Gutierrez E., Shin B.S., Woolstenhulme C.J., Kim J.R., Saini P., Buskirk A.R., Dever T.E. eIF5A promotes translation of polyproline motifs. 2013. Mol Cell. Vol. 51. P. 35–45.

Hafner A.-S., Donlin-Asp P.G., Leitch B., Herzog E. and Schuman E.M. Local protein synthesis is a ubiquitous feature of neuronal pre- and postsynaptic compartments. 2019. Science. Vol. 364.

Halliday M., Radford H., Zents K.A.M., Molloy C., Moreno J.A., Verity N.C., Smith E., Ortori C.A., Barrett D.A., Bushell M., Mallucci G.R. Repurposed drugs targeting eIF2α-P-mediated translational repression prevent neurodegeneration in mice. 2017. Brain. Vol. 140. P. 1768-1783.

Han W. and Šestan N. Cortical projection neurons: Sprung from the same root. 2013. Neuron. Vol. 80. P. 1103–1105.

Hatanaka Y., Hisanaga S., Heizmann C.W., Murakami F. Distinct migratory behavior of early- and late-born neurons derived from the cortical ventricular zone. 2004. J Comp Neurol. Vol. 479(1). P. 1-14.

Haubensak W., Attardo A., Denk W. Huttner W.B. Neurons arise in the basal neuroepithelium of the early mammalian telencephalon: a major site of neurogenesis. 2004. Proc. Natl. Acad. Sci. U. S. A. Vol. 101. P. 3196–3201.

He S., Li Z., Ge S., Yu Y.C., Shi S.H. Inside-Out Radial Migration Facilitates Lineage-Dependent Neocortical Microcircuit Assembly. 2015. Neuron. Vol. 86(5). P. 1159-1166.

Hebert D.N., Garman S.C., Molinari M. The glycan code of the endoplasmic reticulum: asparagine-linked carbohydrates as protein maturation and quality-control tags. 2005. Trends Cell Biol. Vol. 15(7). P. 364–370.

Henley J.M. and Wilkinson K.A. Synaptic AMPA receptor composition in development, plasticity and disease. 2016. Nat. Rev. Neurosci. Vol. 17. P. 337-350.

Hetz C., Chevet E., Oakes S.A. Proteostasis control by the unfolded protein response. 2015. Nat. Cell Biol. Vol. 17. P. 829–838.

Hinnebusch A.G. The scanning mechanism of eukaryotic translation initiation. 2014. Annu. Rev. Biochem. Vol. 83. P. 779-812.

Hinnebusch A.G., Ivanov I.P., Sonenberg N. Translational control by 5'-untranslated regions of eukaryotic mRNAs. 2016. Science. Vol. 352. P. 1413-1416.

Hirota Y. and Nakajima K. Control of Neuronal Migration and Aggregation by Reelin Signaling in the Developing Cerebral Cortex. 2017. Front. Cell Dev. Biol. Vol. 5:40.

Hoeffel G. and Ginhoux F. Ontogeny of tissue-resident macrophages. 2015. Front. Immunol. Vol. 6. P. 486.

Horton R.W., Prestwich S.A., Meldrum B.S. Gamma-aminobutyric acid and benzodiazepine binding sites in audiogenic seizure-susceptible mice. 1982. J Neurochem. Vol. 39. P. 864–870.

Huang G., Yao J., Zeng W., Mizuno Y., Kamm K.E., Stull J.T. et al. ER stress disrupts Ca2+-signaling complexes and Ca2+ regulation in secretory and muscle cells from PERK-knockout mice. 2006. J Cell Sci. Vol. 119. P. 153–161.

Huberfeld G., De La Pride L.M., Pallud J., Cohen L., Le Van Quyen M. et al. Glutamatergic pre-ictal discharges emerge at the transition to seizure in human epilepsy . Nat Neurosci. 2011. Vol. 14. P. 627-634.

Ingolia N.T., Lareau L.F., Weissman, J.S. Ribosome profiling of mouse embryonic stem cells reveals the complexity and dynamics of mammalian proteomes. 2011. Cell. Vol. 147. P. 789–802.

Ishimura R., Nagy G., Dotu I., Zhou H., Yang X.L., Schimmel P., Senju S., Nishimura Y., Chuang J.H., Ackerman S.L. Ribosome stalling induced by mutation of a CNS-specific tRNA causes neurodegeneration. 2014. Science. Vol. 345. P. 455-459.

Iwawaki T., Akai R., Yamanaka S., Kohno K. Function of IRE1 alpha in the placenta is essential for placental development and embryonic viability. PNAS. 2009. Vol. 106(39). P. 16657-16662.

Jabadoun D. Fate and freedom in developing neocortical circuits. 2017. Nat Commun. Vol.8.

Jackson R.J., Hellen C.U.T., Pestova T.V. The mechanism of eukariotic translation initiation and principles of its regulation. 2010. Vol. 11. P. 113-127.

Jacquemyn J., Cascalho A., Goodchild R.E. The ins and outs of endoplasmic reticulum-controlled lipid biosynthesis. 2017. Vol. 18(11). P. 1905-1921.

Jan C.H., Williams C.C., Weissman J.S. Principles of ER cotranslational translocation revealed by proximity-specific ribosome profiling. 2014. Science. Vol. 346(6210).

Jobe P.C. and Browning R.A. Mammalian models of genetic epilepsy characterized by sensory-evoked seizures and generalized seizure susceptibility. 2006. Model. seizures epilepsy. P. 261–271.

Johnson A.E. and van Waes M.A. The Translocon: a dynamic gateway at the ER membrane. 1999. Annu Rev Cell Dev Biol. Vol. 15. P. 799-842.

Johnson E.W., De Lanerolle N.C., Kim J.H. et al. “Central” and “peripheral” benzodiazepine receptors: opposite changes in human epileptogenic tissue. 1992. Neurology. Vol. 42. P. 811–815.

Kapur M., Monaghan C.E., Ackerman S.L. Regulation of mRNA Translation in Neurons—A Matter of Life and Death. 2017. Neuron. Vol. 96(13). P. 616-637.

Kennedy C.L. and O’Bryan M.K. N-ethyl-N-nitrosourea (ENU) mutagenesis and male fertility research. 2006. Human Reproduction Update. Vol. 12(3). P. 293-301.

Kharel P., Becker G., Tsvetkov V., Ivanov P. Properties and biological impact of RNA G-quadruplexes: from order to turmoil and back. 2020. Nucleic Acids Research. Vol. 48(22). P. 12534-12555.

Klinge S. and Woolford Jr. J.L. Ribosome assembly coming into focus. 2018. Nature Reviews Molecular Cell Biology. Vol. 20. P. 116-131.

Koester S.E. and O’Leary D.D. Connectional distinction between callosal and subcortically projecting cortical neurons is determined prior to axon extension. 1993. Dev. Biol. Vol. 160. P. 1–14.

Korennykh A.V., Egea P.F., Korostelev A.A., Finer-Moore J., Zhang C., Shokat K.M., Stroud R.M., Walter P. The unfolded protein response signals through high-order assembly of Ire1. 2009. Nature. Vol. 457(7230). P. 687-693.

Koromilas A.E., Lazaris-Karatzas A., Sonenberg N. mRNAs containing extensive secondary structure in their 5' non-coding region translate efficiently in cells overexpressing initiation factor eIF-4E. 1992. EMBO J. Vol. 11. P. 4153-4158.

Koutmou K.S., Schuller A.P., Brunelle J.L., Radhakrishnan A., Djuranovic S., Green R. Ribosomes slide on lysine-encoding homopolymeric A stretches. 2015. eLife. Vol. 4.

Kovacevic J., Maroteaux G., Schut D., Loos M., Dubey M., Pitsch J., Remmelink E., Koopmans B., Crowley J., Cornelisse L.N., Sullivan P.F., Schoch S., Toonen R.F., Stiedl O., Verhage M. Protein instability, haploinsufficiency, and cortical hyper-excitability underlie STXBP1 encephalopathy. 2018. Brain. Vol. 141(5). P. 1350-1374.

Kramer M.A. and Cash S.S. Epilepsy as a Disorder of Cortical Network Organisation. 2012. Neuroscientist. Vol. 18(4). P. 360-372.

Kraushar M.L., Krupp F., Harnett D., Turko P., Ambrozkiewicz M.C., Sprink T., Imami K., Günnigmann M., Zinnall U., Vieira-Vieira C.H., et al. Protein Synthesis in the Developing Neocortex at Near-Atomic Resolution Reveals Ebp1-Mediated Neuronal Proteostasis at the 60S Tunnel Exit. 2021. Molecular Cell. Vol. 81. P. 304-322.

Kriegstein A. and Alvarez-Buylla A. The glial nature of embryonic and adult neural stem cells. 2009. Annu. Rev. Neurosci. Vol. 32. P. 149-184.

Kriegstein A.R. and Noctor S.C. Patterns of neuronal migration in the embryonic cortex. 2004. Trends Neurosci. Vol. 27. P. 392-399.

Kwan P., Arzimanoglou A., Berg A.T., Brodie M.J., Allen Hauser W., Mathern G., Moshe S.L., Perucca E., Wiebe S., French J. Definition of drug resistant epilepsy: consensus proposal by the ad hoc Task Force of the ILAE Commission on Therapeutic Strategies. 2010. Epilepsia. Vol. 51(6). P. 1069-1077.

Lambert de Rouvroil C. and Goffinet A.M. Neuronal migration. 2001. Mechanisms of Development. Vol. 105 (1-2). P. 47-56.

Lee K.P.K., Dey M., Neculai D., Cao C., Dever T.E. and Sicheri F. Structure of the dual enzyme Ire1 reveals the basis for catalysis and regulation in nonconventional RNA splicing. 2008. Cell. Vol. 132. P. 89–100.

Lee S., Liu B., Lee S., Qian S.-B. Global mapping of translation initiation sites in mammalian cells at single-nucleotide resolution. 2012. PNAS. Vol. 109(37).

Lelouard H., Schmidt E.K., Camosseto V., Clavarino G., Ceppi M., Hsu H.-T., Pierre P. Regulation of translation is required for dendritic cell function and survival during activation. 2007. J Cell Biol. Vol. 179(7). P. 1427–1439.

León K., Boulo T., Musnier A., Morales J., Gauthier C., Dupuy L., Heyne S., Backofen R., Poupon A., Cormier P. et al. Activation of a GPCR leads to eIF4G

phosphorylation at the 5′ cap and to IRES-dependent translation. 2014. J. Mol. Endocrinol. Vol. 52.

Leventer R.J., Phelan E.M., Coleman L.T., Kean M.J., Jackson G.D., Harvey A.S. Clinical and imaging features of cortical malformations in childhood. 1999. Neurology. Vol. 53. P. 715-722.

Lin H., Walter P., Yen T.S.B. Endoplasmic Reticulum Stress in Disease Pathogenesis. 2008. Annu Rev Pathol. Vol. 3. P. 399-425.

Liu S.J., Nowakowski T.J., Pollen A.A., Lui J.H., Horlbeck M.A., Attenello F.J., He D., Weissman J.S., Kriegstein A.R., Diaz A.A., Lim D.A. "Single-cell analysis of long non-coding RNAs in the developing human neocortex". 2016. Genome Biol. Vol. 17(67).

Liu W., An D., Xiao J., Li J., Hao N., Zhou P. Malformations of cortical development and epilepsy: A cohort of 150 patients in western China. 2015. Seizure. Vol. 32. P. 92-99.

Lodato S. and Arlotta P. Generating neuronal diversity in the mammalian cerebral cortex. 2015. Annu Rev Cell Dev Biol. Vol. 31. P. 699-720.

López-Erauskin J., Tadokoro T., Baughn M.W., Myers B., McAlonis-Downes M., Chillon-Marinas C., Asiaban J.N., Artates J., Bui A.T., Vetto A.P., Lee S.K., Le A.V., Sun Y., Jambeau M., Boubaker J., Swing D., Qiu J., Hicks G.G., Ouyang Z., Fu X.-D., Tessarollo L., Ling S.-C., Parone P.A., Shaw C.E., Marsala M., Lagier-Tourenne C., Cleveland D.W. ALS/FTD-Linked Mutation in FUS Suppresses Intra-axonal Protein Synthesis and Drives Disease Without Nuclear Loss-of-Function of FUS. 2018. Neuron. Vol. 100(4). P. 816-830.

Lortie A., Plouin P., Chiron C., Delalande O., Dulac O. Characterisation of epilepsy in focal cortical dysplasia in infancy. 2002. Epilepsy Research. Vol. 51(1-2). P. 133-145.

Löscher W., Potschka H., Sisodiya S.M., Vezzani A. Drug Resistance in Epilepsy: Clinical Impact, Potential Mechanisms, and New Innovative Treatment Options. Pharmacol Rev. 2020. Vol. 72(3). P. 606-638.

Luzzati F. A hypothesis for the evolution of the upper layers of the neocortex through co-option of the olfactory cortex developmental program. 2015. Front. Neurosci. Vol. 9. P. 162.

Macdonald R.L. Mechanisms of anticonvulsant drug action. 1983. In: Pedley TA, Meldrum BS, eds. Recent advances in epilepsy I. Edinburgh: Churchill Livingstone. P. 1–23.

Mahmood T. and Yang P.-C. Western Blot: Technique, Theory, and Trouble Shooting. 2012. N Am J Med Sci. Vol. 4(9). P. 429-434.

Mamane Y., Petroulakis E., Martineau Y., Sato Y.A., Larsson O., Rajasekhar V.K., Sonenberg N. Epigenetic activation of a subset of mRNAs by eIF4E explains its effects on cell proliferation. 2007. PLoS One. Vol. 2.

Manno G.L., Siletti K., Furlan A., Gyllborg D., Vinsland E., Albiach A.M., Langseth C.M., Khven I., Lederer A.R., Dratva L.M., Johnson A., Nilsson M., Lönnerberg P., Linnarsson S. Molecular architecture of the developing mouse brain. 2021. Nature. Vol. 596. P. 92-96.

Manzin M.C. and Walsh C.A. What disorders of cortical development tell us about the cortex: one plus one does not always make two. 2011. Curr Opin Genet Dev. Vol. 21(3). P. 333-339.

Marín O. and Rubenstein J.L.R. Cell migration in the forebrain. 2003. Annu. Rev. Neurosci. Vol. 26. P. 441–483.

Marintchev A., Edmonds K.A., Marintcheva B., Hendrickson E., Oberer M., Suzuki C., Herdy B., Sonenberg N., Wagner G. Topology and regulation of the human eIF4A/4G/4H helicase complex in translation initiation. 2009. Cell. Vol. 136. P. 447-460.

Martínez G., Vidal R.L., Mardones P., Serrano F.G., Ardiles A.O., Wirth C., et al. Regulation of memory formation by the transcription factor XBP1. 2016. Cell Rep. Vol. 14. P. 1382–1394.

McTague A., Howell K.B., Cross J.H., Kurian M.A., Scheffer I.E. The genetic landscape of the epileptic encephalopathies of infancy and childhood. 2016. Lancet Neurol. Vol. 15(3). P. 304-316.

Metcalf M.G., Higuchi-Sanabria R., Garcia G., Tsui C.K., Dillin A. Beyond the cell factory: Homeostatic regulation of and by the UPRER. 2020. Science Advances. Vol. 6(29).

Meyer D.I., Krause E., Dobberstein B. Secretory protein translocation across membranes the role of the “docking protein’. 1982. Nature. Vol. 297(5868). P. 647–650.

Meyer K., Feldman H.M., Lu T., Drake D., Lim E.T., Ling K.-H., Bishop N.A., Pan Y., Seo J., Lin Y.-T., Su S.C., Church G.M., Tsai L.-H., Yankner B.A. REST and neural gene network dysregulation in iPSC models of Alzheimer’s disease. 2019. Cell Rep. Vol. 26. P. 1112-1127.

Migliore M. and Shepherd G.M. Opinion: an integrated approach to classifying neuronal phenotypes. 2005. Nat. Rev. Neurosci. Vol. 6. P. 810–818.

Miyata T. Asymmetric production of surface-dividing and non-surfacedividing cortical progenitor cells. 2004. Development. Vol. 131. P. 3133–3145.

Molnár Z. and Cheung A.F.P. Towards the classification of subpopulations of layer V pyramidal projection neurons. 2006. Neurosci. Res. Vol. 55. P. 105–115.

Molyneaux B.J., Arlotta P., Menezes J.R.L. and Macklis J.D. Neuronal subtype specification in the cerebral cortex. 2007. Nat. Rev. Neurosci. Vol. 8. P. 427–437.

Mori K., Ma W., Gething M.J., Sambrook J. A transmembrane protein with a cdc2+/CDC28-related kinase activity is required for signaling from the ER to the nucleus. 1993. Cell. Vol. 74. P. 743-756.

Nadarajah B., Brunstrom J.E., Grutzendler J., Wong R.O., Pearlman A.L. Two modes of radial migration in early development of the cerebral cortex. 2001. Nat. Neurosci. Vol. 4. P. 143-150.

Namba T., Kibe Y., Fanahashi Y., Nakamuta S., Takano T., Ueno T. et al. Pioneering Axons Regulate Neuronal Polarisation in the Developing Cerebral Cortex. 2014. Neuron. Vol. 81(4). P. 814-829.

Needs H.I., Henley B.S., Cavallo D., Gurung S., Modebadze T., Woodhall G., Henley J.M. Changes in excitatory and inhibitory receptor expression and network activity during induction and establishment of epilepsy in the rat Reduced Intensity Status Epilepticus (RISE) mode. 2019. Neuropharmacology. Vol. 158.

Neelagandan N., Gonnella G., Dang s., Janiesch P.C., Miller K.K., Küchler K., Marques R.F., Indenbirken D., Alawi M., Grundhoff A., Kurtz S., Duncan K.E. TDP-43 enhances translation of specific mRNAs linked to neurodegenerative disease. 2019. Nucleic Acids Res. Vol. 47(1). P. 341–361.

Neubauer C., Gillet R., Kelley A.C., Ramakrishnan V. Decoding in the absence of a codon by tmRNA and SmpB in the ribosome. 2012. Science. Vol. 335. P. 1366–1369.

Nishitoh H., Matsuzawa A., Tobiume K., Saegusa K., Takeda K. et al. ASK1 is essential for endoplasmic reticulum stress-induced neuronal cell death triggered by expanded polyglutamine repeats. 2002. Genes Dev. Vol. 16. P. 1345–1355.

Noctor S.C., Flint A.C., Weissman T.A., Wong W.S., Clinton B.K., Kriegstein A.R. Dividing precursor cells of the embryonic cortical ventricular zone have morphological and molecular characteristics of radial glia. 2002. J. Neurosci. Vol. 22. P. 3161–3173.

Noctor S.C., Martinez-Cerdeno V., Ivic L., Kriegstein A.R. Cortical neurons arise in symmetric and asymmetric division zones and migrate through specific phases. 2004. Nat Neurosci. Vol. 7(2). P. 136-144.

Noctor S.C., Martinez-Cerdeno V., Kriegstein A.R. Neural stem and progenitor cells in cortical development. 2007. Novartis Found. Symp. Vol. 288. P. 59-73.

Nowakowski T.J., Bhaduri A., Pollen A.A., Alvarado B., Mostajo-Radji M.A., Di Lullo E., Haeussler M., Sandoval-Espinosa C., Liu S.J., Velmeshev D. et al. Spatiotemporal gene expression trajectories reveal developmental hierarchies of the human cortex. 2017. Science. Vol. 358. P. 1318-1323.

Oakes S.A. and Papa F.R. The role of endoplasmic reticulum stress in human pathology. 2015. Annu Rev Pathol. Vol. 10. P. 173–194.

Ochiari W., Minobe S., Ogawa M., Miyata T. Transformation of pin-like ventricular zone cells into cortical neurons. 2007. Neuroscience Research. Vol. 57(2). P. 326-329.

Olsen R.W., Wamsley J.K., McCabe R.T. et al. Midbrain GABA receptor deficit in genetic animal models of epilepsy. 1986. In: Nistico G, Morselli PL, Lloyd KG, et al., eds. Neurotransmitters, seizures and epilepsy III. New York: Raven Press. P. 279–291.

Palmini A. Revising the classification of focal cortical dysplasias. 2011. Epilepsia. Vol. 52. P. 188-190.

Paoletti P., Bellone C., Zhou Q. NMDA receptor subunit diversity: impact on receptor properties, synaptic plasticity and disease. 2013. Vol. 14. P. 383-400.

Park S., Park J. M., Kim S., Kim J.-A., Shepherd J. D., Smith-Hicks C. L. et al. Elongation Factor 2 and Fragile X Mental Retardation Protein Control the Dynamic Translation of Arc/Arg3.1 Essential for mGluR-LTD. 2008. Neuron. Vol. 59. P. 70–83.

Pederick D.T., Homan C.C., Jaehne E.J., Piltz S.G., Haines B.P., Baune B.T., Jolly L.A., Hughes J.N., Gecz J., Thomas P.Q. Pcdh19 Loss-of-Function Increases Neuronal Migration In Vitro but is Dispensable for Brain Development in Mice. 2016. Scientific Reports. Vol. 6.

Perucca P. and Gilliam F.G. Adverse effects of antiepileptic drugs. 2012. The Lancet Neurology. Vol. 9. P. 792-802.

Pestova T.V., Kolupaeva V.G., Lomakin I.B., Pilipenko E.V., Shatsky N., Agol V.I., Hellen C.U. Molecular mechanisms of translation initiation in eucariotes. 2001. Proc Natt Acad Sci USA. Vol. 98(13). P. 7029-7036.

Polleux F. and Snider W. Initiating and Growing an Axon. 2010. Cold Spring Harb Perspect Biol. Vol. 2(4).

Prabhakar A., Choi J., Wang J., Petrov A., Puglisi J.D. Dynamic basis of fidelity and speed in translation: Coordinated multistep mechanisms of elongation and termination. 2017. Protein Sci. Vol. 26. P. 1352-1362.

Rakic P. Evolution of the neocortex: a perspective from developmental biology. Nat. Rev. Neurosci. 2009. Vol. 10. P. 724–735.

Rapoport T.A. Protein translocation across the eukaryotic endoplasmic reticulum and bacterial plasma membranes. 2007. Nature. Vol. 450(7170). P. 663–669.

Raza F., Waldron J.A., Quesne J.L. Translational dysregulation in cancer: eIF4A isoforms and sequence determinants of eIF4A dependence. 2015. Biochem. Soc. Trans., Vol. 43. P. 1227-1233.

Reid C.A., Berkovic S.F., Petrou S. Mechanisms of human inherited epilepsies. Prog Neurobiol. 2009. Vol. 87. P. 41-57.

Reid D.W., Nicchitta C.V. Diversity and selectivity in mRNA translation on the endoplasmic reticulum. 2015. Nat Rev Mol Cell Biol. Vol.16(4). P. 221–231.

Richter J.D. and Coller J. Pausing on Polyribosomes: Make Way for Elongation in Translational Control. 2015. Cell. Vol. 163(2). P. 292-300.

Rodrigues D.C., Mufteev M., Weatheritt R.J., Djuric U., Ha K.C.H., Ross P.J., Wei W., Piekna A., Sartori M.A., Byres L., Mok R.S.F., Zaslavsky K., Pasceri P., Diamandis P., Morris Q., Blencowe B.J., Ellis J. Shifts in Ribosome Engagement Impact Key Gene Sets in Neurodevelopment and Ubiquitination in Rett Syndrome. 2020. Cell Reports. Vol. 30(12). P. 4179-4196.

Rogers G.W. Jr., Lima W.F., Merrick W.C. Further characterization of the helicase activity of eIF4A. Substrate specificity. 2001. J. Biol. Chem. Vol. 276. P. 12598–12608.

Romero C.D.J. and Borrell V. Coevolution of radial glial cells and the cerebral cortex. 2015. Glia. Vol. 63(8). P. 1303-1319.

Saito T. In vivo electroporation in the embryonic mouse central nervous system. 2006. Nat Protoc. Vol. 1(3). P. 1552-1558.

Salinger A.P., Justice M.J. Mouse mutagenesis using N-Ethyl-N-Nitrosourea (ENU). CSH Protoc 2008. 2008. Vol. 5.

Salzer J.L. An unfolding role for ankyrin-G at the axon initial segment. 2019. PNAS. Vol. 116(39). P. 19228-19230.

Samuel C.E. "Mechanism of interferon action: Phosphorylation of protein synthesis initiation factor eIF-2 in interferon-treated human cells by a ribosome-associated kinase processing site specificity similar to hemin-regulated rabbit reticulocyte kinase". 1979. Proc Natl Acad Sci USA. Vol. 76(2). P. 600–604.

Sasaki S., Tabata H., Tachikawa K., Nakajima K. The cortical subventricular zone-specific molecule Svet1 is part of the nuclear RNA coded by the putative netrin receptor gene Unc5d and is expressed in multipolar migrating cells. 2008. Mol Cell Neurosci. Vol. 38(4). P. 474-483.

Schmidt E.K., Clavarino G., Ceppi M., Pierre P. SUnSET, a nonradioactive method to monitor protein synthesis. 2009. Nature Methods. Vol. 6. P. 275–277.

Schneider-Poetsch T., Ju J., Eyler D.E., Dang Y., Bhat S., Merrick W.C., Green R., Shen B., Liu J.O. Inhibition of Eukaryotic Translation Elongation by Cycloheximide and Lactimidomycin. 2010. Nat Chem Biol. Vol. 6(3). P. 209–217.

Schubert D., Kötter R. and Staiger J. F. Mapping functional connectivity in barrel-related columns reveals layer- and cell type-specific microcircuits. Brain Struct. Funct. 2007. Vol. 212. P. 107–119.

Schwarz D.S. and Blower M.D. The endoplasmic reticulum structure, function and response to cellular signaling. 2016. Cell Mol Life Sci. Vol. 73. P. 79-94.

Shan S., Schmid S.L., Zhang X. Signal recognition particle (SRP) and SRP receptor: A new paradigm for multi-state regulatory GTPases. 2009. Biochemistry. Vol. 48(29). P. 6696-6704.

Shao L.-R., Habela C.W., Stafstrom C.E. Pediatric Epilepsy Mechanisms: Expanding the Paradigm of Excitation/Inhibition Imbalance. Children (Basel). 2019. Vol. 6(2). P. 23.

Shen J., Chen X., Hendershot L., Prywes R. ER stress regulation of ATF6 localization by dissociation of BiP/GRP78 binding and unmasking of Golgi localization signals. 2002. Dev Cell. Vol. 3(1). P. 99–111.

Sieghart W. and Savic M.M. International union of basic and clinical pharmacology. CVI: GABAA receptor subtype- and function-selective ligands: key issues in translation to humans. 2018. Pharmacol. Rev. Vol. 70. P. 836-878.

Sirven J.I. Epilepsy: A Spectrum Disorder. 2015. Cold Spring Harb Perspect Med. Vol. 5(9).

Sisodiya S.M. Malformations of cortical development: burdens and insights from important causes of human epilepsy. 2004. Lancet Neurol. Vol. 3. P. 29-38.

Sonenberg N. and Hinnebusch A.G. Regulation of Translation Initiation in Eukaryotes: Mechanisms and Biological Targets. 2009. Cell. Vol. 136(4). P. 731-735.

Staiger E.A., Tseng C.T., Miller D., Cassano J.M., Nasir L., Garrick D., Brooks S.A., Antczak D.F. Host genetic influence on papillomavirus-induced tumors in the horse. 2016. International Journal of Cancer. Vol. 139(4). P. 784-792.

Stottman R. and Beier D.R. ENU mutagenesis in the mouse. Curr Protoc Hum Genet. 2014. Vol.82. P. 1-10.

Suh Y.H., Chang K., Roche K.W. Metabotropic glutamate receptor trafficking. 2018. Mol. Cell. Neurosci. Vol. 91. P.10-24.

Sun T. and Hevner R.F. Growth and folding of the mammalian cerebral cortex: from molecules to malformations. 2014. Nat. Rev. Neurosci. Vol. 15. P. 217-232.

Sundaram A., Plumb R., Appathurai S., Mariappan M. The Sec61 translocon limits IRE1α signaling during the unfolded protein response. 2017. eLife. Vol. 6.

Suri M., Evers J.M.G., Laskowski R.A., O'Brien S., Baker K., Clayton-Smith J., Dabir T., Josifova D., Joss S., Kerr B., Kraus A., McEntagart M., Morton J., Smith A., Splitt M., Thornton J.M., DDD Study., Wright C.F. Protein structure and phenotypic analysis of pathogenic and population missense variants in STXBP1. 2017. Mol Genet Genomic Med. Vol. 5(5). P. 495-507.

Svitkin Y.V., Pause A., Haghighat A., Pyronnet S., Witherell G., Belsham G.J., Sonenberg N. The requirement for eukaryotic initiation factor 4A (eIF4A) in translation is in direct proportion to the degree of mRNA 5’ secondary structure. 2001. RNA. Vol. 7. P. 382-394.

Tabata H. and Nakajima K. Multipolar migration: the third mode of radial neuronal migration in the developing cerebral cortex. 2003. Neurosci. Vol. 23. P. 9996-10001.

Takyar S., Hickerson R.P., Noller H.F. mRNA helicase activity of the ribosome. 2005. Cell. Vol. 120(1). P. 49-58.

Tanenbaum M.E., Gilbert L.A., Qi L.S., Weissman J.S., Vale R.D. A Protein-Tagging System for Signal Amplification in Gene Expression and Fluorescence Imaging. 2014. Cell. Vol. 159(3). P. 635-646.

Tarabykin V., Stoykova A., Usman N. and Gruss P. Cortical upper layer neurons derive from the subventricular zone as indicated by Svet1 gene expression. 2001. Development. Vol. 128. P. 1983–1993.

Taverna E., Gotz M. and Huttner W.B. The cell biology of neurogenesis: toward an understanding of the development and evolution of the neocortex. 2014. Annu Rev Cell Dev Biol. Vol. 30. P. 465-502.

Telley L., Agirman G., Prados J., Amberg N., Fievre S., Oberst P., Bartolini G., Vitali I., Cadilhac C., Hippenmeyer S., Nguyen L., Dayer A., Jabaudon D. Temporal patterning of apical progenitors and their daughter neurons in the developing neocortex. 2019. Science. Vol. 364(6440).

Toma K. and Hanashima C. Switching modes in corticogenesis: mechanisms of neuronal subtype transitions and integration in the cerebral cortex. 2015. Front Neurosci. Vol. 9. P. 274.

Tsai C.J., Sauna Z.E., Kimchi-Sarfaty C., Ambudkar S.V., Gottesman M.M., Nussinov R. Synonymous mutations and ribosome stalling can lead to altered folding pathways and distinct minima. 2008. J. Mol. Biol. Vol. 383. P. 281-291.

Tuller T., Carmi A., Vestsigian K., Navon S., Dorfan Y., Zaborske J., Pan T., Dahan O., Furman I., Pilpel Y. An evolutionarily conserved mechanism for controlling the efficiency of protein translation. 2010. Cell. Vol. 141. P. 344-354.

Urano F., Wang X., Bertolotti A., Zhang Y., Chung P. et al. Coupling of stress in the ER to activation of JNK protein kinases by transmembrane protein kinase IRE1. 2000. Science. Vol. 287. P. 664–666.

Urra H., Henriquez D.R., Cánovas J., Villarroel-Campos D., Carreras-Sureda A., Pulgar E., Molina E., Hazari Y.M., Limia C.M., Alvarez-Rojas S. et al. IRE1α governs cytoskeleton remodelling and cell migration through a direct interaction with filamin A. 2018. Nat. Cell Biol. Vol. 20. P. 942–953.

van Beuningen S.F.B. and Hoogenraad C.C. Neuronal polarity: remodeling microtubule organization. 2016. Current Opinion in Neurobiology. Vol. 39. P. 1-7.

Vlaskamp D.R.M., Callenbach P.M.C., Rump P., Giannini L.A.A., Dijkhuizen T., Brouwer O.F., van Ravenswaaij-Arts C.M.A. Copy number variation in a hospital-based cohort of children with epilepsy. 2017. Epilepsia Open. Vol. 2(2). P. 244-254.

Walter P. and Blobel G. Translocation of proteins across the endoplasmic reticulum. II. Signal recognition protein (SRP) mediates the selective binding to microsomal membranes of in-vitro-assembled polysomes synthesizing secretory protein. 1981. J Cell Biol. Vol. 91(2 Pt 1). P. 551–556.

Walter P. and Ron D. The Unfolded Protein Response: From Stress Pathway to Homeostatic Regulation. 2011. Science. Vol. 334(6059). P. 1081-1086.

Walter P., Ibrahimi I., Blobel G. Translocation of proteins across the endoplasmic reticulum. I. Signal recognition protein (SRP) binds to in-vitro-assembled polysomes synthesizing secretory protein. 1981. J Cell Biol. Vol. 91(2 Pt 1). P. 545–550.

Wang H., Wu Q., Li S., Zhang B., Chi Z., Hao L. Unc5D regulates p53-dependent apoptosis in neuroblastoma cells. 2014. Mol Med Rep. Vol. 9(6). P. 2411-2416.

Wang M. and Kaufman R. J. Protein misfolding in the endoplasmic reticulum as a conduit to human disease. 2016. Nature. Vol. 529. P. 326–335.

Wang X.Z., Harding H.P., Zhang Y., Jolicoeur E.M., Kuroda M., Ron D. Cloning of mammalian Ire1 reveals diversity in the ER stress responses. 1998. EMBO J. Vol. 17(19). P. 5708–5717.

Wassie A.T., Zhao Y., Boyden E.S. Expansion microscopy: principles and uses in biological research. 2018. Nature Methods. Vol. 16. P. 33-41.

Westrate L.M., Lee J.E., Prinz W.A., Voeltz G.K. Form follows function: the importance of endoplasmic reticulum shape. 2015. Annu Rev Biochem. Vol. 84. P. 791–811.

Willemsen R., Levenga J., Oostra B.A. CGG repeat in the FMR1 gene: size matters. 2011. Clin Genet. Vol. 80. P. 214-225.

Wolfe A.L., Singh K., Zhong Y., Drewe P., Rajasekhar V.K., Sanghvi V.R., Mavrakis K.J., Jiang M., Roderick J.E/. Van der Meulen J., Schatz J.H., Rodrigo C.M., Zhao C., Rondou P., de Stanchina E., Teruya-Feldstein J., Kelliher M.A., Speleman F., Porco J.A.Jr., Pelletier J., Rätsch G., Wendel H.-G. RNA G-quadruplexes cause eIF4A-dependent oncogene translation in cancer. 2014. Nature. Vol. 513(7516). P. 65–70.

Wonders C.P. and Anderson S.A. The origin and specification of cortical interneurons. 2006. Nat. Rev Neurosci. Vol. 7. P. 687–696.

Wu J., Cai Y., Wu X., Ying Y., Tai Y., He M. Transcardiac Perfusion of the Mouse for Brain Tissue Dissection and Fixation. 2021. Bio Protoc. Vol. 11(5).

Wyllie E., Comair Y.G., Kotagal P., Raja S., Ruggier P. Epilepsy Surgery in Infants. 1996. Epilepsia. Vol. 37. P. 625-637.

Xiang X., Corsi G.I., Anthon C., Qu K., Pan X., Liang X., Han P., Dong Z., Liu L., Zhong J., Ma T., Wang J., Zhang X., Jiang H., Xu F., Liu X., Xu X., Wang J., Yang H., Bolund L., Church G.M., Lin L., Gorodkin J., Luo Y. Enhancing CRISPR-Cas9 gRNA efficiency prediction by data integration and deep learning. 2021. Nature Communications. Vol. 12.

Yan X., Hoek T.A., Vale R.D., Tanenbaum M.E. Dynamics of Translation of Single mRNA Molecules In Vivo. 2016. Cell. Vol. 165. P. 976-989.

Ye H. and Kaszuba S. Inhibitory or excitatory? Optogenetic interrogation of the functional roles of GABAergic interneurons in epileptogenesis. Journal of Biomedical Science. 2017. Vol.24.

Ye S., Dhillon S., Ke X., Collins A.R. and Day I.M.N. An efficient procedure for genotyping single nucleotide polymorphisms. Nucleic Acid Res. 2001; 29.

Zhang W., Xiao W., Wei H., Zhang J., Tian Z. mRNA secondary structure at start AUG codon is a key limiting factor for human protein expression in Escherichia coli. 2006. Biochem. Biophys. Res. Commun. Vol. 349. P. 69–78.

8. Publication list

Levin-Kravets O, Kordonsky A, Shusterman A, Biswas S, Persaud A, Elias S, Langut Y, Florentin A, Simpson-Lavy KJ, Yariv E, Avishid R, Sror M, Almog O, Marshanski T, David NB, Manori B, Fischer Z, Lilly J, **Borisova E**, Ambrozkiewicz MC, Tarabykin V, Kupiec M, Thaker M, Rotin D, Prag G. *Split chloramphenicol acetyl-transferase assay reveals self-ubiquitylation-dependent regulation of UBE3B*. Journal of Molecular Biology. 2021 Sep; 1672-76.

Parthasarathy S, Srivatsa S, Weber AI, Gräber N, Britanova OV, **Borisova E**, Bessa P, Ambrozkiewicz MC, Rosário M, Tarabykin V. *TrkC-T1, the Non-Catalytic Isoform of TrkC, Governs Neocortical Progenitor Fate Specification by Inhibition of MAP Kinase Signaling*. Cerebral Cortex. 2021 Jul; 00:1-17.

Epifanova E, Salina V, Lajkó D, Textoris-Taube K, Naumann T, Bormuth O, Bormuth I, Horan S, Schaub T, **Borisova E**, Ambrozkiewicz MC, Tarabykin V, Rosário M. *Adhesion dynamics in the neocortex determine the start of migration and the post-migratory orientation of neurons*. Science Advances. 2021 Jul; 7(27).

Harnett D, Ambrozkiewicz MC, Zinnall U, **Borisova E**, Rusanova A, Dannenberg R, Imami K, Münster-Wandowski A, Fauler B, Mielke T, Selbach M, Landthaler M, Spahn CMT, Tarabykin V, Ohler U, Kraushar ML. *Timed global reorganization of protein synthesis during neocortex neurogenesis at codon resolution*. bioRxiv. 2021 Jun.

Ambrozkiewicz MC, **Borisova E**, Newman AG, Kraushar ML, Schaub T, Dannenberg R, Brockmann M, Rosário M, Turko P, Jahn O, Kaplan DR, Iwawaki T, Spahn CMT, Rosenmund C, Tarabykin V. *Ire1α-Regulated Rate of mRNA Translation is Required for Acquisition of Identity and Polarity in Upper Layer Cortical Neurons*. bioRxiv. 2021 Jun.

Kraushar ML, Krupp F, Harnett D, Turko P, Ambrozkiewicz MC, Sprink T, Imami K, Günnigmann M, Zinnall M, Vieira-Vieira CH, Schaub T, Münster-Wandowski A, Bürger J, **Borisova E**, Yamamoto H, Rasin M-R, Ohler U, Beule D, Mielke T, Tarabykin V, Landthaler M, Kramer G, Vida I, Selbach M, Spahn CMT. *Protein synthesis in the developing neocortex at near-atomic resolution reveals Ebp1-mediated neuronal proteostasis at the 60S tunnel exit.* Molecular cell. 2021 Jan; 81(2):304-322.

Borisova EV, Turovsky EA, Turovskaya MV, Tomilin AN, Nedospasov SA, Tarabykin VS. *ENU mutagenesis as a tool for identifying novel mouse models of epilepsy.* Opera Medica et Physiologica. 2021; 8(1):5-11.

Ambrozkiewicz MC, **Borisova E**, Schwark M, Ripamonti S, Schaub T, Smorodchenko A, Weber AI, Rhee HJ, Altas B, Yilmaz R, Mueller S, Piepkorn L, Horan ST, Straussberg R, Zaqout S, Jahn O, Dere E, Rosário M, Boehm-Sturm P, Borck G, Willig KI, Rhee JS, Tarabykin V, Kawabe H. *The murine ortholog of Kaufman oculocerebrofacial syndrome protein Ube3b regulates synapse number by ubiquitinating Ppp3cc.* Molecular psychiatry. 2020 Apr; 26:1980-1995.

Ambrozkiewicz MC, Schwark M, Kishimoto-Suga M, **Borisova E**, Hori K, Salazar-Lázaro A, Rusanova A, Altas B, Piepkorn L, Bessa P, Schaub T, Zhang X, Rabe T, Ripamonti S, Rosário M, Akiyama H, Jahn O, Kobayashi T, Hoshino M, Tarabykin V, Kawabe H. *Polarity acquisition in cortical neurons is driven by synergistic action of Sox9-regulated Wwp1 and Wwp2 E3 ubiquitin ligases and intronic miR-140*. Neuron. 2018 Dec; 100(5):1097-1115.

Borisova EV, Epifanova EA, Tutukova SA, Belousova II, Zhidkova NM, Rusanova AM, Salina VA, Turovsky EA, Turovskaya MV, Tarabykin VS, Babaev AA. *Identification of novel mutations controlling cerebral cortex malformations caused by ENU-induced mutagenesis in the mouse*. Modern technologies in medicine. 2018; 10(3):70-76.

Belousova II, Zhidkova NM, **Borisova EV**, Epifanova EA, Salina VA, Tutukova SA, Lapshin RD, Babaev AA, Mukhina IV, Tarabykin VS. *Phenotypic Variations in the Behavior of Sip1 Knockout Mice.* Modern technologies in medicine. 2018; 10(2):20-28.

Salina V, Tutukova S, **Borisova E**, Epifanova E, Zhidkova N, Rusanova A, Turovsky E, Turovskaya M, Babaev A, Tarabykin V. *ENU mutagenesis screening in mice identifies a mutation that causes microcephaly*. JOURNAL OF NEUROCHEMISTRY. 2017 Aug; 142:142.

Borisova E, Epifanova E, Tutukova S, Salina V, Zhidkowa N, Rusanova A, Turovsky E, Turovskaya M, Babaev A, Tarabykin V. *ENU mutagenesis screening to identify mutations that control corpus callosum development*. JOURNAL OF NEUROCHEMISTRY. 2017 Aug; 142:137.

Turovskaya MV, Babaev AA, Zinchenko VP, Epifanova EA, **Borisova EV**, Tarabykin VS, Turovsky EA. *Sip-1 mutations cause disturbances in the activity of NMDA-and AMPA-, but not kainate receptors of neurons in the cerebral cortex*. Neuroscience letters. 2017 May; 650:180-186.

Epifanova EA, **Borisova EV**, Salina VA, Babaev AA. *Viral Vectors for Delivering Gene Material into Cells and Their Application in Neurobiology*. Modern technologies in medicine. 2017; 9(1):162-173.

Borisova EV, Epifanova EA, Tutukova SA, Salina VA, Babaev AA. *Optogenetic approaches in neurobiology*. Molecular Genetics, Microbiology and Virology. 2016 Oct; 31(4):203-207.

Acknowledgements

Firstly, I would like to thank my supervisors Victor and Mateusz.

Victor, thank you for your constant support and guidance throughout my PhD years. Thank you for being an example of a scientist full of enthusiasm and love for science, and for the “high-fives”!

Mateusz, thank you from the bottom of my heart for your daily support, even in the most challenging moments, for believing in me, and for pleasant conversations not only about science. Thank you for all the time, work and patience you put into me! You are exactly the teacher I dreamed of! Bardzo dziękuję!

Many thanks to all the people in the lab who have created a wonderful atmosphere over the years, for their helpfulness and all the pleasant moments! Thank you Olga and Ingo, Marta, Jutta, Andrew, Diana, Ulrike, Kuo, Katie!

A special thank you to Theres for her willingness to help with all my requests! Thank you, Denis, for your help and the fantastic talks and conversations about art! Thank you, Rike, for your assistance with the projects and your wonderful sense of humor! Ich danke Ihnen von ganzem Herzen!

Thank you to my girls with whom we have been fighting through PhD together! Thank you for your support, for our inner humor, and for the time we spent together and not just in the lab. Thank you Katya aka Катеришкинс, Valya aka Валенти, Sveta, Alexandra aka Алекзашечкин, Lara and Tanya! I am endlessly happy that you are in my life! Вы лучшие!

Despite the distance, they never stopped thinking of me, supporting me, sharing sweet moments, and reminding me of old times. Thank you, Natasha and Zakhar, Nastya, Nastya and Dasha, Sergei, Nastya, for your love and kindness!

Thank you, my dear Evgenij, for all the wonderful moments and your invaluable support! I am looking forward to new adventures together 😉

Words cannot express how grateful I am to my amazing parents and grandmothers! Thank you for your love, care, support and faith that I feel all the time! Thank you to my grandfathers, who always believed in me and taught me never to be discouraged, to like animals and to be creative. Люблю вас всем сердцем!